A THEORETICAL STUDY OF CH···X (X= O, N, S, P AND π) INTERACTIONS

RAN JIONG

NATIONAL UNIVERSITY OF SINGAPORE

2006

A THEORETICAL STUDY OF CH···X (X= O, N, S, P AND π) INTERACTIONS

RAN JIONG

(B.S., LANZHOU UNIVERSITY, P. R. CHINA)

A THESIS SUBMITTED

FOR THE DEGREE OF DOCTOR OF PHILOSOPHY

DEPARTMENT OF CHEMISTRY

NATIONAL UNIVERSITY OF SINGAPORE

2006

Acknowledgements

First and foremost, I would like to thank to my supervisor Assoc Prof Wong Ming Wah, Richard, for his constant guidance throughout the course of my study.

I thank NUS for its financial support, the department of chemistry and the computer centre for providing workstation and supercomputing facilities.

I thank my colleagues, Dr. Kiruba, Dr. Goh Sor Koon, Wong Chiong Teck, Chwee Tsz Sian, Adrian Matthew Mak Weng Kin and Mien Ham and Joshua, Lau Boon Wei for putting up with me and for maintaining a peaceful, lively and healthy working atmosphere.

I am especially thankful to my friends, Yang TianCai, HanJun, Qian JianTing, Zhang WenHua, Kuang ZhiHai and Cai LiPing for all their help.

Finally, I would like to thank my beloved parents, sister, my wife and my daughter from the bottom of my heart, for being my source of inspiration and for their constant encouragement, profound love, care and prayers.

Table of Contents

Summary

This thesis deals with the computational quantum chemical study of weak CH···X (X= O, N, S, P and π) interactions in organic as well as biological molecules.

Chapter 1 gives a general introduction of hydrogen bond studied in this thesis.

Chapter 2 provides the theoretical background of all type of calculations included in this thesis.

Chapter 3 investigate the cooperative CH/π effects between the π face of benzene and several modeled saturated hydrocarbons, propane, isobutane, cyclopropane, cyclobutane, cyclopentane, cyclohexane, cyclopentane, cyclooctane and bicyclo[2.2.2]octane by high-level ab initio calculations at the CCSD(T)/aug-cc-pVTZ//MP2/aug(d,p)-6-311G(d,p) level. In all cases, multiple C-H groups (2–4) are found to interact with the π face of benzene, with one C–H group points close to the centre of the benzene ring. The geometries of these complexes are governed predominantly by electrostatic interaction between the interacting systems. The calculated interaction energies (10–15 kJ mol^{-1}) are two to three times larger than that of the prototypical methane–benzene complex. The trends of geometries, interaction energies, binding properties as well as electron-density topological properties were analyzed. The calculated interaction energies correlate well with the polarizabilities of the hydrocarbons. The AIM analysis confirms the hydrogen-bonded nature of the CH/π interactions. Significant changes in proton chemical shift and stretching frequency (blue shift) are predicted for the ring C–H bond in these complexes.

Chapter 4 deals with the study of intermolecular complexes of benzene with cyclohexane and its heterocyclic analogues $C_{6-n}X_nH_{12-2n}$ (X= O, S, NH, PH, SiH_2 and n=1, 2, 3) to investigate the effect of heteroatom substitution on the multiple CH/π interactions. Geometries were optimized at the MP2/6-31G* level and the binding energies were computed at CCSD(T)/aug(d,p)-6-311G** + ZPE, including BSSE correction. Our studies showed that oxygen and nitrogen substitution have little effect on the geometry and interaction energy. On the other hand, sulfur, phosphorus and silicon substitution strengthen the multiple CH/π complexes, with binding energy range from 13.2 to 18.6 kJ mol^{-1}. The binding energy increases with the number of heteroatom substitution. Each second-row atom substitution yields a rather uniform increase of binding energy (2.5 kJ mol^{-1}).

Chapter 5 deals with the study of cooperative XH/π (X=C or N) effects between the π face of benzene and phenylalanine and several modeled biological molecules, pyrrolidine-2-carbaldehyde (PCA), cyclopentanecarbaldehyde (CCA) and proline. In all cases, multiple X–H groups (2–4) are found to interact with the π face of benzene or phenylalanine, with one X–H (C or N) group points close to the centre of the aromatic ring. The geometries of these complexes are governed predominantly by electrostatic interaction between the interacting systems. The calculated interaction energies cover a wild range (15-49 kJ mol^{-1}) at CCSD (T)/aug(d,p)-6-311G(d,p)//MP2/6-31G(d) level. The trends of geometries, interaction energies, binding properties as well as electron-density topological properties were analyzed. The AIM analysis confirmed the hydrogen-bonded nature of the XH/π interactions.

Chapter 6 deals with the study of gauche/trans conformational equilibrium of a series of XCH_2CH_2Y (X, Y= NMe_2, PMe_2, OMe and SMe) molecules by ab *initio* and DFT methods. The relevant intramolecular CH···X (X= O, N, S and P) interaction was examined by G3(MP2) level. The calculations show that intramolcular CH···X interaction stabilizes the gauche conformation significantly. The estimated CH···O and CH···N interaction energies are in the range 4-6 kJ mol^{-1}. Systems with mixed hetero atoms, such as OS, ON, OP, NS and NP prefer a *gauche* conformer. The repulsion between heavy atoms also contribute to the conformational preference. Due to the small difference in dipole moment between *gauche* and *trans* forms, the calculated solvent effect is generally small. All the intramolecular CH···X(X= O, N, S and P) interactions are confirmed to be hydrogen bonding in nature based on AIM analysis.

Chapter 7 deals with the study of Conformations of 4,4-bisphenylsulfonyl-*N*,*N*-dimethylbutylamine (BPSDMBA) were examined by ab initio calculations. Intramolecular C–H···N, C–H···O and π···π interactions are found to play an important role in governing the conformational properties. This finding is supported by the AIM charge density. The calculated structure and ^1H chemical shifts of BPSDMBA confirm the existence of an intramolecular C–H···N hydrogen bond, with an estimated interaction energy of 14 kJ mol^{-1}. The sulfonyl oxygens in BPSDMBA interact with neighboring methylene, methyl and phenyl hydrogens via the C–H···O=S hydrogen bond. In agreement with experiment, SCRF calculations indicate that these weaker intramolecular interactions prevail in an aprotic polar medium.

Chapter 1 General introduction

The hydrogen bond was discovered almost 100 years ago, but it is still a hot topic of current scientific research. The reason for this long-standing interest lies in the eminent importance of hydrogen bonds for the structure, function, and dynamics of a vast number of chemical systems, ranging from inorganic to biological compounds. Hydrogen bonds are important in diverse scientific disciplines which include mineralogy, material science, general inorganic and organic chemistry, supramolecular chemistry, biochemistry, molecular medicine, and pharmacy. In recent years, research in hydrogen bonds have greatly expanded in depth as well as in breadth, as new concepts have been established, and the complexity of the phenomena considered has increased dramatically. There are dozens of different types of XH···Y hydrogen bonds that occur commonly in the condensed phases, and in addition there are numerous less common ones. Dissociation energies span more than two orders of magnitude (1.0-160 kJ mol^{-1}). Within this range, the nature of the interaction is not uniform, with its electrostatic, covalent, and dispersion contributions vary greatly in relative weights. The hydrogen bond has broad transition regions that merge continuously with the covalent bond, the van der Waals interaction, the ionic interaction, and also the cation-π interaction. In this chapter, the fundamental aspects on the various types of weak XH···Y hydrogen bond will be reviewed.

1.1 Definitions of Hydrogen Bond

The definition of the hydrogen bond has been a subject of strong controversy. The early definition by Pimentel and McClellan[1] stated that: "A hydrogen bond exists between

X–H and an atom (or group of atoms) A, if the interaction between X–H and A (1) is bonding, and (2) sterically involves the hydrogen atom". This is a very general definition, which leaves the chemical nature of X–H and A, including their polarities and charges, unspecified. No restriction is made on the geometry of the interaction, as long as it is bonding in nature and it involves a hydrogen atom. The crucial requirement is the existence of a "bond", which is not easy to define. In practice, the difficulty is to demonstrate the bonding nature of a given arrangement. Unlike other definitions, that of Pimentel and McClellan is flexible enough to cover the wide range from the strongest hydrogen bonds,[2] over 'normal' ('moderate') hydrogen bonding to the weak bonding which is present for example in directional CH···A or CH···π interactions.

Apart from the general chemical definitions, there are many specialized definitions of hydrogen bonds that are based on certain sets of properties that can be studied with a particular technique. For example, hydrogen bonds have been defined on the basis of interaction geometries in crystal structures (short contact distance and almost "linear angle" θ), certain effects in IR absorption spectra (red-shift and intensity increase of υ_{XH}, etc.), or certain properties of experimental electron density distributions (existence of a "bond critical point" between H and A, with numerical parameters within certain ranges). The practical scientist often prefers to use a technical definition, and an automated data treatment procedure for identifying a hydrogen bond. It is outside the scope of this chapter to discuss any set of threshold values that a "hydrogen bond" must pass in any particular type of technical definition. It is worth mentioning that the "van der Waals cutoff" definition for identifying hydrogen bonds on a structural basis (requiring that the H···A distance is substantially shorter than the sum of the van der Waals radii of H and A) is far too restrictive and should no longer be applied.[3] If distance cutoff limits must be used, X–

H···A interactions with H···A distances up to 3.0 or even 3.2 Å should be considered as potentially hydrogen bonding.[4] An angular cutoff can be set at >90º or, somewhat more conservatively, at >110º. A necessary geometric criterion for hydrogen bonding is a positive directionality preference, that is, linear X–H···A angles must be statistically favored over the bent ones.[5] In a hydrogen bond X–H···A, the group X–H is called the donor and A is called the acceptor (short for "proton donor" and "proton acceptor", respectively). Some authors prefer the reverse nomenclature (X–H = electron acceptor, Y = electron donor), which is equally justified.

1.2 Components of Interaction

A hydrogen bond is a complex interaction composed of several components that are different in their natures.[6] The most popular partition schemes follow essentially that employed by Morokuma.[7] The total energy of a hydrogen bond (E_{tot}) is split into contributions from electrostatics (E_{el}), polarization (E_{pol}), charge transfer (E_{ct}), dispersion (E_{disp}), and exchange repulsion (E_{er}) terms. Somewhat different, but related partitioning schemes were also in use. The distance and angular characteristics of various components are very different. The electrostatic term is directional and of long range (diminishing only slowly as $-r^{-3}$ for dipole-dipole and as $-r^{-2}$ for dipole-monopole interactions). Polarization decreases faster ($-r^{-4}$) and the charge-transfer term decreases even faster, approximately following e^{-r}. According to natural bond orbital analysis,[8] charge transfer occurs from an electron lone pair of A to an antibonding orbital of X–H, that is $n_A \rightarrow \sigma^*$ of X–H for hydrogen bond. The dispersion term is isotropic with a distance dependence of $-r^{-6}$. The exchange repulsion term increases sharply with reducing distance (as $+r^{-12}$). The

dispersion and exchange repulsion terms are often combined into an isotropic "van der Waals" contribution that is approximately described by the well-known Lennard-Jones potential ($E_{vdw} \sim Ar^{-12}\text{-}Br^{-6}$). Depending on the particular chemical donor-acceptor combination, and the details of the contact geometry, all these terms contribute with different weights. It cannot be generally stated that the hydrogen bond as such is dominated by this or that term in any case. Some general conclusions can be drawn from the overall distance characteristics. In particular, it is important that of all the energy terms, the electrostatic contribution reduces most slowly with increasing distance. The hydrogen bond potential for any particular donor-acceptor combination is, therefore, dominated by electrostatics term at long distances, even if charge transfer plays an important role at optimal geometry. Elongation of a hydrogen bond from optimal geometry always makes it more electrostatic in nature. In "normal" hydrogen bonds, E_{el} is the largest term, but a certain charge-transfer contribution is also present. The van der Waals terms too are always present, and for the weakest kinds of hydrogen bonds dispersion may contribute as much as electrostatics to the total bond energy. Purely "electrostatic plus van der Waals" models can be quite successful despite their simplicity for hydrogen bonds of weak to intermediate strengths.[9]

1.3 Properties of hydrogen bonds

There are two features which are common to all generally accepted definitions of hydrogen bond.[10] First, there is a significant charge transfer from the proton acceptor (Y) to the proton donor (X–H). Second, formation of the X–H···Y H-bond results in weakening of the X–H bond. This weakening is accompanied by a bond elongation and a

concomitant decrease of the X–H stretch vibration frequency compared to the noninteracting species. A shift to lower frequencies is called a red shift and represents the most important, easily detectable (in liquid, gas, and solid phases) manifestation of the formation of a H-bond. Note that these "significant" changes of molecular properties upon complex formation are actually quite small: the change in energies, bond lengths, frequencies, and electron densities are two or more orders of magnitude smaller than those of the typical chemical changes. The red shift of the X–H stretch vibration, which varies between several tens or hundreds of wavenumbers, represents, until recently, an unambiguous information about the formation of a H-bond, since the formation of a H-bond in a XH···Y system is accompanied by weakening of the X–H covalent bond. This is the basis for several spectroscopic, structural, and thermodynamic techniques for the detection and investigation of H-bonds. The characteristic features of X–H···Y H-bond are as follows: (i) the X–H covalent bond stretches in correlation with the strength of the H-bond; (ii) a small amount of electron density (0.01-0.03 e) is transferred from the proton-acceptor (Y) to the proton-donor molecule (X–H); (iii) the band which corresponds to the X–H stretch shifts to lower frequency (red shift), increases in intensity, and broadens. The value of the red shift and the strength of the H-bond are correlated.[6] Frequency shifts correlate with various characteristics of the H-bonded system. Recently relationships were found between experimental proton affinities and frequency shifts as well as between *ab* initio-calculated bond distances, interaction energies, and frequency shifts, deduced from intermolecular complexes of pyridines, pyrimidines, and imidazoles with water[11] and pyridine derivatives with water.[12]

1.4 The CH···X Weak Hydrogen Bond

1. 4.1 General introduction

The weak hydrogen bond has been defined as an interaction XH···Y, wherein a hydrogen atom forms a bond between two structural moieties X and Y, of which one or even both are only of moderate to low electronegativity.[3] The oldest and certainly the prototype interaction is the CH···O, but one would also include others such as PH···O, CH···N, CH···S, CH···P and MH···O ((M) metal) interactions of which a weak donor associates with a strong acceptor. The alternative situation of which a strong donor associates with a weak acceptor is exemplified by OH···π, NH···π, OH···M, and OH···S. Finally, and at the limit of the hydrogen bond phenomenon, one needs to consider the association of a weak donor with a weak acceptor such as CH···π.

The introduction of the idea of CH···O bonding is usually attributed to Glasstone in 1937.[13] It has long been known that mixtures of chloroform with liquids like acetone or ether have abnormal physical properties, such as vapour pressures, viscosities and dielectric constants. Glasstone investigated such systems by polarisation measurements on liquid complexes of haloforms with ethers, acetone and quinoline. He found that the molar polarisation of the mixtures is larger than those of the pure components, in other words, the dipole moment of each constituent in the mixtures is greater than in the pure forms. He explained the observed result in terms of the association of the molecules by directional electrostatic interactions. This idea was rapidly accepted by spectroscopists, and Gordy,[14] based on infrared (IR) spectroscopic evidence, already called this interaction a 'hydrogen bond'. In the following years, numerous related studies were performed, in which the focus was on the reduction of C–H IR stretching frequencies υ_{CH} in the presence of

electronegative atoms. The largest frequency shifts >100 cm^{-1}, which come close to υ_{XH} shifts in OH···A or NH···A bonds, are observed for 'activated' C–H groups like in acetylenes, C≡C–H, or C–H adjacent to highly electronegative groups. Allerhand and Schleyer[15] in 1963 interpreted a series of such experiments in a well-known review. One of their main conclusions is:

"The ability of a C–H group to act as a proton donor depends on the carbon hybridization, C(sp)–H>C(sp^2)–H>C(sp^3)–H, and increases with the number of adjacent electron-withdrawing groups".

Two early crystal structures showing C–H···X hydrogen bonding are those of HCN[16] and cyanoacetylene, [17] both structures are composed of infinite linear chains, and the authors have no problem in interpreting the short ≡C–H···N≡ contacts as hydrogen bonds. This was well supported by IR spectroscopic data: in solid HCN, the C–H stretching frequency is 180 cm^{-1} lower than in the gaseous state, which is almost half the shift observed for O–H in ice.[18] Another relevant early crystal structure is that of dimethyl oxalate, reported by Dougill and Jeffrey.[19] The authors noted that in the crystal, carbonyl O-atoms co-ordinate tightly around the methyl group, roughly in the expected directions of the C–H bonds (the H-atoms could not be seen). Dougill and Jeffrey associate these contacts with a significant bonding interaction, which they call "polarisation bonding". The authors suggested that these interactions are the reason for the anomalous melting point of the substance, which is about 100 ºC higher than that of most related carboxylic esters. The structure analysis was (with a different background) repeated by Jones, Cornell, Horn and Tiekink, [20] who located the H-atom positions. On this basis, a dense

network of CH···O contacts can actually be shown. The H···O separations (2.5–2.8 Å) are much longer than in the ≡C–H···N≡ bonds, but one can suppose that due to their large number, they are in fact responsible for the unusually stable molecular association of dimethyl oxalate. The study of Dougill and Jeffrey can be taken as the first evidence of hydrogen bonding of a methyl group.

The CH···π interaction was first proposed by Nishio[21] and co-workers to explain the preference of conformations in which bulky alkyl and phenyl groups had close contact. In the following two decades, several experimental studies, which support the existence of the attraction, have been reported. The close contact was observed in stable conformations of a lot of molecules. Statistical analysis of the crystal database indicates that the short contact of the C–H bond and the π system is observed in large number of organic crystals[22] and crystals of proteins.[23] The CH···π interaction is believed as a crucial driving force of crystal packing.[24]

The CH···π geometry is very common but the interaction is of variable character because of the wide range of C–H group acidity and *π*-basicity. The interaction has also been called by different names; organic chemists have termed it a "CH···*π* interaction", structural biologists prefer the term "phenyl interactions",[25] and in the crystal engineering literature they are referred to as "herringbone" interactions[26] or "hybrid" interactions.[27]
A distinctive feature of *π*-acceptors is that they are of the multi-atom type. While CH···π interactions to phenyl rings have been often identified, their directional properties also vary greatly different that the C–H bond can point at the aromatic center, at a particular C-C bond or even at an individual C-atom, but in most cases shows a trend that these interactions are directed toward the centroids of the respective phenyl rings. This preference may arise from either or both steric and electronic reasons.

One of the unique properties of the CH···π hydrogen bond is that many C–H and π groups may cooperatively participate in the interaction. Although contribution from a unit CH···π bond is small, total interaction energy may become significant by the cooperation of many CH/π bonds. Frequently used ligands such as 2, 2'-bipyridyl, 1, 10-phenanthryl and triphenylphosphine are aromatic. They are effective as a C–H acceptor as well as a donor. It is a common experience of organic chemists and crystallographers that an aromatic compound generally has a higher melting point and is easier to crystallize than its aliphatic analog. Grouped arrangement of C–H bonds is common in organic compounds. A methyl group, for instance, has C3 symmetry. A long-chain aliphatic group has many C–H bonds united into a single moiety. Every aromatic group has the plane of symmetry with large surface. Consequently, the Gibbs energy of a CH···π interacted system increases. Such a condition is not anticipated for in the conventional hydrogen bond. Recognition of the above two features is crucial in understanding the role of CH···π interaction. Lastly, the CH···π hydrogen bond plays its role in polar protic media such as water, and by implication in the physiological environment. This is because the energy of the CH···π bond comes mostly from the dispersion force. This is of utmost importance when considering the effect of nonpolar or weak hydrogen bonds in the biochemical process. The Coulomb force and the ordinary hydrogen bond, on the contrary, are not very effective in polar solvents.

The scope of weak hydrogen bonding has been extended considerably by inclusion of organometallic examples. This topic has been reviewed in detail elsewhere by Braga, and others.[28, 29] In other words, with the advantages of polarizable donors and acceptors and of cooperativity effects it is possible to have metal-containing species as donors and

acceptors in hydrogen bonding situations. In the end, it appears that even with minimum residual electrostatic character, an interaction XH···A shows many hydrogen bond-like properties. The difficulty in understanding interactions formed by the association of weak donors with weak acceptors is that the major stabilization arises from dispersion. The transition from a hydrogen bond to a van der Waals interaction is gradual and several situations may be found in the gray area that lies between these regions.

1. 4.2 The general properties of CH···X hydrogen bond

As we mentioned above, the standard hydrogen bonding of the type XH···Y is characterized by weakening of the X–H bond which causes elongation of this bond and a red shift of the corresponding X–H stretch frequency. However, there are a number of cases where the proton donor (X–H bond) is sp^3-hybridized (e.g. CF_3H, acetone) its interaction with a proton acceptor leads to the shortening of the C–H bond, associated with this uncharacteristic bond shortening is the blue shift of the stretching frequency, in contrast to the normally expected red shift. This situation is happened in CH···X hydrogen extremely common, especially in sp^2-and sp^3-hybridized C–H bond, but for the sp-hybridized C–H donors, in most times, the red shift was observed**.** The first indication that the situation is more complicated appeared in 1989 when Buděšínský, Fiedler, and Arnold reported the preparation and spectra of triformylmethane (TFM).[30] They measured the IR spectrum of TFM in chloroform and detected the presence of a distinct, sharp band close to the C–H stretch of chloroform but slightly shifted toward higher wavenumbers (3028 cm^{-1} compared to 3021 cm^{-1}, the typical C–H stretch value for chloroform). Therefore, instead of the normal red shift of the C–H stretch frequency, a blue shift was observed.

The authors were certainly aware of the peculiarity of their finding: "We find it rather strange that this remarkable effect has not been observed by other authors[31] during their detailed examination of the IR spectrum of TFM". The second observation of the blue shift was reported in 1997 by Boldeskul et al.[32] They measured the IR spectra of chloroform, deuterochloroform, and bromoform in mixed systems containing proton acceptors such as carboxy, nitro, and sulfur-containing compounds. The formation of intermolecular complexes was accompanied by shifts of the haloform C–H/D stretch vibration absorption band by 3-8 cm^{-1} to a higher frequency compared to their position in CCl_4. The unusual shift was explained by a strengthening of the C–H/D bond due to increase of its *s* character caused by molecular deformation resulting from intermolecular forces. An attempt to explain this unusual behavior of haloforms by semi-empirical MNDO-H quantum chemical method failed.[32] Contrary to experimental findings, calculations predicted a decrease of the C–H frequency (i.e. a red shift) upon formation of the intermolecular complexes.

The first systematic investigation of the blue shift of the X–H stretch frequency in XH···Y complexes was a theoretical study of the interaction of benzene with C–H proton donors, [33] where it was shown that the formation of benzene···HCX (CX = CH_3, CCl_3, C_6H_5) complexes leads to a C–H bond contraction and an increase of the respective stretch frequency (blue-shift). Because the most important feature (the shortening of the proton-donor C–H bond and the blue shift) were opposite to those characteristics of classical H-bonds (the elongation of the proton donor X–H bond and the red shift), this type interaction originally was called an "anti-hydrogen bond". The term anti-hydrogen bond was later rightfully criticized as misleading mainly because it could suggest a destabilizing interaction of the subsystems or suggest a complex with anti-hydrogen. The

anti-H bonded complexes are formally the same as the classical hydrogen bond: the proton is placed between both subsystems, charge is transferred from proton acceptor to proton donor system, and stabilization of the complex is comparable to a normal H-bond. Because of this characteristic feature is opposite, the term of H-bond for the classical, red-shifting and improper, blue-shifting were appeared.

The blue shift of the C–H stretch frequency of chloroform was first detected in solutions of TFM in chloroform[30] and nitrobenzene in chloroform.[32] Direct evidence of the blue shift in the gas phase was missing until 1999, when a complex between fluorobenzene and chloroform was investigated using the double-resonance infrared ion-depletion spectroscopy.[34] The experimental value of the blue shift of the chloroform C–H stretch frequency (14 cm^{-1}) agreed well with the theoretical prediction (12 cm^{-1}) using a good quality ab initio treatment. The same technique was later used for a complex of fluorobenzene with fluoroform, and again, the agreement between the experimental blue shift and its theoretical prediction was good. The blue shift of the C–H stretch frequency was also theoretically predicted for CH···O contacts. The first system investigated was fluoroform···oxirane, where a significant blue shift of 30 cm^{-1} was predicted.[35] The family of CH···O complexes exhibiting a blue shift of the C–H stretch frequency upon complexation was later extended to dimers of $F_nH_{3-n}CH$ with H_2O, CH_3OH, and H_2CO.[36] These theoretical calculations predicted the largest blue shift of 47 cm^{-1} for the $F_3CH\cdots OHCH_3$ complex. A very large blue shift of the C–H stretch frequency, more than 100 cm^{-1}, was detected recently from infrared spectra of $X\cdots H_3CY$ ionic complexes (X = Cl, Y = Br; X,Y = I), which were also thoroughly investigated theoretically,[37] with excellent agreement with experimental values.

1. 4.3 The interaction energy of CH···X hydrogen bond

Interaction energy of weak hydrogen bond lies in 2 - 20 kJ mol^{-1}, with the majority < 10 kJ mol^{-1}. At the low energy end of the range, the CH···F hydrogen bond gradually fades into a van der Waals interaction. The strong end of the interaction has not yet been well explored. CH···X bonds stronger than 18 kJ mol^{-1} can readily be predicted to occur when very acidic C–H (e.g., ≡CH) or very basic acceptor groups are involved. According to the theoretical calculations, stabilization of the CH···X hydrogen bond comes, essentially, from the dispersion force.[38] Energetic contribution from the electrostatic energy is insignificant except for cases involving strong C–H donors such as chloroform or acetylenic C–H bond, but it very important in determining the complex structure.

1. 4.4 The nature of blue shift of CH···X hydrogen bond.

From its first discovery, blue shift CH···X hydrogen bonding received much attention from theoreticians who suggested several explanations for this phenomenon. The first line of thought, introduced by Hobza and co-workers,[10] concentrated on differences between classical and improper H-bonding such as an increased importance of disperse interactions and of changes in the remote parts of the molecule, e.g., electron transfer to C–F bonds in a complex of fluoroform and water which occur in addition to more common hyperconjugative charge transfer from the lone pair of a heteroatom to the σ^* (C–H) orbital (n→σ*(C-H) interaction). The second school of thought views conventional and improper hydrogen bonds as very similar in nature. As a representative example, Scheiner and co-workers have shown in a thorough study that improper and normal H-bond formation leads to similar changes in the remote parts of the H-bond acceptor, [39] and

that there are no fundamental distinctions between the mechanism of formation of improper and normal H-bonds.[36] This is consistent with the results of AIM ("Atoms-In-Molecules")[40] analysis of Cubero et al. who found no essential differences between electron density distributions for normal and blue-shifted hydrogen-bonds.[41] Several other studies which concentrate on the importance of electrostatic contributions to H-bonding and the effect of the electric field on C–H bond length support this conclusion. Earlier studies of Dykstra and co-workers were able to predict the nature of H-bonding (blue or red-shift) based on electrical moments and polarization of H-bond donors.[42] Recently, Dannenberg and co-workers have shown that at small electric fields "electron density from the hydrogen moves into the C–H bond" shortening and strengthening it",[43] whereas Hermansson has modeled the electric field of H-bond acceptor with a highly accurate "electrostatic potential derived point charges" and concluded that the reasons for the blue-shift is "the sign of the dipole moment derivative with respect to the stretching coordinate combined with electronic exchange overlap at moderate and shorter H-bonded distances."[44] In a very recent paper, Li et al. suggested that C–H bond shortening in blue-shift H-bonding is a result of repulsive (Pauli) steric interactions between the two molecules which balance the attractive (electrostatic) forces at the equilibrium geometry.[45] Qian and Krimm analyzed the dynamic properties of the H-bond donor group, with particular emphasis on the force on the bond resulting from "the interaction of the external electric field created by the proton acceptor atom with the permanent and induced dipole derivatives of the X-H bond." They concluded that the effect of the electric field is more complicated such that "when the field and dipole moments are parallel, the bond lengthens, as in the case of OH···O, when the field and dipole derivative are antiparallel, as in the case of CH···O, the bond shortens."[46] Finally, Alabugin et al proposed that the

X–H bond length in XH···Y hydrogen bonded complexes is controlled by a balance of two main factors acting in opposite directions. "X–H bond lengthening" due to n(Y) →σ*(H-X) hyperconjugative interaction is balanced by "X–H bond shortening" due to increase in the ***s***-character and polarization of the X–H bond. When hyperconjugation dominates, X–H bond elongation is reflected in a concomitant red shift of the corresponding IR stretching frequency. When the hyperconjugative interaction is weak and the X-hybrid orbital in the X-H bond is able to undergo a sufficient change in hybridization and polarization, rehybridization dominates leading to a shortening of the X–H bond and a blue shift in the X–H stretching.[47] All these explanations are only meaningful for a particular case. There appears no uniform theory which can be explain all types of hydrogen bond, so the nature of blue shift is still under debated.

1. 4.5 The common methods used in studying CH···X hydrogen bond

1. 4.5.1 IR and NMR Spectroscopy

IR and NMR spectroscopy have both become standard methods to investigate CH···X weak hydrogen bonds in the condensed phase. Formation of a hydrogen bond affects the vibrational modes of the groups involved in several ways. For relatively simple systems, these effects can be studied quantitatively by IR spectroscopy. The frequency of the donor C–H stretching vibration (υ_{CH}) is best studied because it is quite easy to identify in absorption spectra, and like as in classic hydrogen bond system which in most cases sensitive to the formation of hydrogen bonds. The difference between the υ_{CH} value of free and hydrogen-bonded C–H groups, $\Delta\upsilon_{CH}$, increases systematically with decreasing H···X (or C···X) distance. In principle, the H···X stretching vibration is the most direct

spectroscopic indicator of hydrogen bonding.

In most hydrogen bonds several nuclei may be observed by NMR spectroscopy. In particular, the proton is increasingly deshielded with increasing hydrogen bond strength, which leads to ^{1}H downfield shifts that are correlated with the lengths of the CH···X hydrogen bond. Thus, NMR shift data can be used to estimate lengths of hydrogen bonds. Chemical constants and differences in the ^{1}H and ^{2}H signals in H/D exchange experiments can give additional information on CH···X bonds.

1.4.5.2 Atoms in molecules (AIM)

The precise mapping of the distribution of charge density in CH···X hydrogen-bonded systems is a classical topic in structural chemistry,[48] with a large number of individual studies reported.[49] Currently, Bader's quantum theory of atoms in molecules (AIM) is the most frequently used formalism in theoretical analyses of charge density.[40] Each point in space is characterized by a charge density $\rho(r)$, and further quantities such as the gradient of $\rho(r)$, the Laplacian function of $\rho(r)$, and the matrix of the second derivatives of $\rho(r)$ (Hessian matrix). The relevant definitions and the topology of $\rho(r)$ in a molecule or molecular complex can be best understood by means of "bond critical point" (BCP).

Different kinds of chemical bonds have different numerical properties at the BCP, such as different electron density ρ_{BCP} and different values of the Laplacian function. The electron density at the bond critical point (ρ_{BCP}) is higher in strong bonds than in weak ones. The values of ρ_{BCP} in H···X increases with increasing of CH···X hydrogen bond strength.

1. 4.5.3 Crystallography

The crystallographic method provides strong evidence for a weak CH···X hydrogen bond, especially when effects from the electronic substituent are supplied. Distance and angle parameters of the putative hydrogen-bonded atoms are used in evaluating the strength of the interaction.

1. 4.5.4 Theoretical calculation

Theoretical calculation of the improper, blue-shifting intermolecular H-bond is still the best way to determine the interaction energy and the most accurate techniques should be applied. For the most CH···X hydrogen bond complexes (except CH···π) the DFT method is good enough to calculate the interaction energy and predict the reasonable vibrational frequency and ^{1}H chemical shift which agree very well with the experimental observations. For the CH···π hydrogen bond, on the other hand, the DFT method gives a poor result due to its bad approximation of long-range exchange-correlation function, so the MP series or coupled-cluster method is the preferred choice to obtain the promising results.

1. 4.6 The Intramolecular CH···X hydrogen bond

It must be mentioned, however, that in addition to intermolecular H-bonds, intramolecular CH···X hydrogen bonds also exist, which are known to be important in molecular structures of many compounds. Characterization of the intramolecular weak hydrogen is not easy since the unperturbed characteristics are missing for comparison. In

the case of the intermolecular H-bond, we describe the formation of the H-bond comparing the bond characteristics (bond length, vibrational frequency, etc.) in the isolated systems and the hydrogen bonded system, which is impossible for the intramolecular CH···X hydrogen bond. The intramolecular H-bond is mostly studied in the liquid phase using the NMR spin-spin X–H coupling constants, which are decisive for the bond formation. In recently, a blue shift intramolecular CH···O hydrogen bond was observed by matrix-isolation infrared spectroscopy. The contraction of the C–H bond upon formation of the intramolecular CH···X contacts and blue shift were predicted from ab initio calculations. And also the Bader AIM analysis gives evidence about the formation of the CH···X intramolecular H-bond.

To better understand the role of multiple CH···π interactions, in chapter 3 we have investigated systematically the benzene complexes of propane, isobutane and several saturated cyclic compounds, namely cyclopropane, cyclobutane, cyclopentane, cyclohexane, cycloheptane, cyclooctane and bicyclo[2.2.2]octane, using high-level ab initio calculations. These hydrocarbon models are characterized by several "axial" hydrogens in close proximity. The geometrical features, interaction energies, binding properties and topological properties have been examined to gain further insight into the nature of CH···π interactions in this series of hydrocarbon–benzene complexes.

In chapter 4, we have systematically investigated the benzene complexes of cyclohexane, and its heterocyclic analogues, namely $C_5H_{10}O$, $C_4H_8O_2$, $C_3H_6O_3$, $C_5H_{10}S$, $C_4H_8S_2$, $C_3H_6S_3$, $C_5H_{11}N$, $C_4H_{10}N_2$, $C_3H_9N_3$, $C_5H_{11}P$, $C_4H_{10}P_2$, $C_3H_9P_3$, $C_5H_{12}Si$, $C_4H_{12}Si_2$, and $C_3H_{12}Si_3$, using high-level *ab initio* calculations to evaluate the magnitude of substitution effect and the relationship between interaction energy and number of substituent. Up to

three heteroatom (N, O, S, Si or P) substitutions were considered. In all cases, only complex with three axial C–H bonds perpendicular the π face of benzene considered. The geometrical features, interaction energies, charge transfer and topological properties were investigated to obtain the influence of heteroatom substitution on the strength of multiple CH···π complexes.

The intermolecular interaction of the natural amino acids is of special interest because it determines the functional specificity of proteins and polypeptides. Proline has a very special conformation among 20 natural amino acids. Its nitrogen atom is bonded to the aliphatic side chain forming the five member pyrrolidine ring. This cyclic conformation may interact with aromatic ring forming a strong complex by cooperative XH/π interaction. In addition, the high polar NH bond will also contribute to total interaction energy by substantial stronger NH···π interaction. In chapter 5, we present a high level *ab initio* study of pyrrolidine-2-carbaldehyd-cyclopentanecarbaldehyde-benzene and proline-benzene, proline-phenalanine complexes to investigate the magnitude of interaction energy in the amino acid complex and the directionality of such complex.

Recently, the CH···X hydrogen bond has attracted strong attention from researchers in chemists and biochemists because of its potential capacity in stabilizing structures of molecules and molecular assemblies. The majority of works focus mainly on the intermolecular CH···X interaction have been done. There are very few investigations on the types of intramolecular CH···X interaction. To gain further insight into the role of the CH···X (X = O, N, S and P) intramolecular interactions in the conformational properities of a series of molecules, in chapter 6, we have investigated the *gauche/trans* conformational equilibrium of disubstituted ethane XCH_2CH_2Y (X, Y= NMe_2, PMe_2,

OMe or SMe) using high-level G3(MP2) theory. Our main goal is to estimate the magnitude of the CH···X intramolecular interaction and their influence on the conformational preference.

In chapter 7, we examined in detail the role of the weak C–H···N hydrogen bond in the conformational stability of BPSDMBA and BPSTDA in the gas phase and in solution. In addition, we attempted to provide an estimate the bond strength of this weak C–H···N intramolecular hydrogen bond using the topological analysis based on the Bader's theory of atoms in molecules (AIM). Unexpectedly, we found that C–H···O and π-π interactions also play an important role in governing the conformational stability of these disulfone compounds.

1.5 References

1. Pimentel, G. C.; McClellan, A. L. *The Hydrogen Bond*. San Francisco: Freeman **1990**.
2. Hibbert, F.; Emsley, J. *Adv. Phys. Org. Chem*. **1990**, *26*, 255.
3. Desiraju, G. R.; Steiner, T. *The Weak Hydrogen Bond in Structural Chemistry and Biology,* Oxford University Press, Oxford, **1999**.
4. Jeffrey, G. A. *An Introduction to Hydrogen Bonding*, Oxford University Press, Oxford, **1997**.
5. Steiner, T.; Desiraju, G. R. *Chem. Commun*. **1998**, 891.
6. Scheiner, S. *Hydrogen Bonding. A Theoretical Perspective*, Oxford University Press, Oxford, **1997**.
7. Morokuma, K. *Acc. Chem. Res*. **1977**, *10*, 294.
8. Reed, A. E.; Curtiss, L. A.; Weinhold, F. *Chem. Rev.* **1988,** *88*, 899.
9. Coombes, D. S.; Price, S. L.; Willock, D. J.; Leslie, M. *J. Phys. Chem*. **1996**, *100***,** 7352.
10. Hobza, P.; Havlas, Z. *Chem. Rev*. **2000**, *100*, 4253.
11. Maes, G.; Smets, J.; Adamowicz, L.; McCarthy, W.; VanBael, M. K.; Houben, L.; Schoone, K. *J. Mol. Struct*. **1997**, *410-411*, 315.
12. Smets, J.; McCarthy, W.; Maes, G.; Adamowicz, L. *J. Mol. Struct*. **1999**, *476,* 27.
13. Glasstone, S. *Trans. Faraday Soc*. **937**,200.
14. Gordy, W. *J. Chem. Phys*. **1939**, *7*, 163.
15. Allerhand, A.; Schleyer, P. R. *J. Am. Chem. Soc*. **1963**, *85*, 1715.
16. Dulmage, W. J. ; Lipscomb, W. N. *Acta Crystallogr*. **1951**, *4*, 330.

17. Shallcross, F. V.; Carpenter, G. B. *Acta Crystallogr*. **1958**, *11*, 490.

18. Green, R. D. *Hydrogen Bonding by C–H Groups*. London: Macmillan. **1974**.

19. Dougill, M. W.; Jeffrey, G. A. *Acta Crystallogr***. 1953**, *6,* 831.

20. Jones, G. P.; Cornell, B. A.; Horn, E.; Tiekink, E. R. T. *J. Spectrosc. Res*. **1989**, *19*, 715.

21. Kodama, Y.; Nishihata, K.; Nishio, M.; Nakagawa, N. *Tetrahedron Lett.* **1977**, 2105.

22. Takahashi, H.; Tsuboyama, S.; Umezawa, Y.; Honda, K.; Nishio, M. *Tetrahedron* **2000***, 56*, 6185, and references therein.

23. Umezawa, Y.; Nishio, M. *Bioorg. Med. Chem*. **1998**, *6*, 493.

24. Nishio, M. *Cryst. Eng. Comm*. **2004**, *6*, 130.

25. Burley, S. K.; Petsko, G. A. *FEBS Lett*. **1986**, *203*, 139.

26. Desiraju, G. R.; *Crystal engineering*. *The design of organic solids*; Elsevier: Amsterdam, **1989**.

27. Ciunik, Z.; Jarosz, S. *J. Mol. Struct*. **1998**, 442.

28. Braga, D.; Grepioni, F.; Desiraju, G. R. *Chem. Rev*. **1998**, *98,* 1375.

29. Desiraju, G. R. *J. Chem. Soc., Dalton Trans*. **2000**, 3745.

30. Buděšínský, M.; Fiedler, P.; Arnold, Z. *Synthesis* **1989**, 858.

31. Keshavarz, K. M.; Cox, S. D.; Angus, R. O.; Wudl, F. *Synthesis* **1988**, 641.

32. Boldeskul, I. E.; Tsymbal, I. F.; Ryltsev, E. V.; Latajka, Z.; Barnes, A. J. *J. Mol. Struct*. **1997**, *436*, 167.

33. Hobza, P.; Sÿ pirko, V.; Selzle, H. L.; Schlag, E. W. *J. Phys. Chem. A* **1998**, *102*, 2501.

34. Hobza, P.; Sÿ pirko, V.; Havlas, Z.; Buchhold, K.; Reimann, B.; Barth, H. D.;

Brutschy, B. *Chem. Phys. Lett.* **1999**, *299*, 180.

35. Hobza, P.; Havlas, Z. *Chem. Phys. Lett*. **1999**, *303*, 447.

36. Gu, Y.; Scheiner, S. *J. Am. Chem. Soc.* **1999**, *121*, 9411.

37. Van der Veken, B. J.; Herrebout, W. A.; Szostak, R.; Shchepkin, D. N.; Havlas, Z.; Hobza, P. *J. Am. Chem. Soc*. **2001**, *123,* 12290.

38. Tsuzuki, S. ; Honda, K. ; Uchimaru, T. ; Mkami, M. ; Tanabe, K. *J. Am. Chem. Soc.* **2000**, *122*, 3746.

39. Scheiner, S.; Kar, T. *J. Phys. Chem. A* **2002**, *106*, 1784.

40. Bader, R. W. F. Atoms *in Molecules. A Quantum Theory*; Oxford University Press: Oxford, U.K., **1990.**

41. Cubero, E.; Orozco, M.; Hobza, P.; Luque, F. J. *J. Phys. Chem. A* **1999**, *103*, 6394.

42. Parish, C. A.; Dykstra, C. E. *J. Phys. Chem.* **1993**, *97*, 9374.

43. Masunov, A.; Danenberg, J. J.; Contreras, R. H. *J. Phys. Chem. A* **2001**, *105*, 4737.

44. Hermansson, K. *J. Chem. Phys.* **1993**, *99*, 861.

45. Li, X.; Liu, L.; Schlegel, H. B. *J. Am. Chem. Soc.* **2002**, *124*, 9639.

46. Qian, W.; Krimm, S. *J. Phys. Chem. A* **2002**, *106*, 6628.

47. Alabugin, I. V.; Maanoharan, M.; Peabody, S.; Weinhold, F. *J. Am. Chem. Soc.* **2003**, *125*, 5973.

48. Coppens, P. *X-Ray Charge Densities and Chemical Bonding*, Oxford University Press, Oxford, **1997.**

49. Macchi, P. ; Iversen, B. ; Sironi, A. ; Chakoumakos, B. C. ; Larsen, F. K. *Angew. Chem. Int. Ed*. **2000***, 39*, 2719.

Chapter 2 Theoretical Methodology

2.1 The Schrödinger Equation

Quantum mechanics[1] is based on Schrödinger equation:

$$H|\Psi\rangle = E|\Psi\rangle, \tag{2.1}$$

where here H is the Hamiltonian operator[2] for a system consisting of nuclei and electrons, Ψ is the wavefunction known as the eigenfunction and E is the energy of the system known as the eigenvalue. The Hamiltonian operator is a sum of the kinetic and potential energy terms of the system.

$$H = T + V \tag{2.2}$$

The Hamiltonian operator for a system with N electrons and M nuclei is

$$H = -\sum_{i=1}^{N}\frac{1}{2}\nabla_i^2 - \sum_{A=1}^{M}\frac{1}{2M_A}\nabla_A^2 - \sum_{i=1}^{N}\sum_{A=1}^{M}\frac{Z_A}{r_{iA}} + \sum_{i=1}^{N}\sum_{j>i}^{N}\frac{1}{r_{ij}} + \sum_{A=1}^{M}\sum_{B>A}^{M}\frac{Z_A Z_B}{R_{AB}} \tag{2.3}$$

In the above equation, M_A is the ratio of the mass of nucleus A to the mass of the electron, Z_A is the atomic number of nucleus A. The Laplacian operators ∇_i^2 and ∇_A^2 involve differentiation with respect to the coordinates of the ith electron and the Ath nucleus.

$$\nabla^2 = \frac{d^2}{dx^2} + \frac{d^2}{dy^2} + \frac{d^2}{dz^2} \tag{2.4}$$

The first term in Eq. 2.3 is the operator for the kinetic energy of the electrons; the second term is the operator for the kinetic energy of the nuclei; the third term represents the Coulomb attraction between electrons and nuclei; the fourth and fifth terms represent the repulsion between electrons and between nuclei, respectively.

2.2 Approximations Used to Solve the Schrödinger Equation

It is impossible to obtain an exact solution to the Schrödinger equation for any system except the hydrogen atom. Therefore a number of approximations are incorporated to solve the Schrödinger equation. The key approximations are as follows:

1. The Born-Oppenheimer Approximation,
2. The One-Electron Approximation,
3. The Linear Combination of Atomic Orbital (LCAO) Approximation.

2.2.1 The Born-Oppenheimer Approximation[2]

One of the most important approximations relating to applying quantum mechanics to molecules is known as the Born-Oppenheimer (BO) approximation.[2] According to this approximation, one can consider the electrons in a molecule to be moving in a field of fixed nuclei because the nuclei are much heavier than the electrons (eg. even a H nucleus weighs nearly 2000 times what are electron weighs). Therefore, Ψ can be approximated as a product of electronic and nuclear wavefunctions.

$$\Psi = \Psi_{elec}\Psi_{nucl} \tag{2.5}$$

The electronic wavefunction, Ψ_{elec} can be obtained by assuming the electrons to be moving in a field of fixed nuclei and the nuclear wavefunction, Ψ_{nucl} can be obtained by assuming the nuclei to be moving in an average electronic field.

Upon applying the Born-Oppenheimer approximation to Eq. 2.3 the second term representing the kinetic energy of the nuclei can be removed from consideration of the electronic energy and the fifth term representing the repulsion between the nuclei

becomes a constant. As a result, any constant added to an operator adds only to the operator eigenvalues but has no effect on the operator eigenfunctions. Therefore, Eq. 2.3 becomes

$$H_{elec} = -\sum_{i=1}^{N} \frac{1}{2}\nabla_i^2 - \sum_{i=1}^{N}\sum_{A=1}^{M} \frac{Z_A}{r_{iA}} + \sum_{i=1}^{N}\sum_{j>i}^{N} \frac{1}{r_{ij}}, \tag{2.6}$$

where H_{elec} is known as the electronic Hamiltonian, i.e. Hamiltonian describing the motion of N electrons in a field of M point charges. Solution of the electronic Schrödinger equation,

$$H_{elec}\Psi_{elec} = E_{elec}\Psi_{elec}, \tag{2.7}$$

gives the electronic wavefunction, Ψ_{elec} and the electronic energy, E_{elec}. The electronic wavefunction,

$$\Psi_{elec} = \Psi_{elec}\left(\{r_i\};\{R_A\}\right), \tag{2.8}$$

describes the motion of the electrons or represents the molecular orbitals and the electronic energy,

$$E_{elec} = E_{elec}\left(\{R_A\}\right), \tag{2.9}$$

represents the energies of the molecular orbitals. The electronic wavefunction and electronic energy obtained by solving the electronic Schrödinger equation depends explicitly on the electronic coordinates and depends parametrically on the nuclear coordinates. Parametric dependence means that, for different arrangements of the nuclei, Ψ_{elec} is a different function of the electronic coordinates. The total energy of a system with fixed nuclei is given by

$$E_{tot} = E_{elec} + \sum_{A=1}^{M}\sum_{B>A}^{M} \frac{Z_A Z_B}{R_{AB}}. \tag{2.10}$$

Eqs. 2.8 to 2.10 constitute the electronic problem. If one has solved the electronic problem, it is possible to solve for the motion of nuclei as well by using the same assumption as that used to solve the electronic problem. Since the electrons move much faster than the nuclei, it is a reasonable approximation to replace the electronic coordinates in Eq. 2.3 by their average values, averaged over the electronic wavefunction. This then generates a nuclear Hamiltonian (H_{nucl}) for the motion of the nuclei in an average electronic field.

$$H_{nucl} = -\sum_{A=1}^{M} \frac{1}{2M_A} \nabla_A^2 + \left\langle -\sum_{i=1}^{N} \frac{1}{2} \nabla_i^2 - \sum_{i=1}^{N} \sum_{A=1}^{M} \frac{Z_A}{r_{iA}} + \sum_{i=1}^{N} \sum_{j>i}^{N} \frac{1}{r_{ij}} \right\rangle + \sum_{A=1}^{M} \sum_{B>A}^{M} \frac{Z_A Z_B}{R_{AB}}$$

$$= -\sum_{A=1}^{M} \frac{1}{2M_A} \nabla_A^2 + E_{elec}\left(\{R_A\}\right) + \sum_{A=1}^{M} \sum_{B>A}^{M} \frac{Z_A Z_B}{R_{AB}}$$

$$= -\sum_{A=1}^{M} \frac{1}{2M_A} \nabla_A^2 + E_{tot}\left(\{R_A\}\right) \qquad (2.11)$$

The total energy $E_{tot}\left(\{R_A\}\right)$ provides a potential for the nuclear motion. Therefore, the nuclei in the framework of the Born-Oppenheimer approximation move on a potential energy surface obtained by solving the electronic problem. Solving the nuclear Schrödinger equation,

$$H_{nucl} \Psi_{nucl} = E \Psi_{nucl} , \qquad (2.12)$$

gives the nuclear wavefunction Ψ_{nucl} which describes the rotation, vibration and translation of a molecule and the energy E which is a sum of the rotational, vibrational and translational energy of a molecule.

2.2.2 The One-Electron Approximation

By using the BO approximation to the Schrödinger equation helps to separate this complex Schrödinger equation into two parts, namely the electronic (Eq. 2.8) and nuclear (Eq. 2.12) Schrödinger equations. The electronic wavefunction, Ψ_{elec}, is a function of the spatial coordinates of all the *n* electrons and it would be easier to solve the electronic Schrödinger equation if we assume Ψ_{elec} as a product of *n* one-electron wavefunctions:

$$\Psi_{elec}(1,2,...,n) = \Psi_1(1)\Psi_2(2)...\Psi_n(n), \tag{2.13}$$

where $\Psi_i(i)$ is a function of only the three dimension coordinates of the i^{th} electron. Now the Hamiltonian operator can be expressed as a sum of one-electron operators. The Hamiltonian can be written as a function of zero, one and two electron terms:

$$H_0 = e^2 \sum_{\alpha<\beta} \sum_{\alpha<\beta} \frac{Z_\alpha Z_\beta}{R_{\alpha\beta}} \tag{2.14}$$

$$H_1 = \sum_{i=1}^{n} \left(\frac{\hbar^2}{2m} \nabla_i^2 - \sum_{\alpha} \frac{e^2 Z_\alpha}{r_{\alpha i}} \right) = \sum_{i=1}^{n} h_i(i) \tag{2.15}$$

$$H_2 = \sum_{i<j} \sum_{i<j} \frac{e^2}{r_{ij}} \tag{2.16}$$

Where H_0, H_1 and H_2 correspond to the Hamiltonians which are function of zero, one and two electrons, respectively. H_0 is a constant since the nuclei are considered to be stationary and H_1 presents no obstacle to the separation of variables since it is a function of one-electron terms. But the H_2 operator will cause a problem in separating the Hamiltonian into a sum of one-electron operators. It can be simplified by simply ignoring the H_2 operator. For example, let us consider a three electron system and construct its Schrödinger equation using a product wavefunction.

$$H\Psi(1,2,3) = E\Psi(1,2,3) \tag{2.17}$$

$$\left[h_1(1) + h_1(2) + h_1(3)\right]\phi_1(1)\phi_2(2)\phi_3(3) = \left(\varepsilon_1 + \varepsilon_2 + \varepsilon_3\right)\phi_1(1)\phi_2(2)\phi_3(3)$$

After dividing the above equation by $\phi_1(1)\phi_2(2)\phi_3(3)$ the equation will become :

$$\frac{1}{\phi_1(1)}h_1(1)\phi_1(1) + \frac{1}{\phi_2(2)}h_1(2)\phi_2(2) + \frac{1}{\phi_3(3)}h_1(3)\phi_3(3) = \varepsilon_1 + \varepsilon_2 + \varepsilon_3 \tag{2.18}$$

And involves three independent one-electron Schrödinger equations:

$$h_1\phi_1 = \varepsilon_1\phi_1 \tag{2.19}$$

$$h_1\phi_2 = \varepsilon_2\phi_2 \tag{2.20}$$

$$h_1\phi_3 = \varepsilon_3\phi_3 \tag{2.21}$$

Since h_1 is the same in all the three equations, one only need is to solve one equation. Therefore it is quite simple to solve the Schrödinger equation by neglecting the two electron terms. However, the two electron terms are so important in the molecular energy expression that their omission would lead to an unreliable result. Hence, the two electrons terms should take into account at the separated Hamiltonian. Considered a two electron system and the product wavefunction of which would be

$$\Psi_1(1)\Psi_2(2)$$

The above product wavefunction is surely not antisymmetric. However, an antisymmetric linear combination of the above wavefunction

$$N\left[\Psi_1(1)\Psi_2(2) - \Psi_1(2)\Psi_2(1)\right]$$

is antisymmetric (N is a normalization constant) with respect to the exchange of two electrons. This wavefunction includes only the spatial coordinates of the electrons. It is necessary to include the spin coordinates as well. Therefore the one-electron

wavefunction can be written as a product of one-electron orbital Ψ and one-electron spin η functions:

$$\phi_i = \Psi_i \eta_1 \tag{2.22}$$

Rewriting the above antisymmetric wavefunction by including the spin-orbit functions:

$$N\left[\phi_1(1)\phi_2(2) - \phi_1(2)\phi_2(1)\right]$$

So it is very straightforward to obtain an antisymmetric wavefunction for any system by writing the complete spin-orbital wavefunction in the form of a determinant. For a two-electron system:

$$N\begin{vmatrix}\phi_1(1) & \phi_1(2)\\ \phi_2(1) & \phi_2(2)\end{vmatrix} = N\left[\phi_1(1)\phi_2(2) - \phi_1(2)\phi_2(1)\right] \tag{2.23}$$

and for an *n*-electron (including the normalization constant):

$$\Phi \equiv \frac{1}{\sqrt{n!}}\begin{vmatrix}\phi_1(1) & \cdots & \phi_1(n)\\ \vdots & & \\ \phi_n(1) & \cdots & \phi_n(n)\end{vmatrix} \tag{2.24}$$

This determinant is known as a *Slater determinant*. Now let us assume that each electron moves in a field of all other electrons, i.e., each electron experiences an average field of all other electrons. This would mean that each electron is formally independent of all the other electrons. This is known as the *independent particle model*. This model behaves computationally as a one-electron model, even though in practice the effective field depends on all the electrons; i.e., for the calculation of the effective potential, we should know the states of all the electrons. Due to this interdependence, the equation has to be solved by an iterative procedure. The quality of the model depends on how well the effective one-electron potential approximates the real two-electron potential:

$$\sum_{i<j}^{n}\sum_{i<j}^{n}\frac{e^2}{r_{ij}} \rightarrow \sum_{i}^{n} V_1^{eff}(i)\,, \tag{2.25}$$

where $V_1^{eff}(i)$ depends on all the electrons except the i^{th} electron. Now the Hamiltonian can be expressed as

$$H \cong \sum_{i=1}^{n}\left[h_1(i) + V_1^{eff}(i)\right] = \sum_{i=1}^{n} F(i) \tag{2.26}$$

and

$$F(i)\phi_i = \varepsilon_i \phi_i \tag{2.27}$$

The one-electron wavefunction ϕ_i can be used to construct the many-electron determinant wavefunction Φ and the energy ε_i can be used to determine the energy *E*, of the system.

2.2.3 The Linear Combination of Atomic Orbital (LCAO) Approximation

In the LCAO approximation, a molecular orbital can be constructed by a linear combination of one-electron basis functions, usually the atomic orbitals (AOs) which are normally centered on each nucleus,

$$\Psi = \sum_{\mu}^{AO} C_{\mu}^{i} \chi_{\mu}\,. \tag{2.28}$$

C_{μ}^{i} is the coefficient of the μ th atomic orbital χ_{μ} in the *i*th MO.[3] The LCAO approximation provides us an efficient approach to obtain a trial linear variational function to describe the MOs in a molecule. The orbital coefficients are the variational parameters of the quantum mechanical calculations and their best values will give the optimum calculated energy.

2.3 The Variation Method

The *variational principle* is the basis for the variational determination of a wavefunction. The variational principle states that the expectation value or average value of the energy for an approximate wave function always lies above or equal to the exact solution of the Schrödinger equation for the same Hamiltonian operator[4]. This means that if we have a wave function that contains adjustable parameters and we adjust them to minimize the expectation value of the energy, then we are approaching the exact result.

Assume the ground state energy[5] of the system be E_0 with the corresponding wavefunction Ψ_0, and let Ψ be an arbitrary function, the expectation value of energy with the trial wavefunction Ψ can be expressed as

$$E = \frac{\langle \Psi | H | \Psi \rangle}{\langle \Psi | \Psi \rangle} \tag{2.29}$$

where the denominator is required for normalization. As stated above, according to the variation theorem for any Ψ it is true that $E_0 \le E$ and equality holds only if $\Psi = k\Psi_0$ (and $|k| = 1$). In order to find the ground-state energy of the system, we have to minimize Eq. 2.29. To achieve this, we have to select a set of known basis functions $\{\phi_n\}$, express the trial wavefunction, Ψ, as a linear combination of these, and substitute the result into Eq. 2.29:

$$E = \frac{\left\langle \left(\sum_i c_i \phi_i \right) | H | \left(\sum_j c_j \phi_j \right) \right\rangle}{\left\langle \sum_i \sum_j c_i \phi_i | c_j \phi_j \right\rangle} \tag{2.30}$$

On expanding the above equation, we get

$$E = \frac{\sum_i \sum_j c_i^* c_j \langle \phi_i | H | \phi_j \rangle}{\sum_i \sum_j c_i^* c_j \langle \phi_i | \phi_j \rangle} \quad (2.31)$$

where

$$\langle \phi_i | H | \phi_j \rangle = H_{ij} \quad \text{(Coulomb Integral)} \quad (2.32)$$

and

$$\langle \phi_i | \phi_j \rangle = S_{ij} \quad \text{(Exchange Integral).} \quad (2.33)$$

By substituting Eq. 2.32 and 2.33 into Eq. 2.31, we get

$$E = \frac{\sum_i \sum_j c_i^* c_j H_{ij}}{\sum_i \sum_j c_i^* c_j S_{ij}} \quad (2.34)$$

In order to determine the minimum value of E, we have to calculate the $\frac{\partial E}{\partial c_i}$ partial derivative for each c_i and set it equal to zero. This results in the following set of linear equations:

$$c_1(H_{11} - S_{11}E) + c_2(H_{12} - S_{12}E) + \cdots = 0$$

$$c_1(H_{21} - S_{21}E) + c_2(H_{22} - S_{22}E) + \cdots = 0 \quad (2.35)$$

or more briefly:

$$\sum_j c_j \left(H_{ij} - ES_{ij}\right) = 0 \qquad (i = 1, 2, \ldots) \qquad (2.36)$$

This equation can also be written in the matrix form:

$$[\mathbf{H} - E\mathbf{S}]\mathbf{c} = 0, \qquad (2.37)$$

which has a trivial solution ($\boldsymbol{c}$ = 0) and also a non-trivial solution $|\mathbf{H} - E\mathbf{S}| = 0$. This determinant is called the *secular determinant*. The solutions of the resulting polynomial, E_0, E_1, E_2,…, E_k… are the energy eigenvalues of the system. Once the value of $\boldsymbol{c}$ is known, the trial wavefunction can be written as:

$$\Psi = \sum_{i=1}^{k} c_i \phi_i . \qquad (2.38)$$

2.4 The Hartree-Fock Method

The Hartree-Fock (HF)[5] or self-consistent field (SCF) calculation scheme is a self-consistent iterative *variational* procedure to calculate the Slater determinant (or the molecular orbitals which it is made of) for which the expectation value of the electronic molecular Hamiltonian is minimum. Whilst it calculates the exchange energy exactly, it does not include the effect of electron correlation. The procedure is named after Douglas Hartree, who devised the self-consistent field method, and V. A. Fock, who demonstrated the rigour of Hartree's method and reformulated it into the matrix form used today.

based on Eqs. (2.14) - (2.16), the total energy of a system can be expressed as

$$E = \langle \Phi | H | \Phi \rangle = \langle \Phi | H_0 | \Phi \rangle + \left\langle \Phi \left| \sum_{i=1}^{n} h_1(i) \right| \Phi \right\rangle + \left\langle \Phi \left| \sum_{i<j}^{n} \sum_{i<j}^{n} h_2(ij) \right| \Phi \right\rangle \qquad (2.39)$$

where Φ is the Slater determinant of the system under study, $h_1(i)$ is the one-electron operator and $h_2(ij) = \left(e^2/r_{ij}\right)$, the two-electron operator. We know that the determinant is simply the linear combination of product wavefunctions. Since the $h_1(i)$ operators affect only one function (the i^{th}) from such a product and $h_2(ij)$ affects only two (the i^{th} and j^{th}), a number of integrals will vanish from Eq. 2.54. After a long and strenuous derivation, we finally reach the following complex-looking expression of the total energy:

$$E = E_0 + \sum_{i=1}^{n} \left\langle \phi_i(i) \middle| h_1(i) \middle| \phi_i(i) \right\rangle$$

$$+ \sum_{i<j}^{n} \sum_{i<j}^{n} \left[\left\langle \phi_i(i)\phi_j(j) \middle| h_2(ij) \middle| \phi_i(i)\phi_j(j) \right\rangle - \left\langle \phi_i(i)\phi_j(j) \middle| h_2(ij) \middle| \phi_i(j)\phi_j(i) \right\rangle \right]$$

$$= E_0 + \sum_{i=1}^{n} \left\langle \phi_i(i) \middle| h(i) \middle| \phi_i(i) \right\rangle + \frac{1}{2} \sum_{i=1}^{n} \sum_{j=1}^{n} \left\langle \phi_i(i)\phi_j(j) \middle| h_2(ij)\left(1 - P_{ij}\right) \middle| \phi_i(i)\phi_j(j) \right\rangle \quad (2.40)$$

We have replaced $\sum_{i<j}^{n}\sum_{i<j}^{n}$ term by $\frac{1}{2}\sum_{i=1}^{n}\sum_{j=1}^{n}$ in Eq. 2.53. This is because the first term of the double sum (the *Coulomb interaction*) and the second term (the *exchange interaction*) are equal and cancel out if *i*=*j*. This is why the $V_1^{eff}(i)$ potential indeed describes the interaction of an electron with the field of *n*-1 other electrons. For finding the minimum of the energy expression (refer the appendix for derivation) described by Eq. 2.53, we have to follow the conditions $\left\langle \phi_i \middle| \phi_j \right\rangle = \partial_{ij}$ with the parameters ε_{ij}, and add them to the above equation. Following this procedure, we obtain the following much simpler equations:

$$F(i)\phi_i = \sum_j \varepsilon_{ij}\phi_j \qquad i = 1,2,...,n \quad (2.41)$$

where *n* is the number of electrons and the *Fock operator*, $F(i)$, has the following form:

$$F(i) = h_1(i) + \sum_{j=1}^{n} \left\langle \phi_j(j) \middle| h_2(ij)\left(1 - P_{ij}\right) \middle| \phi_j(j) \right\rangle . \qquad (2.42)$$

The equations in (2.54) are called the *Hartree-Fock* (abbreviated as HF) *equations* (there are n equations). We can also write them in the form of matrix:

$$F\phi = \phi\varepsilon = F\left(\phi_1\phi_2 ... \phi_n\right) = \left(\phi_1\phi_2 ... \phi_n\right) \begin{pmatrix} \varepsilon_{11} & \varepsilon_{12} & \cdots & \varepsilon_{1n} \\ \varepsilon_{21} & \cdots & & \\ \vdots & & & \\ \varepsilon_{n1} & \cdots & & \varepsilon_{nn} \end{pmatrix}, \qquad (2.43)$$

where ϕ is a row vector and ε is a square matrix. Since the latter is symmetric, it can be made diagonal using similarity transformation. Using the appropriate transformation matrix, $\mathbf{Q}$, the HF equation can be written as:

$$F\underbrace{\phi \times \mathbf{Q}}_{\phi'} = \underbrace{\phi}_{\phi'}\underbrace{\mathbf{Q}\mathbf{Q}^{-1}\varepsilon\mathbf{Q}}_{\varepsilon'} = F\phi' = \phi'\varepsilon' , \qquad (2.44)$$

which has the component

$$F(i)\phi_i = \varepsilon_i\phi_i \qquad i = 1,2,...,n \qquad (2.45)$$

These eigenvalue equations are called *canonical Hartree-Fock equations*. We notice that the Fock operator, F remains unchanged, whereas, the individual functions, ϕ_j, are altered after the similarity transformation. It can be easily proved (refer to the appendix for the proof) that similarity transformation does not change the value of any determinant. Since the individual functions, ϕ_j, have no physical meaning, unlike the determinant Φ,

there is no harm in performing a similarity transformation in order to transform the original HF equations into the canonical HF equations, which are much easier to handle.

It is obvious from Eq. 2.55 that the Fock operator, F, itself contains the ϕ_i functions that are to be evaluated. Therefore, the HF equation has to be solved *iteratively*. First we choose a series of one-electron functions ϕ_1^0, ϕ_2^0, ϕ_n^0, construct an initial Fock operator (F_0), and by solving the HF equations we obtain the new series ϕ_1^1, ϕ_2^1, ϕ_n^1. We then construct a new F^1 from the ϕ_1^1, ϕ_2^1, ϕ_n^1 one-electron functions. This procedure is repeated until convergence has been reached. In other words, a *self-consistent field* (SCF)[6] is reached and the algorithm is, therefore, called the *SCF procedure*.

2.4.1 Restricted Hartree-Fock Method

A restricted Hartree-Fock calculation is commonly used for closed-shell systems. It forces each electron pair in a molecule to occupy a single molecular orbital (MO). RHF treatment of a closed-shell system will therefore result in all doubly occupied MOs, whereas, that of an open-shell system will result in both singly and doubly occupied MOs (Figure 1). In RHF treatment, the ground state energy[7] for a closed-shell system can be written as:

$$E = 2\sum_{i=1}^{N/2}\varepsilon_i - \sum_{i=1}^{N/2}\sum_{j=1}^{N/2}(2J_{ij} - K_{ij}) \qquad (2.46)$$

where N is the number of MOs, J_{ij} and K_{ij} are the Coulomb and exchange integrals, respectively. The corresponding n electron wavefunction is an eigenfunction of the total spin operator S^2.

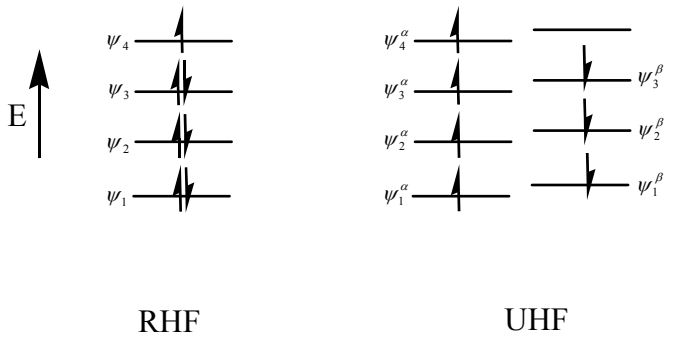

Figure 2.1 MOs for RHF and UHF theories

2.4.2 Unrestricted Hartree-Fock Method

Unrestricted Hartree-Fock calculations are commonly used for open-shell systems such as radicals. In this approach, different spatial orbitals are assigned to α and β electrons (Figure 1). Therefore, there are two distinct sets of molecular orbitals, which are defined by two sets of MO expansion coefficients:

$$\psi_i^\alpha = \sum_{\mu=1}^{N} c_{\mu i}^\alpha \phi_\mu ; \qquad \psi_i^\beta = \sum_{\mu=1}^{N} c_{\mu i}^\beta \phi_\mu \tag{2.47}$$

The coefficients $c_{\mu i}$ are varied independently, leading to the UHF generalization of the Roothaan-Hall equation, the Pople-Nesbet equations:

$$\sum_{\upsilon=1}^{N} (F_{\mu\upsilon}^\alpha - \varepsilon_i^\alpha S_{\mu\upsilon}) c_{\upsilon i}^\alpha = 0 ; \tag{2.48}$$

$$\sum_{\upsilon=1}^{N}(F_{\mu\upsilon}^{\beta}-\varepsilon_i^{\beta}S_{\mu\upsilon})c_{\upsilon i}^{\beta}=0\,,\qquad \mu=1,2,...,N \tag{2.49}$$

If we assume N_α and N_β are the total number of spatial orbitals for α and β spins, then the HF ground state energy[8] using unrestricted spin orbitals can be written as:

$$E=\sum_{i=1}^{N_\alpha}\varepsilon_i^{\alpha}+\sum_{i=1}^{N_\beta}\varepsilon_i^{\beta}+\frac{1}{2}\sum_{i=1}^{N_\alpha}\sum_{j=1}^{N_\alpha}(J_{ij}^{\alpha\alpha}-K_{ij}^{\alpha\alpha})+\frac{1}{2}\sum_{i=1}^{N_\beta}\sum_{j=1}^{N_\beta}(J_{ij}^{\beta\beta}-K_{ij}^{\beta\beta})+\sum_{i=1}^{N_\alpha}\sum_{j=1}^{N_\beta}J_{ij}^{\alpha\beta} \tag{2.50}$$

The UHF method is capable of providing a qualitatively correct description of bond dissociation, and it is mathematically more straightforward than RHF for open-shell systems. One of the major drawbacks of the UHF method is that the resulting wavefunction is not always an exact eigenfunction of the total spin operator $<S^2>$, and it may be contaminated by states of higher spin multiplicity. The true eigenvalue of $<S^2>$ is $S(S+1)$, where S is the total electronic spin of the wavefunction, and the degree of contamination is reflected in the amount by which $<S^2>$ (UHF) exceeds $S(S+1)$.

2.5 The Perturbation Method

Perturbation theory works on the idea that if we know the answer to one problem we can work out an answer to a closely related problem. Perturbation theory offers another method for finding quantum mechanical wavefunctions. It is especially suited to problems that are similar to model or ideal situations differing in only some small way, which is the perturbation. In perturbation theory, the Hamiltonian for any problem is partitioned into two or more parts. The first part is one for which the eigenfunctions and eigenvalues are known, while everything else represents the perturbation. This first part and the associated

eigenfunctions and eigenvalues are distinguished in notation by a zero superscript. Assume the Schrödinger equation for the model system is written as

$$H^{(0)}\Psi^{(0)} = E^{(0)}\Psi^{(0)}, \tag{2.51}$$

then the Schrödinger equation of the true system can be expressed as

$$H\Psi = E\Psi \text{ , where } H = H^{(0)} + \lambda V \tag{2.52}$$

Here, V is the potential representing the difference between the two systems and λ is a dimensionless parameter, the *perturbation parameter*. If we can describe the true system as a small perturbation of the model, Ψ and E will not be very different from $\Psi^{(0)}$ and $E^{(0)}$, and both can be expressed using powers of λ:

$$\Psi = \Psi^{(0)} + \lambda\Psi^{(1)} + \lambda^2\Psi^{(2)} + \ldots \tag{2.53}$$

$$E = E^{(0)} + \lambda E^{(1)} + \lambda^2 E^{(2)} + \ldots \tag{2.54}$$

To simplify the mathematics, we choose the perturbed wavefunctions to be orthogonal to $\Psi^{(0)}$. By inserting the proceeding two equations into Eq. 2.40, we obtain

$$\begin{aligned}&\left(H^{(0)} + \lambda V\right)\left(\Psi^{(0)} + \lambda\Psi^{(1)} + \lambda^2\Psi^{(2)} + \ldots\right)\\ &= \left(E^{(0)} + \lambda E^{(1)} + \lambda^2 E^{(2)} + \ldots\right)\left(\Psi^{(0)} + \lambda\Psi^{(1)} + \lambda^2\Psi^{(2)} + \ldots\right).\end{aligned} \tag{2.55}$$

Collecting the powers of λ, leads to:

$$\begin{aligned}&H^{(0)}\Psi^{(0)} + \lambda\left[V\Psi^{(0)} + H^{(0)}\Psi^{(1)}\right] + \lambda^{(2)}\left[V\Psi^{(1)} + H^{(0)}\Psi^{(2)}\right] + \ldots\\ &= E^{(0)}\Psi^{(0)} + \lambda\left[E^{(1)}\Psi^{(0)} + E^{(0)}\Psi^{(1)}\right] + \lambda^2\left[E^2\Psi^{(0)} + E^{(1)}\Psi^{(1)} + E^{(0)}\Psi^{(2)}\right] + \ldots\end{aligned}. \tag{2.56}$$

This equation can only be satisfied for an arbitrary value of λ if the coefficients for different powers of λ are the same:

$$\begin{aligned}
&H^{(0)}\Psi^{(0)} = E^{(0)}\Psi^{(0)} \\
&V\Psi^{(0)} + H^{(0)}\Psi^{(1)} = E^{(1)}\Psi^{(0)} + E^{(0)}\Psi^{(1)} \\
&V\Psi^{(1)} + H^{(0)}\Psi^{(2)} = E^{(2)}\Psi^{(0)} + E^{(1)}\Psi^{(1)} + E^{(0)}\Psi^{(2)} \\
&\vdots \\
&V\Psi^{(k-1)} + H^{(0)}\Psi^{(k)} = \sum_{i=0}^{k} E^{(k-i)}\Psi^{(i)}
\end{aligned} \tag{2.57}$$

Depending on the power of λ we truncate this expression. We refer to them as the first, second, …, etc. order of perturbation. First-order perturbation theory delivers $\Psi^{(1)}$ and $E^{(1)}$, while we obtain $\Psi^{(2)}$ and $E^{(2)}$ at the second order.

Let us first examine the first-order equations. By multiplying from the left with $\Psi^{(0)}$ and integrating over all space, we get

$$\left\langle \Psi^{(0)} \middle| V \middle| \Psi^{(0)} \right\rangle + \left\langle \Psi^{(0)} \middle| H^{(0)} \middle| \Psi^{(1)} \right\rangle = E^{(1)} \left\langle \Psi^{(0)} \middle| \Psi^{(0)} \right\rangle + E^{(0)} \left\langle \Psi^{(0)} \middle| \Psi^{(1)} \right\rangle . \tag{2.58}$$

The second term of this equation can be written as

$$\left\langle \Psi^{(0)} \middle| H^{(0)} \middle| \Psi^{(1)} \right\rangle = \left\langle H^{(0)}\Psi^{(0)} \middle| \Psi^{(1)} \right\rangle = E^{(0)} \left\langle \Psi^{(0)} \middle| \Psi^{(1)} \right\rangle = 0 . \tag{2.59}$$

The first term of the right-hand side of this equation is $E^{(1)}$, while the second term is zero due to the orthogonality condition. Therefore, the first-order energy correction is

$$E^{(1)} = \left\langle \Psi^{(0)} \middle| V \middle| \Psi^{(0)} \right\rangle . \tag{2.60}$$

Since the perturbation operator V and $\Psi^{(0)}$ are known, $E^{(1)}$ can be calculated without having to determine the perturbed wavefunction. Of course, we need this wavefunction to determine the higher-order energy corrections.

$$\begin{aligned} E^{(2)} &= \left\langle \Psi^{(0)} \middle| V \middle| \Psi^{(1)} \right\rangle \\ &\vdots \\ E^{(k)} &= \left\langle \Psi^{(0)} \middle| V \middle| \Psi^{(k-1)} \right\rangle \end{aligned} \tag{2.61}$$

and the true energy of the system is

$$E = E^{(0)} + \sum_{i=1}^{\infty} \lambda^i \left\langle \Psi^{(0)} \middle| V \middle| \Psi^{(i-1)} \right\rangle . \tag{2.62}$$

$\Psi^{(1)}$ can be expressed as follows:

$$\Psi^{(1)} = \sum_i \frac{\left\langle \Psi_i^{(0)} \middle| V \middle| \Psi^{(0)} \right\rangle}{E^{(0)} - E_i^{(0)}} \Psi_i^{(0)} . \tag{2.63}$$

The conclusion from all of this is that if we only require the perturbed energy to the first-order, it is sufficient to know the unperturbed wavefunction of the given state. In contrast, if we are after the perturbed wavefunction, we need to know all the eigenfunctions of the unperturbed system. By inserting, Eq. 2.63, into the second-order energy expression (Eq. 2.61), we can calculate $E^{(2)}$. In a similar way we can go on to $\Psi^{(2)}$, and so on.

Inspecting the denominator of expression (Eq. 2.63), it appears that only states energetically close to $E^{(0)}$ contribute appreciably to the true energy of the system. On the other hand, we might argue that the sheer numbers of higher-lying states might affect the

results. However, it can be proved that many of these higher states vanish from the numerator. To estimate the zero or nonzero value of an integral, e.g., $\left\langle \Psi_i^{(0)} \middle| V \middle| \Psi^{(0)} \right\rangle$, we recall our knowledge of group theory. The result of an integration of a function from $-\infty$ to $+\infty$ is zero if the function is antisymmetric and nonzero if it is symmetric. Therefore, if the product function $\Psi_i^{(0)} V \Psi^{(0)}$ is totally symmetric, the integration gives a nonzero result. In this case, the direct product $\Gamma^{(i)} \otimes \Gamma^{(pert)} \otimes \Gamma^{(0)}$ must contain the totally symmetric species. In other words, if the distortion picked up by the system has the same symmetry as the disturbing perturbation, the close-in energy state indeed plays a dominant role.

Another important question that arises is whether the perturbation series (Eq. 2.53) converges. In most practical cases, it does converge well (although it cannot be taken for granted). An important shortcoming of the perturbation theory is that it is not variational; i.e., perturbation theory does not provide an upper bound to the energy of the system. It is reasonable to expect, however, that by including the higher-energy terms, we may improve the quality of the results.

2.6 Electron Correlation

Because electrons repel each other according to Coulomb's law, there is a tendency for them to keep out of each other's way**.** In Hartree-Fock theory, this instantaneous electron-electron repulsion is replaced by the repulsion of each electron with an average electron charge cloud. This approximation introduces an error in the wavefunction and the energy. The error in energy is called the total correlation energy. The error in the total energy is about 1 eV per electron pair in a bond or lone pair. This correlation between the

motion of electrons is referred to as “electron correlation”. Thus, the HF method provides an inadequate treatment of the correlation between the motions of electrons within a molecular system, especially that arising between electrons of opposite spins. It however, accounts for the correlation between the motions of electrons of same spin. This correlation is termed as exchange correlation and is automatically taken into account by the antisymmetry requirement of the wavefunction.

The difference between HF energy and the exact (for a simplified non relativistic Hamiltonian) energy of a system is referred to as “correlation energy”. Correlation energy is small compared to the total energy but it is of the same order of magnitude as the quantities of chemical interest. Any method which goes beyond SCF in attempting to treat electron correlation properly is known as an electron correlation method (despite the fact that HF theory does include some correlation effects) or a post-SCF method.

Most ab initio methods dealing with electron correlation are based on the HF reference wavefunction. Almost all the post-SCF methods, such as, configuration interaction (CI), coupled cluster (CC), multi-reference configuration interaction (MRCI), multi-configuration self-consistent field (MCSCF) and complete active space self-consistent field (CASSCF), use one of the following approaches to improve upon the HF wavefunction:

a) Optimizing only the coefficients of the Slater determinants.

b) Optimizing both the coefficients of the Slater determinants and the coefficients of the one-electron wavefunctions forming the Slater determinant.

Approach a) is the basic idea behind all the CI methods. The Hartree-Fock wavefunction, ψ_{HF} , is only one of the $N!/(N-n)!n!$ possible arrangements (or configurations) of n electrons in the N spin orbitals. In this approach, all other determinantal wavefunctions are derived from the reference HF wavefunction by substitution of occupied spinorbitals by virtual spinorbitals. This substitution is actually the excitation of electrons from the occupied orbitals to the unoccupied or virtual orbitals. Depending on the number of electrons excited, we have singly-excited configurations, doubly-excited configurations and so on. These excited configurations are often abbreviated as singles, doubles, and so forth. The full CI wavefunction is a linear combination of all single, double and multiple substitutions:

$$\psi = a_{HF}\psi_{HF} + \sum a_s \psi_s \tag{2.64}$$

The above expression represents a mixing of all possible electronic configurations of the molecules, all of which have some probability of being attained according to the laws of quantum mechanics. A full CI method is the most complete non-relativistic treatment possible within the limitations imposed by the basis set. As the basis set becomes more and more flexible, the results of a full CI treatment approaches the exact solution of the non-relativistic, Born-Oppenheimer approximated, Schrödinger equation. The full CI method has the advantage of being well defined, size-consistent (energy of well separated molecules is equal to the sum of energies of individual molecules) and variational (provides an upper bound to energy). Because of the enormous amount of computation time required to perform a full CI calculation, it is practically impossible to treat molecules with more than a few heavy atoms.

Therefore, limited CI methods, such as, CIS, CID, CISD are used in which the CI series is truncated at a given level of substitution. For example, in the CISD method, the wavefunction is composed of only single and double excitation terms along with the reference HF determinant. Similarly, a CID wavefunction is composed of determinants resulting from only double excitations and the reference HF determinant. The most severe disadvantage of these limited CI methods is that they are not size-consistent.[9] To overcome this deficiency, the quadratic configuration interaction (QCI) method was developed. Corresponding to CID and CISD methods, are the QCID and QCISD methods. QCISD(T) is the QCI method obtained by adding triplet substitutions to QCISD in an iterative manner. Coupled cluster (CC) methods were also developed to correct the size-consistency problem of limited CI methods. The CCD, CCSD and CCSD(T) methods[10,11] include the double, single and double, single, double and triple excitations, respectively. CC methods are size-consistent but they are not variational and they are computationally less efficient than the limited CI methods.

Approach b) is the basic idea behind multi-configuration self-consistent field (MCSCF) method and the complete active space self-consistent field (CASSCF) method.

Another electron correlation method which is developed to improve upon the HF wavefunction is the Møller-Plesset perturbation theory. In this approach, electron interaction is treated as a perturbation to the sum of one-electron Hamiltonians. If the perturbation correction to energy is truncated at the second, third, fourth or fifth order, the method is known as MP2[12], MP3[13,14], MP4[15] and MP5[16] respectively.

2.7 Basis Set

A basis set is a mathematical function (basis function). The molecular orbitals Ψ_i in a Hartree-Fock treatment are expressed as a linear combination of a pre-defined set of one-electron functions or N nuclear-centered functions known as basis functions ϕ_μ $(\mu = 1,2,...,N)$,

$$\Psi_i = \sum_{\mu=1}^{N} c_{\mu i}\phi_\mu \tag{2.65}$$

Basis sets assign a group of basis functions to each atom within a molecule to approximate its orbitals. The following two types of basis functions are most widely used: (1) Slater-type functions and (2) Gaussian-type functions.

The Slater-type orbitals (STOs) are characterized by the exponential factor $\exp(-\xi r)$ and are represented by the following expression:

$$\phi_i = N_j(x,y,z)\exp(-\xi r) \tag{2.66}$$

STOs provide a very good representation of atomic orbitals because they possess a cusp at the nucleus. It is, however, very difficult to evaluate the two-electron integrals using STOs.

Gaussian-type functions (GTFs) are characterized by the exponential factor $\exp(-\alpha r^2)$ and are represented by the following expression:

$$\phi_i = N_j(x,y,z)\exp(-\alpha r^2) \tag{2.67}$$

GTFs lack the proper cusp behavior of the STOs as the distance between the nucleus and electrons approaches zero and they die off quickly at large distances. Even though the GTFs do not represent atomic orbitals as well as STOs, they are widely used because the evaluation of two-electron integrals is much easier using the GTFs. Due to the ease of calculating two-electron integrals with GTFs, most ab initio electronic structure programs use GTFs rather than STFs as basis functions. In order to provide an improved description, the individual basis functions in a Gaussian basis set are often taken as a linear combination of GTFs

$$\phi_\mu = \sum_k d_{\mu k} g_k \tag{2.68}$$

where the coefficients $d_{\mu k}$ are fixed and the individual functions g_k are all of the same type. Such basis functions ϕ_μ are known as "contracted Gaussians" and the individual functions g_k are known as "primitives". A basis function consisting of a single Gaussian function is referred to as "uncontracted". A brief description of various types of basis set is given below.

2.7.1 Minimal Basis Sets

A minimal basis set is the one which contains the minimum number of basis functions needed for each atom, while maintaining the overall spherical symmetry. Minimal basis set use fixed atomic-type orbitals. For instance, the "STO-KG" basis set is a minimal basis set which approximates the expansion of Slater-type atomic orbitals

(STOs) by taking a linear combination of K gaussian functions. The commonly used STO-KG minimal basis set is STO-3G[17,18] which uses three gaussian primitives (3G) per basis function. "STO" stands for Slater-type orbitals and the STO-3G basis set approximates the Slater-type atomic orbitals using three gaussian primitives. An example of the atomic orbitals required by a minimal basis set for any theoretical calculation with carbon and hydrogen atoms is shown below.

H: 1s

C: 1s, 2s, $2p_x$, $2p_y$, $2p_z$

2.7.2 Split Valence Basis Sets

A basis set has to be very flexible in order to be able to provide a realistic description of atomic orbitals. To increase the flexibility of a basis set, one has to increase its size and the simplest way of doing this is to increase the number of basis functions on each atom. A basis set obtained by doubling all the functions of a minimal basis set is referred to as a "double-zeta" basis set. An example of a double-zeta basis set is the Dunning-Huzinaga basis set (D95), in which all the molecular orbitals are formed by a linear combination of two different functions for each atomic orbital.

A much simpler way of extending a basis set is to just double the valence functions of a minimal basis set. Such a basis set is known as a "split valence" basis set in general and a "double split valence" basis set in particular. The commonly used double split valence basis sets are 3-21G[19-21] and 6-31G[22,23] basis set. A 3-21G basis set is formed

by taking a linear combination of three GTO's to form the core orbitals and the valence orbitals are split into two parts, formed by taking a linear combination of two and one GTO's for the inner and outer parts respectively. For example, hydrogen and carbon atoms using a double split valence basis set are represented as follows:

H: 1s, 1s´

C: 1s, 2s, 2s´, $2p_x$, $2p_x$´, $2p_y$, $2p_y$´, $2p_z$, $2p_z$´

A triple split valence basis set, such as 6-311G, is formed by splitting the valence orbitals into three parts.

2.7.3 Polarized Basis Set

Split valence basis sets allow orbitals to change size, but do not allow them to change shape. Polarized basis sets remove this limitation by adding orbitals with angular momentum beyond what is required for the ground state to the description of each atom. For example, polarized basis sets add *p* functions to hydrogen atoms, *d* functions to carbon atoms and *f* functions to transition metals. The most commonly used polarized basis set, 6-31G(*d*) (also represented as 6-31G*) is formed by adding *d* functions to all the heavy atoms. The other commonly used basis set, 6-31G(*d,p*) (also represented as 6-31G**) is formed from the 6-31G(*d*) basis set by adding *p* functions to hydrogen atoms. In a similar manner, the 6-31G(*mdf, npd*) basis set is formed from the 6-31G basis set by adding *m* sets of *d* functions and one set of *f* function to heavy atoms and *n* sets of *p* functions and one set of *d* function to hydrogen and helium. For cases where the

description of hydrogen atoms is important, a set of *p* functions is usually added to hydrogen atoms.

2.7.4 Diffuse Basis Sets

Diffuse functions are larger-size versions of *s*-and *p*-type functions. They allow orbitals to occupy a larger region of space. Basis sets with diffuse functions are important for systems where electrons are relatively far from the nucleus: molecules with lone pairs, anions and other systems with significant negative charge, systems in their excited states, systems with low ionization potentials, description of absolute acidities, and so on. The 6-31+G(d) basis set is an example of a diffuse function basis set. It is formed from the 6-31G(d) basis set by incorporating a set of *s* and *p* diffuse functions to the heavy atoms.

In selecting a basis set, the number of expansion and the nature of the functions ϕ_i need to be considered. A limiting HF treatment would involve an infinite set of basis functions ϕ_i. This is clearly impractical in terms of the basis set expansion required to describe various properties satisfactorily. In general, a larger basis set, more accurately approximates the orbitals by imposing fewer restrictions on the location of electrons in space.

2.8 G3(MP2) Theory

The G3(MP2) theory[24] developed by Pople et al., is a general procedure based on ab initio molecular orbital theory for the accurate calculation of energies. In the G3(MP2)

approach, all the structures are optimized at the MP2(full)/6-31G(*d*) level using both the core and the valence electrons. Followed by the geometry optimization, a series of single point energy calculations are carried out at higher levels of theory. All the subsequent single point energy calculations include only the valence electrons in the treatment of electron correlation, i.e., frozen core (fc) approximation. The first high level calculation is performed at the quadratic configuration interaction level of theory with the 6-31G(*d*) basis set, i.e., QCISD(T)/6-31G(*d*). This energy is then modified by a series of corrections to obtain the total energy, $E_0[G3(MP2)]$

$$E_0[G3(MP2)] = QCISD(T)/6\text{-}31G(d) + \Delta E_{MP2} + \Delta E(SO) + E(HLC) + E(ZPE), \quad (2.69)$$

where ΔE_{MP2} is the correction at the second order Møller-plesset level[12] (MP2) given by

$$\Delta E_{MP2} = [E(MP2/G3MP2large)] - [E(MP2/6\text{-}31G(d))] \quad (2.70)$$

The G3MP2large basis set is the same as the G3large basis set used in the G3 theory, except that the core polarization functions are not included. $\Delta E(SO)$ is the spin-orbit correction and it is included only for the atomic species. The zero-point energy correction, $E(ZPE)$ is obtained from scaled HF/6-31G(*d*) frequencies. The frequencies are scaled by a factor of 0.8929. $E(HLC)$ is the "high-level correction" term which is added to take into account the remaining deficiencies in the energy calculation. $E(HLC)$ is given by

$$E(HLC) = -An_\beta - B(n_\alpha - n_\beta) \quad (2.71)$$

for molecules and by

$$E(HLC) = -Cn_\beta - D(n_\alpha - n_\beta) \quad (2.72)$$

for atoms and atomic ions, where n_α and n_β are the number of α and β valence electrons respectively, with $n_\alpha \geq n_\beta$. A, B, C and D are constants. For G3(MP2) theory, A=9.279 mhartrees, B=4.471 mhartrees, C=9.345 mhartrees and D=2.021 mhartrees. The average absolute deviation from experiment of G3(MP2) theory is 5.5 kJ mol^{-1} for energies and 5.0 kJ mol^{-1} for enthalpies.

2.9 Density Functional Theory (DFT)

Traditional methods in electronic structure, like Hartree-Fock theory are based on the complicated many-electron wavefunction. The main objective of density functional theory is to replace the many-body electronic wavefunction with the electronic density as the basic quantity. Whereas the many-body wavefunction is dependent on 3N variables, three spatial variables for each of the N electrons, the density is only a function of three variables and is a simpler quantity to deal with both conceptually and practically.

In 1964, Hohenberg and Kohn proved that the ground-state molecular energy, wavefunction, and all other molecular electronic properties are uniquely determined by the electron probability density $\rho(x, y, z)$, a function of only three variables.[25] Therefore, the ground-state energy E_0 is a functional of electron probability density ρ and can be written as $E_0 = E_0[\rho]$.

In the traditional quantum-chemical approach, one determines the wavefunction ψ first and then the electron probability density ρ by integrating ψ. The Hohenberg-Kohn theorem on the other hand tells us that if we know the ground-state electron density $\rho(x, y, z)$, then all the ground-state molecular properties can be calculated from it. It

however, does not tell us how to calculate E_0 from ρ or how to find ρ without first finding ψ. Later in 1965, Kohn and Sham[26] showed that the exact ground-state purely electronic energy E_0 of an n-electron system with ground-state electron probability density ρ can be written as

$$E_0 = -\frac{1}{2}\sum_{i=1}^{n}\left\langle \psi_i(1)\middle|\nabla_1^2\middle|\psi_i(1)\right\rangle - \sum_{\alpha}\int \frac{Z_\alpha \rho(1)}{r_{1\alpha}}dv_1 + \frac{1}{2}\iint \frac{\rho(1)\rho(2)}{r_{12}}dv_1 dv_2 + E_{XC}[\rho], \quad (2.73)$$

where $\psi_i(1)$ are the Kohn and Sham orbitals and $E_{XC}[\rho]$ is the exchange-correlation energy. Kohn-Sham also showed that the exact ground-state ρ can be found from ψ_i's, according to

$$\rho = \sum_{i=1}^{n}\left|\psi_i\right|^2 \quad (2.74)$$

The Kohn-Sham orbitals are obtained by solving the one-electron equations

$$\hat{F}_{KS}(1)\psi_i(1) = \varepsilon_{i,KS}\psi_i(1), \quad (2.75)$$

where the Kohn-Sham operator $\hat{F}_{KS}$ is given by

$$\hat{F}_{KS} \equiv -\frac{1}{2}\nabla_1^2 - \sum_{\alpha}\frac{Z_\alpha}{r_{1\alpha}} + \sum_{j=1}^{n}\hat{J}_j(1) + V_{XC}(1) \quad (2.76)$$

where $\hat{J}_j(1)$ is the Coulomb operator defined by

$$\hat{J}_j(1) = \int \left|\phi_j(2)\right|^2 \frac{1}{r_{12}}dv_2 \quad (2.77)$$

and V_{XC} is the exchange-correlation potential defined by

$$V_{XC} = \delta E_{XC}[\rho]/\delta\rho \tag{2.78}$$

The Hartree-Fock operator $\hat{F}$ for electron *m* in a molecule of *n*-electrons is given by

$$\hat{F} \equiv -\frac{1}{2}\nabla_m^2 - \sum_{\alpha}\frac{Z_\alpha}{r_{m\alpha}} + \sum_{j=1}^{n}\left[\hat{J}_j(m) - \hat{K}_j(m)\right] \tag{2.79}$$

This V_{XC} handles the effects of both exchange (antisymmetry) and electron correlation. The density functional theory (DFT) methods are self-consistent methods like the Hartree-Fock method.

The only problem with density functional methods is that the correct functional form of $E_{XC}[\rho]$ is not known and it is too complicated to be evaluated analytically. Therefore, numerical quadrature must be used which may lead to significant loss of precision. In practice E_{XC} is divided into two parts, exchange E_X and correlation E_C,

$$E_{XC} = E_X + E_C \tag{2.80}$$

2.9.1 Exchange Functionals

Listed below are some of the commonly used exchange functionals.

Exchange functional proposed by **Slater**[27]

$$E_X^{LDA}[\rho] = -\int \frac{3}{4}\left(\frac{3}{\pi}\right)^{\frac{1}{3}} \rho(r)^{\frac{4}{3}}\, dr \qquad (2.81)$$

The corresponding potential is

$$\varepsilon_X^{LDA}[\rho] = -\left(\frac{3}{\pi}\rho(r)\right)^{\frac{1}{3}} \qquad (2.82)$$

Becke's 1988 exchange functional (**B88**)[28]

$$\varepsilon_X^{B88}[\rho] = -\varepsilon_X^{LDA}[\rho]\left[1 - \frac{\beta}{2^{\frac{1}{3}} A_X}\frac{z^2}{1 + 6\beta z \sinh^{-1}(z)}\right] \qquad (2.83)$$

where

$$z = 2^{\frac{1}{3}}\frac{|\nabla\rho|}{\rho^{\frac{4}{3}}}, \qquad A = \frac{3}{4}\left(\frac{3}{\pi}\right)^{\frac{1}{3}} \qquad \text{and} \qquad \beta = 0.0042\,.$$

Perdew-Wang (PW91)[29,30] exchange functional

$$\varepsilon_X^{PW91} = \varepsilon_X^{LDA}(\rho)\left[\frac{1 + sa_1\sinh^{-1}(sa_2) + \left(a_3 + a_4 e^{-100s^2}\right)s^2}{1 + sa_1\sinh^{-1}(sa_2) + a_5 s^4}\right] \qquad (2.84)$$

where

$s = \dfrac{|\nabla\rho|}{\left(24\pi^2\right)^{\frac{1}{3}}\rho^{\frac{4}{3}}}$, a_1=0.19645, a_2=7.7956, a_3=0.2743, a_4=-0.1508 and a_5=0.004.

2.9.2 Correlation Functionals

Listed below are some of the commonly used correlation functionals.

Vosko, Wilk and Nusair correlation functional (**VWN**)[31]

$$\varepsilon_C^{VWN}[\rho]=\frac{A}{2}\left[\ln\frac{x}{X(x)}+\frac{2b}{Q}\tan^{-1}\frac{Q}{2x-b}-\frac{bx_0}{X(x_0)}\left(\ln\frac{(x-x_0)^2}{X(x)}+\frac{2(b+2x_0)}{Q}\tan^{-1}\frac{Q}{2x+b}\right)\right] \qquad (2.85)$$

where the functions x, X and Q are given by

$$x=r_s^{\frac{1}{2}},\quad r_s=\left(\frac{4\pi\rho}{3}\right)^{-\frac{1}{3}},\quad X(x)=x^2+bx+x,\quad Q=(4c-b^2)^{1/2}$$

and the constants are A = 0.0621814, x_0 = -0.409286, b = 13.0720 and c = 42.7198.

Lee, Yang and Parr correlation functional (**LYP**)[32]

$$\varepsilon_C^{LYP}[\rho]=-a\frac{1}{1+d\rho^{-\frac{1}{3}}}\left\{\rho+b\rho^{-\frac{2}{3}}\left[C_F\rho^{\frac{5}{3}}-2t_w+\frac{1}{9}\left(t_w+\frac{1}{2}\nabla^2\rho\right)\right]e^{-c\rho^{-\frac{1}{3}}}\right\} \qquad (2.86)$$

where

$$t_w=\frac{1}{8}\left(\frac{|\nabla\rho|^2}{\rho}-\nabla^2\rho\right),\quad C_F=\frac{3}{10}\left(3\pi^2\right)^{\frac{2}{3}},\quad a=0.04918,\ b=0.132,\ c=0.2533 \text{ and } d=0.349.$$

Perdew-Wang (**PW91**) correlation functional

$$V_C^{PW91}[\rho]=\varepsilon_C^{LDA}[\rho]+\rho H[\rho,s,t] \qquad (2.87)$$

where

$$H = \frac{\beta^2}{2\alpha}\ln\left[1+\frac{2\alpha}{\beta}\frac{t^2+At^4}{1+At^2+A^2t^4}\right]+C_{c0}\left[C_c(\rho)-C_{c1}\right]t^2e^{-100s^2} \qquad (2.88)$$

with

$$A = \frac{2\alpha}{\beta}\left[e^{\frac{2\alpha\varepsilon_C^{LDA}(\rho)}{\rho\beta^3}}-1\right]^{-1} \qquad (2.89)$$

s is the same as in PW91 exchange functional, and

$t = \frac{\left(\frac{\pi}{3}\right)^{\frac{1}{6}}}{4}\frac{|\nabla\rho|}{\rho^{\frac{7}{6}}}$, $\alpha = 0.09, \beta = 0.0667263212, C_{c0} = 15.7559, C_{c1} = 0.0035521$, and

$$C_c(\rho) = C_1 + \frac{C_2 + C_3 r_s + C_4 r_s^2}{1 + C_5 r_s + C_6 r_s^2 + C_7 r_s^3} \qquad (2.90)$$

with $C_1 = 0.001667$, $C_2 = 0.002568$, $C_3 = 0.023266$, $C_4 = 7.389\times10^{-6}$ $C_5 = 8.723$, $C_6 = 0.472$ and $C_7 = 0.07389$.

There are three different categories of DFT methods and they all differ in the way they handle $E_{XC}[\rho]$.

1) The **Local DFT methods** based on the local density approximation (LDA), approximates $E_{xc}[\rho]$ as

$$E_{XC}^{LDA}[\rho] = \int \varepsilon_{XC}^{LDA}[\rho(r)]\rho(r)dr \qquad (2.91)$$

For example, the S-VWN method which is a combination of Slater-type exchange functional and the VWN correlation functional parameterized on the homogenous electron gas.

2) The **Non-Local or Gradient-Corrected DFT methods** which contain gradient-corrected exchange and correlation functionals (e.g., B-LYP and B-P86 methods).

$$E_{XC}^{NL}[\rho] = \int \varepsilon_{XC}\left[\rho(r)|\nabla\rho(r)|\nabla^2\rho(r)\right]dr \qquad (2.92)$$

3) The **Hybrid DFT methods** contain a mixture of Hartree-Fock exchange energy and DFT exchange correlation energy. For example, B3LYP, B3P86 and B3PW91 methods. The three-parameter mixing scheme proposed by Becke in 1993 is[33]

$$E_{XC} = E_{XC}^{LDA} + a_0\left(E_X^{HF} - E_X^{LDA}\right) + a_X\Delta E_X^{B88} + a_C\Delta E_C^{non-local} \qquad (2.93)$$

The correlation functional Becke used in his original paper is PW91. The B3LYP functional incorporated in Gaussian 94[34] and Gaussian 98[35] suit of programs is

$$A * E_X^{Slater} + (1-A)E_X^{HF} + B * E_X^{Beck88} + E_C^{VWN} + C * \Delta E_C^{LYP} \qquad (2.94)$$

with A = 0.80, B = 0.72 and C = 0.81 obtained by fitting to G2 test set.

DFT is now a leading method for electronic structure calculations in solid state physics and quantum chemistry fields, especially the Hybrid DFT (for example B3LYP), in many cases, it gives quite satisfactory results. Despite the improvements in DFT, there are still difficulties in using density functional theory to properly describe intermolecular interactions, especially van der Waals forces (dispersion), or in calculations of the

aromatic interaction in biomolecules. Its poor treatment of dispersion renders DFT unsuitable (at least when used alone) for the treatment of systems which are dominated by dispersion (e.g. CH···π interaction) or where dispersion competes significantly with other effects (e.g. in biomolecules). The development of new DFT methods designed to overcome this problem, by alterations to the functional or by the inclusion of additive terms, is still a hot research topic.

2.10 Natural Bond Orbital (NBO) Analysis[36]

Natural Bond Orbitals (NBOs) are localized few-center orbitals ("few" meaning typically 1 or 2, but occasionally more) that describe the Lewis-like molecular bonding pattern of electron pairs (or of individual electrons in the open-shell case) in optimally compact form. More precisely, NBOs are an orthonormal set of localized "maximum occupancy" orbitals whose leading $N/2$ members (or N members in the open-shell case) give the most accurate possible Lewis-like description of the total N-electron density.

Natural Orbitals (NOs) are the unique orbitals chosen by the wavefunction itself as optimal for its own description. Mathematically, the NOs $\{\Theta_i\}$ of a wavefunction Ψ can be defined as the *eigen*orbitals of the first-order reduced density operator Γ,

$$\hat{\Gamma}\theta_k = q_k\theta_k \qquad (2.95)$$

which is formed by 'reducing' the wavefunction probability distribution to the single-particle level,

$$\hat{\Gamma} = N\int \psi(1,2,...,N)\psi^{*}(1',2,...,N)d\tau_2...d\tau_N \qquad (2.96)$$

and whose eigenorbitals are hence 'natural' to ψ itself. As shown by Löwdin[37] and others, rigorous quantum-mechanical questions involving subsystems of an *N*-particle system are best formulated in terms of reduced density operators. In particular, the squared probability amplitude $\left|\langle\psi(1,2,...N)|\phi(1)\rangle\right|^2$ that an electron of $\psi(1,2,...N)$ is 'in' orbital ϕ (i.e., the population of $\phi(1)$ in the wavefunction) is rigorously expressed, for any possible orbital ϕ, as

$$q_\phi = \left\langle \phi \middle| \hat{\Gamma} \middle| \phi \right\rangle \qquad (2.97)$$

The occupancies q_ϕ are intrinsically non-negative and limited by the Pauli exclusion principle, e.g., for spatial orbital $\phi(r)$,

$$0 \le q_\phi \le 2 \qquad (2.98)$$

(The analogous restriction $q_\phi \le 1$ applies to spin orbitals). The sum of occupancies q_k over any complete orthonormal set $\{\phi_k\}$ accounts for all *N* electrons,

$$\sum_k \left\langle \phi_k \middle| \hat{\Gamma} \middle| \phi_k \right\rangle = \sum_k q_k = Tr\{\hat{\Gamma}\} = N \qquad (2.99)$$

The Mulliken populations generally fail to satisfy the physical constraints (Eq. 2.97 and Eq. 2.98)

The chemist's idealized Lewis structure picture describes the *N/2* electron pairs as localized in one-centre (lone pair) or two-centre (bond) regions of the molecule. The natural bond orbital (NBO) algorithm[38,39] leads to an optimal set of one- and two-centre orbitals b_i that are in close correspondence with this picture. In effect, the algorithm searches the density matrix for the set of *N/2* localized Lewis-type lone pair and bond orbitals of near double occupancy that best describe the given wavefunction, with the residual weakly occupied non-Lewis-type antibonding and *Rydberg orbitals* representing small corrections to delocalization.

2.11 Computational Modelling of Solvation[40]

Most of chemical and biochemical reactions occur in solution, and the solvent can have a major effect on the position of chemical equilibrium and on reaction rates[41]. While gas phase predictions are appropriate for many purposes, they are inadequate for describing the characteristics of many molecules in solution. Indeed the properties of molecules and transition states can differ considerably between the gas phase and solution. For example, electrostatic effects are often much less important for species placed in a solvent with high dielectric constant than they are in the gas phase.

Description of solvation requires the application of both quantum chemical and statistical mechanical techniques. Using quantum chemical techniques, one can accurately derive the intermolecular forces of the system under consideration. Solvation can then be

modeled using statistical mechanical techniques or molecular dynamics simulations. Some of the important physical processes involved in solvation are as follows:

1) **Intermolecular forces between pairs of molecules:** The intermolecular forces are usually partitioned into electrostatic, polarization, dispersion and repulsion contributions.

2) **Many-body effects:** The effective force between pairs of molecules is influenced by the presence of neighboring molecules. A simple example of this arises due to molecular polarization; one molecule polarizes another, whose interaction with a third molecule is then affected.

2.11.1 Commonly Used Solvation Models

Some of the commonly used solvation models are as follows:

1) **Solvent/Solute Descriptor Models:** The descriptor models express an observed property γ as the sum $\gamma = \sum_i D_i d_i$, where the sum is over a selected list of molecular properties d_i of the solute (the solute descriptor) and D_i is the solvent's susceptibility to that property (the solvent descriptor). Some of the commonly used solvent descriptors include the solvent polarity, polarizability, Gutmann's hydrogen-bond donor number DN[42] and hydrogen-bond acceptor number AN of Mayer et al.[43]

2) **Statistical Models:** Statistical mechanics offers many techniques for the simplification of problems involving solute-solvent interactions. These usually

involve the introduction of a suitable analytical model for the solvent and yield solutions which relate the observed macroscopic properties to the microscopic properties of the solvent and solute.

3) **Molecular Simulations:** In these approaches the solvent is explicitly represented as individual molecules, allowing the most complete description of the solvent-solute interaction. Solvent effect studies via computer simulations often focus on the change in the geometry of the solute upon solvation; more subtle effects, such as solvation effects on the spectroscopy of the solute, are often studied through the use of models which express the property of interest as a function of the computed solvent structure.[44]

4) **The Supermolecule Approach:** This is the most sophisticated (and computationally demanding) approach and involves the explicit determination of the electronic wavefunction for both the solvent and the solute. A very successful scheme is the local density functional molecular dynamics approach of Car and Parrinello[45] that treats the electronic wavefunctions and liquid structure in a rigorous and sophisticated manner but is at present limited to sample sizes of the order of 32 molecules per unit cell to represent liquid water, for example.

5) **Reaction Field Models:** All the solvation studies in this thesis were carried out using the self-consistent reaction field (SCRF)[46-48] models based on Onsager's reaction field thoery.[49] In the reaction field models, the solvent molecules are represented by a polarizable continuum of uniform dielectric constant ε. The solute molecule is placed in a cavity in the solvent which becomes polarized. The induced solvent reaction field

then interacts with the charge distribution of the solute. There are a variety of reaction field models available and they all differ in the way they define the cavity and the reaction field. The simplest reaction field model is the **Onsager model** in which the solute occupies a fixed spherical cavity of radius a_0 within the solvent field. The solute dipole induces a dipole in the solvent medium and the electric field applied by the solvent dipole in turn interacts with the solute dipole, resulting in net stabilization. One of the major drawbacks of this model is that systems having zero dipole moment will not exhibit any solvent effect.

Another popular reaction field model is the **polarized continuum model** (**PCM**), developed by Tomasi. In the PCM model, the cavity is defined as the union of a series of interlocking atomic spheres. The effect of polarization of the solvent is computed by means of numerical integration rather than by an approximation to the analytical form used in the Onsager model. The reaction field models described above do not provide a realistic picture of solute-solvent interactions because of the assumption of a pre-defined shape such as a sphere or a set of overlapping spheres for the solute cavity. To overcome this shortcoming, isodensity surface models such as **isodensity polarized continuum model** (**IPCM**)[50] and **self-consistent isodensity polarized continuum model** (**SCIPCM**) were developed.

In the IPCM model, the cavity is defined as an isosurface of the total electron density of the solute molecule. This isodensity is determined by an iterative process in which an SCF cycle is performed and converged using the current isodensity cavity. The resultant wavefunction is then used to compute an updated isodensity surface, and

the cycle is repeated until the cavity shape no longer changes upon completion of the SCF.

A cavity defined as an isosurface and the electron density are necessarily coupled. The SCIPCM model was designed to take this effect fully into account. It includes the effect of solvation in the solution of the SCF problem. This procedure solves for the electron density which minimizes the energy including the solvation energy and which itself depends on the cavity which in turn depends on the electron density. In other words, the effects of solvation are folded into the iterative SCF computation rather than comprising an extra step afterwards. SCIPCM model thus accounts for the full coupling between the cavity and the electron density and includes coupling terms that IPCM neglects.

2.12 AIM Theory[51]

Atoms In Molecules (AIM)[51] theory proposed by Professor Richard F.W. Bader at McMaster University makes a link between quantum mechanics and standard chemical concepts such as an atom and a chemical bond. There is no explicit concept of an atom or a bond in the Schrödinger's equation. It is only concerned with particles (electrons and nuclei) in potential fields. However, a lot of the standard chemical knowledge is based on the atomic model. So on one hand we want to make use of the rigor and physically correct quantum mechanics in our calculations and on the other hand we want to have models that are easy to understand and related to conventional chemical intuition. AIM theory is unique in the sense that it provides a rigorous link between intuitive chemical concepts and quantum mechanics through analysis of the electron density $\rho(r)$ (r is a space

coordinate). The AIM theory provides the basis for a *representational front-end* to quantum mechanics where the *topology* of ρ(r) is described by a set of *critical points* (CPs). These CPs are found where ∇ρ(r) =0 where ∇ρ(r) is referred to as the gradient vector field. Such critical points are in a way the "most interesting" points in the scalar field and therefore also constitute a compressed version of the field. However, this is only as a first order Taylor expansion around the critical point. Obviously, in order to capture more of the information, higher derivatives need to be included. It should be mentioned that the ρ(r) is only one of several possible scalar fields that can be subjected to localizing critical points. Another important scalar field is the *Laplacian* of ∇ρ(r): $\nabla^2\rho(r)$. The CPs from this field satisfy $\nabla(\nabla^2\rho(r)) =0$ and provide links to important chemical concepts.

The gradient vector in a scalar field in a single point at r can be defined as:

$$\nabla\rho(r) = \frac{\partial\rho(r)}{\partial x}u_x + \frac{\partial\rho(r)}{\partial y}u_y + \frac{\partial\rho(r)}{\partial z}u_z \tag{2.100}$$

where u_x , u_y , u_z are three unit vectors. The electron density is a scalar field, like e.g. temperature distribution, since only a single number is associated with each point in 3D space. Now let us consider moving a small distance *ds* along the direction of ∇ρ(r).

Compute the gradient vector again to update the direction. By tracing the *path* indicated by ∇ρ(r) for infinitesimal small steps, we obtain a *gradient path*. Now consider starting this process for any point X, Y, Z in the scalar field and we will obtain the *gradient vector field*. Similar type of fields can also be seen in e.g. electrostatics where the curves are referred to as field lines. These are the lines where a positive charge would move if

released somewhere in the system. In general, the force acting on a particle can be written as F=-∇***V*** where ***V*** is the potential. However, the same interpretation is not valid for ∇ρ(r).

The critical points of the electron density distribution are associated with atomic nuclei, bonds, rings and cages. We will concentrate in particular on bond critical points (BCPs). The other critical points encountered are ring critical points (RCPs), cage critical points (CCPs) and the nuclear attractors (NA) for the nuclei. The BCP marks the boundary for the interatomic surface which topologically separates the different atoms into basins. These basins can be used to define the concept of an atom from the electron density. BCP is also located at the center of the interatomic surface. The BCP indicates the point of minimum electron density along the bond path from atom A to B. However, the BCP is a point of maximum electron density in the plane perpendicular to the bond path and constitutes therefore a 3D saddle point in the electron density. The nature of a CP can be determined from the Hessian matrix in that point:

$$H_{ij} = \frac{\partial^2 \rho(r)}{\partial x_i \partial x_j}, \qquad i \in \{1,2,3\} \tag{2.101}$$

for the three spatial dimensions ***x1,x2,x3***. To characterize the different types of CPs, two different measures derived from the Hessian can be used:

- The signature ( ) If λ_i are the eigenvalues of the Hessian, then the signature is defined as the sum of the *signs* of each eigenvalue:

$$S = \sum_{i=1}^{3} sign(\lambda_i) \tag{2.102}$$

- Rank (***r***) This is the number of non-zero eigenvalues of the Hessian.

If any of the eigenvalues are zero, it means that the region along this dimension is locally flat. A CP with rank less than 3 is topologically unstable and can bifurcate into a number of non-degenerate or stable rank 3CPs. This is an important part of how AIM theory can explain chemical reactions and transforms. Thus the coordinate pair (***r,s***)can be used to classify the types of CPs. In the process of finding these CPs the Poincar é-Hopf rule can be used to check the consistency of the results:

$$\mathbf{n-b+r-c=1} \tag{2.103}$$

Where **n** is the number of nuclei, **b** is the number of BCPs, **r** is the number of RCPs and **c** is the number of CCPs.

The bond critical point space

To describe the properties of a BCP in more detail, we need information in addition to the rank and the signature. Three parameters are very useful in this respect:

- The electron density **ρ(r)**
- The Laplacian ($\nabla_2\rho(\mathbf{r})$), which can be written as $\nabla_2\rho(\mathbf{r}) = \lambda_1 + \lambda_{2+} \lambda_3$

- The ellipticity, (ε) is defined as (λ_1 / λ_2) -1 which is always positive since $\lambda_1 < \lambda_2 < 0$. The -1 part is only included to make the ellipticity have a minimum in zero.

So what does the Laplacian in a BCP signify? The $\nabla_2\rho(r)$ determines which curvature dominates in the bonding zone. If $\nabla_2\rho(r) < 0$ then we have a *shared interaction* where charge is concentrated in the internuclear region. If $\nabla_2\rho(r) > 0$ then we have a *closed-shell interaction* where there is a charge *depletion* between the nuclei. It is possible to make a connection to Lewis acids and bases using the Laplacian. A Lewis acid is an electrophile and thus has $\nabla_2\rho(r) > 0$ whereas a Lewis base is a nucleophile and has $\nabla_2\rho(r) < 0$. Shared interactions are associated with covalent and polar bonds. Closed interactions are associated with ionic, hydrogen bonds, noble gas cluster and bonds in van der Waal molecules. The ellipticity ε can be best explained by looking at the following figure.

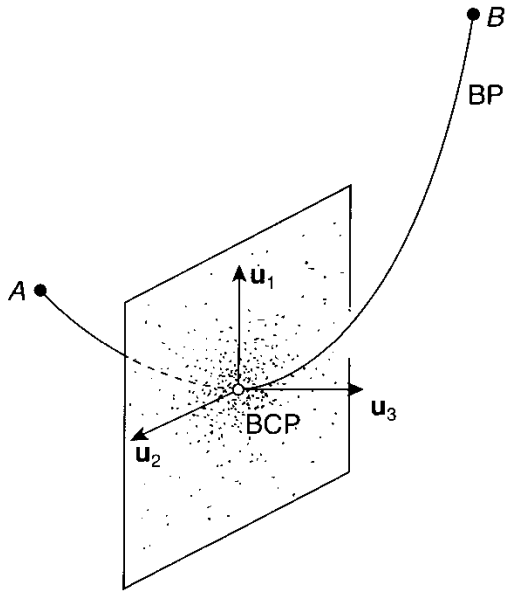

Figure 2.2 Representation of the local structure of the Hessian at the BCP.

Here is shown the plane perpendicular to the bond path (BP) between atoms A and B which is spanned by the two eigenvectors u_1 and u_2 (corresponding eigenvalues are $\lambda_1$and λ_2). u_3 is tangent on the BP and associated with the positive eigenvalue λ_3. The ratio λ_1 / λ_2 measures how much the bond is elongated along u1 direction compared to the u_2 direction. When this ratio is large, we have an elliptic structure that indicates a large π-character of the bond. When $\lambda_{1=} \lambda_2$ we have bond that is more cylindrical. The ellipticity can be used to detect *conjugation*. Formal double bonds involved in a conjugated system will tend to slightly decrease the ellipticity value. Formal single bonds will experience an increase. Similarly the ellipticity will also change in *hyperconjugation*, i.e. when double-bond character is induced in what formally is a single bond. An increase of the ellipticity of the single bond will be detected. In cases when the BCP is close to an RCP, there is a tendency for an increase in the ellipticity. This means that simply closing atoms into a ring, will increase the ellipticity. In spite of being a very powerful tool for measuring ``π -ness" in a bond, there are some exceptions. For instance, ethyne has an ellipticity of zero due to symmetry consideration in the triple bond yet we know it has a large amount of π character.

2.13 References

1. (a) E. Schrödinger, *Ann. Physik*, 1926, 79,361. (b) M. Born.; J. R. Oppenheimer, *Ann. Physik,* 1927,84, 457.
2. Szabo, A.; Ostlund, N. S. *Modern Quantum Chemistry: Introduction to Advanced Electronic Structure Theory*; Dover Pub. Inc. Mineola, New York, 1996.
3. Yamaguchi, Y.; Osamura, Y.; Goddard, J. D.; Schaefer, H. F. *A New Dimension to Quantum Chemistry: Analytic Derivative Methods in Ab Initio Molecular Electronic Structure Theory*; Oxford University Press, New York, 1994.
4. Dykstra, C. E. *Quantum Chemistry and Molecular Spectroscopy*; Prentice Hall, New Jersey, 1992.
5. D. R. Hartree, *Proc. Cambridge Phil. Soc*. **1928**, 24, 111.
6. J. C. Slater, *Phys. Rev*., **1930,** *35*, 210.
7. (a) Roothaan, C. C. J. *Rev. Mod. Phys.* **1960**, *32*, 179. (b) Binkley, J. S.; Pople, J. A.; Dobosh, P. A. *Mol. Phys.* **1974**, *28*, 1423.
8. Pople, J. A.; Nesbet, R. K. *J. Chem. Phys.* **1954**, *22*, 571.
9. Pople, J. A.; Head-Gordon, M.; Raghavachari, K. *J. Chem. Phys*. **1987**, *87*, 5968.
10. Purvis, G. D.; Bartlett, R. J. *J. Chem. Phys*. **1982**, *76*, 1910.
11. Hehre, W. J.; Radom, L.; Schleyer, P. v. R.; Pople, J. A. *Ab initio Molecular Orbital Theory*; John Wiley and Sons, New York, 1996.
12. Almloff, J.; Korsell, K.; Faegri, Jr., K. *J. Comp. Chem*. **1982**, *3*, 385.
13. Pople, J. A.; Binkley, J. S.; Seeger, R. *Int. J. Quantum Chem. Symp*. **1976**, *10*, 1.
14. Pople, J. A.; Seeger, R.; Krishnan, R. *Int. J. Quantum Chem. Symp*. **1977**, *11*, 149.
15. Krishnan, R.; Pople, J. A. *Int. J. Quantum Chem*. **1978**, *14*, 91.

16. Raghavachari, K.; Pople, J. A.; Replogle, E. S.; Head-Gordon, M. *J. Phys. Chem*. **1990**, *94*, 5579.

17. Hehre, W. J.; Stewart, R. F.; Pople, J. A. *J. Chem. Phys*. **1969**, *51*, 2657.

18. Collins, J. B.; Schleyer, P. v. R.; Binkley, J. S.; Pople, J. A. *J. Chem. Phys*. **1976**, *64*, 5142.

19. Binkley, J. S.; Pople, J. A.; Hehre, W. J. *J. Am. Chem. Soc*. **1980**, *102*, 939.

20. Gordon, M. S.; Binkley, J. S.; Pople. J. A.; Pietro, W. J.; Hehre, W. J. *J. Am. Chem. Soc*. **1982**, *104*, 2797.

21. Pietro, W. J.; Francl, M. M.; Hehre, W. J.; Defrees, D. J.; Pople, J. A.; Binkley, J. S. *J. Am. Chem. Soc*. **1982**, *104*, 5039.

22. Ditchfield, R.; Hehre, W. J.; Pople, J. A. *J. Chem. Phys*. **1971**, *54*, 724.

23. Hehre, W. J.; Ditchfield, R.; Pople, J. A. *J. chem.. Phys*. **1972**, *56*, 2257.

24. Curtiss, L. A.; Redfern, P. C.; Raghavachari, K.; Rassolov, V.; Pople, J. A. *J. Chem. Phys.* **1999**, *110*, 4703.

25. Hohenberg, P.; Kohn, W. *Phys. Rev. B* **1964**, *136*, 864.

26. Kohn, W.; Sham, L. J. *Phys. Rev. A* **1965**, *140*, 1133.

27. Slater, J.; *The Self-Consistent Field of Molecules and Solids: Quantum Theory of Molecules and Solids*; Vol. 4, McGraw-Hill, New York, 1974.

28. Becke, A. D. *Phys. Rev. A* **1988**, *33*, 3098.

29. Perdew, J. P.; Wang, Y. *Phys. Rev. B* **1992**, *45*, 13244.

30. Perdew, J. P.; Chevary, J. A.; Vosko, S. H.; Jackson, K. A.; Pederson, M. R.; Singh, D. J.; Fiolhais, C. *Phys. Rev. B* **1992**, *46*, 6671.

31. Vosko, S. H.; Wilk, L.; Nusair, M. *Can. J. Phys.* **1980**, *58*, 1200.

32. Lee, C.; Yang, W.; Parr, R. G. *Phys. Rev. B* **1988**, *37*, 785.

33. Becke, A. D. *J. Chem. Phys.* **1993**, *98*, 5648.

34. Frisch, M. J.; Trucks, G. W.; Schlegel, H. B.; Gill, P. M. W.; Johnson, B. G.; Robb, M. A.; Cheeseman, J. R.; Keith, T.; Petersson, G. A.; Montgomery, J. A.; Raghavachari, K.; Al-Laham, M. A.; Zakrzewski, V. G.; Ortiz, J. V.; Foresman, J. B.; Cioslowski, J.; Stefanov, B. B.; Nanayakkara, A.; Challacombe, M.; Peng, C. Y.; Ayala, P. Y.; Chen, W.; Wong, M. W.; Andres, J. L.; Replogle, E. S.; Gomperts, R.; Martin, R. L.; Fox, D. J.; Binkley, J. S.; Defrees, D. J.; Baker, J.; Stewart, J. P.; Head-Gordon, M.; Gonzalez, C.; and Pople, J. A. Gaussian 94 (Revision E.2), Gaussian, Inc., Pittsburgh PA, 1995.

35. Frisch, M. J.; Trucks, G. W.; Schlegel, H.B.; Scuseria, G. E.; Robb, M. A; Cheeseman, J. R.; Zakrzewski, V. G.; Montgomery, Jr. J. A.; Startmann, R. E.; Burant, J. C.; Dapprich, S.; Millam, J. M.; Daniels, A. D.; Kudin, K. N.; Strain, M. C.; Farkas, O.; Tomasi, J.; Barone, V.; Cossi, M.; Cammi, R.; Mennucci, B.; Pomelli, C.; Adamo, C.; Clifford, S.; Ochterski, J.; Petersson, G. A.; Ayala, P. Y.; Cui, Q.; Morokuma, K.; Malick, D. K.; Rabuck, A. D.; Raghavachari, K.; Foresman, J. B.; Cioslowski, J.; Ortiz, J. V.; Stefanov, B. B.; Liu, G.; Liashenko, A.; Piskorz, P.; Komaromi, I.; Nanayakkara, A.; Gonzalez, C.; Challacombe, M.; Gill, P. M. W.; Johnson, B.; Chen, W.; Wong, M. W.; Andres, J. L.; Gonzalez, C.; Head-Gordon, M.; Replogle, E. S.; and Pople, J. A. Gaussian 98 (Revision A.2), Gaussian, Inc., Pittsburgh PA, 1998.

36. Weinhold, F. *In Encyclopedia of Computational Chemistry;* Schleyer, P. V. R.; Allinger, N. L.; Kollman, P. A.; Clark, T.; Schaefer, H. F.; Gasteiger, J.; Scheiner, P. R., Eds., John Wiely & Sons, 1999, Vol 3, p1792.

37. Löwdin, P. O. *Phys. Rev*. **1955**, *97*, 1474.

38. Foster, J. P.; Weinhold, F. *J. Am. Chem. Soc*. **1980**, *102*, 7211.

39. Reed, A. E.; Weinhold, F. *J. Chem. Phys*. **1983**, *78*, 4066.

40. Bacskay, G. B.; Reimers, J. R. *In Encyclopedia of Computational Chemistry;* Schleyer, P. V. R.; Allinger, N. L.; Kollman, P. A.; Clark, T.; Schaefer, H. F.; Gasteiger, J.; Scheiner, P. R., Eds., John Wiely & Sons, 1999, Vol 4, p2620.

41. C. Reichardt, *Solvents and Solvent Effects in Organic Chemistry*, **1998**, VCH

42. Gutmann, V. *Coord. Chem. Rev*. **1976**, *18*, 225.

43. Mayer, U.; Gutmann, V.; Gerger, W. *Monatsh. Chem*. **1975**, *106*, 1235.

44. Comba, P.; Hambley, T. *Molecular Modelling of Inorganic Systems*; VCH, Weinheim, 1995.

45. Tuckerman, M.; Laasonen, K.; Sprik, M.; Parrinello, M. *J. Chem. Phys*. **1995**, *103*, 150.

46. Tapia, O.; Goscinski, O. *Mol. Phys*. **1975**, *29*, 1653.

47. Wong, M. W.; Frisch, M. J.; Wiberg, K. B. *J. Am. Chem. Soc*. **1991**, *113*, 4776.

48. Wong, M. W.; Wiberg, K. B.; Frisch, M. J. *J. Chem. Phys*. **1991**, *95*, 8991.

49. Onsager. L. *J. Am. Chem. Soc*. **1936**, *58*, 1486.

50. Foresman, J. B.; Keith, T. A.; Wiberg, K. B.; Snoonian, J.; Frisch, M. J. *J. Phys. Chem*. **1996**, *100*, 16098.

51. Bader R.F W. *Atoms in Molecules. A Quantum Theory*, Oxford University Press, Oxford, 1990.

Chapter 3 Saturated Hydrocarbon–Benzene Complexes: A Theoretical Study of Cooperative CH/π Interactions

3.1 Introduction

CH/π interaction, an attractive interaction between a C-H bond and an aromatic π system, has attracted strong recent interests.[1-4] This type of intermolecular force is almost ubiquitous in many fields of organic, inorganic, biochemical and material chemistry.[1,4] The CH/π interaction was first proposed by Nishio and co-workers to explain the preference of conformations in which bulky and phenyl groups are in close contact.[5] It is important to note that the acceptor of the CH/π interaction is not limited to an aromatic π system. Other unsaturated functional groups, such as C=C, C=O, etc, are also good candidates as CH/π acceptors.[1-4] During the last two decades, numerous experimental studies which support the existence of this noncovalent attraction have been reported.[4] In particular, the short contact between a C-H bond and a π system is observed in a very large number of crystals of organic molecules[6,7] peptides,[8] and proteins.[9] It is believed that the CH/π interaction is important in understanding many chemical phenomena such as conformational preference, crystal packing, host-guest complexation, and self-organization processes.[4] The importance of CH/π interaction for structures and properties of biological systems has also been reported.[1,8,9]

In recent years, several theoretical studies of simple benzene complexes have been carried out to evaluate the interaction energy of the CH/π interaction and to gain insight into the nature of the interaction.[10-15] The best calculation of methane–benzene complex

suggests that the CH/π bond strength is about 6 kJ mol^{-1}.[10b] In many organic molecules, there are several C-H protons oriented in such as way that multiple CH/π interactions can occur simultaneously with the π face of an aromatic system. Thus, it is intriguing to ask whether multiple CH/π interactions can interact in a cooperative manner. Recent elegant 2D solid-state NMR study has revealed that multiple CH/π interaction can cooperatively stabilize nanostructures entrapped as guests in channel formed by an aromatic host.[16] To better understand the role of multiple CH/π interactions, we have investigated systematically the benzene complexes (for all the complexes studied in this thesis, only the 1:1 complex is considered) of propane, isobutane and several saturated cyclic compounds, namely cyclopropane, cyclobutane, cyclopentane, cyclohexane, cycloheptane, cyclooctane and bicyclo[2.2.2]octane, using high-level ab initio calculations. These chosen hydrocarbon models are characterized by several "axial" hydrogens in close proximity. In particular, isobutane and cyclohexane have three axial C-H bonds parallel to each other, which readily interact with the π cloud of benzene. Methane– and ethane–benzene complexes have been examined previously, [10-15] but these systems were included in this study for purpose of comparison. The geometrical features, interaction energies, binding properties and topological properties will be examined to gain further insight into the nature of CH/π interactions in this series of hydrocarbon–benzene complexes.

3.2 Computational Methods

Dispersion interaction is important in the proper description of both the geometries and binding energies of CH/π complexes.[2,3,10b,11a,15b] As a consequence, both the

Hartree–Fock (HF) and density functional theory (DFT) methods grossly underestimated the binding energies of the complexes examined here. For instance, the HF and B3LYP interaction energies, corrected for basis set superposition error (BSSE), of isobutane–benzene complex (+0.3, and +1.0, kJ mol^{-1}, respectively) are considerably smaller the MP2 and CCSD(T) values (–4.1 and –2.1 kJ mol^{-1}, respectively) [Table 3.1]. In addition, a large basis set is required for proper description of the weak intermolecular CH/π complexes. Hence, geometry optimizations of the hydrocarbon–benzene CH/π complexes (**1**–**11**) were carried out at MP2/aug(d,p)-6-311G(d,p) level (without BSSE correction). The aug(d,p)-6-311G(d,p) basis set, proposed by Tsuzuki et al,[10b,17] corresponds to the 6-311G(d,p) basis set augmented with diffused *d* functions on carbon and diffuse *p* functions on hydrogen atoms (α_d(C) = 0.1565 and α_p(H) = 0.1875). Frequency analysis was performed at MP2/6-31G(d) level to evaluate zero-point energy (ZPE) correction and to determine the C-H frequency shift in the complex. Previous theoretical studies have established undoubtedly that a large basis set including multiple polarization functions and appropriate electron correlation are necessary to accurately evaluate the interaction energies of CH/π complexes.[2,3,10b,11a,15e] Thus, more reliable prediction of interaction (binding) energies were obtained via higher-level single-point calculations at the CCSD(T)[18] level in conjugation with a larger aug-cc-pVTZ basis set, obtained via additivity approximation at the MP2 level. Correction for basis set superposition error (BSSE), based on the counterpoise method,[19] was included in the final calculated interaction energy. Unless otherwise noted, the interaction energies reported in the text correspond to the CCSD(T)/aug-cc-pVTZ level including zero-point energy (MP2/6-31G(d), scaled by 0.967)[20] and BSSE corrections. NMR chemical shift

calculations were performed using the gauge-independent atomic orbital (GIAO) method.[21] Atomic charges were obtained using the natural bond orbital (NBO) approach, based on the MP2/aug(d,p)-6-311G(d,p) wavefunction.[22] Charge density analysis, based on Bader's theory of atoms in molecules (AIM)[23] was carried out using the MORPHY98 program[24] and the electrostatic potential map was generated using the MOLDEN program.[25] All other calculations were performed using the Molpro 2002,[26] Gaussian 98,[27] and Gaussian 03[28] programs.

3.3 Results and Discussion

3.3.1. Complex geometries

There are several important structural parameters which characterize a CH/π interaction, namely d_1, d_2 and α (see Scheme 3.1). O is the centre (centroid) of the benzene ring, while X represents the projection point of a C-H hydrogen on the molecular plane of benzene. Thus, d_1 corresponds to the non-bonded intermolecular distance, d_2 represents the distance of the projection point away from the benzene centre (O) and α is the CHX angle. Based on previous experimental and theoretical studies,[1-4] the characteristic properties of a typical CH/π interaction are: (1) the intermolecular distance d_1 is in the range 2.6–3.0 Å, (2) the C-H bond points close to the centre of an aromatic ring, and (3) the CHX angle (α) is close to linearity, and (4) the C-H bond length is shorten upon complexation, which leads to a higher C-H stretching frequency.

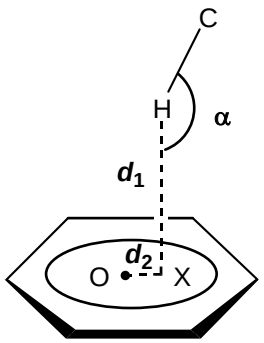

Scheme 3.1

The optimized geometries of all the hydrocarbon–benzene complexes (**1**–**11**) are shown in Fig. 3.1. Selected structural parameters, d_1, d_2 and α, are listed in Table 3.2. The most stable conformation of each complex favors multiple (2–4) CH/π contacts (except for methane and ethane complexes). This clearly demonstrates that several C-H groups of the hydrocarbon can interact with the π face of benzene in a cooperative manner. Let us consider in detail the various possible conformations of the cyclohexane–benzene complex. There are two types of C–H bonds in the chair form of cyclohexane: axial and equatorial. The three axial C–H bonds are parallel to each other. Furthermore, the dimension of these three axial hydrogens is similar to the size of the benzene ring. In other words, multiple CH/π contacts are feasible for benzene to interact with the axial hydrogens. Therefore, one would expect two possible modes of interaction between the cyclohexane and benzene: face-to-face and T-shape. In the first model, both molecules are oriented parallel to each other, with all three axial hydrogens directed toward the face of benzene. In the second model, only one equatorial C–H group is directed toward the centre of the benzene ring. Two different conformations were obtained for the face-to-face model of interaction: symmetrical (C_{3v}, **13**, Fig. 3.2) and asymmetrical (C_1, **8**, Fig. 3.1). In

the symmetrical structure, the 3 axial C–H bonds lie exactly perpendicular to three carbon atoms of benzene (**13**, Fig. 3.2). On the other hand, the asymmetrical structure (**8**) which has one C–H group directs toward to the centre of benzene ring and the other two C–H groups lie outside the benzene ring. The asymmetrical conformation is slightly more stable than the symmetrical form, by 1.0 kJ mol^{-1}. Since the potential energy surface is very flat, it is hard to confirm which one is the most stable form with certainty. Interaction of an equatorial C–H group of cyclohexane with benzene leads to a T-shape structure with one CH/π interaction (d_1 = 2.346 Å, d_2 = 0.094 Å and α = 159.2˚) close to the centre of benzene (C_1, **12**, Fig. 3.2). This T-shape structure is 2.2 kJ mol^{-1} less stable than the most stable form of the complex (**8**). For the isobutane–benzene complex, there exists a similar high-symmetry conformation (C_{3v}, **14**). However, all three C-H groups points perpendicularly to the middle of three C-C π bonds of benzene in this case (**14**, Fig. 3.2). This conformation is predicted to lie very close in energy (0.1 kJ mol^{-1}) to the asymmetrical structure (**4**). Since, the intermolecular potential of this system is very flat, it is likely that both the symmetrical and asymmetrical conformations can coexist. In summary, conformation with multiple CH/π contacts is energetically more favored in the series of hydrocarbon–benzene complexes.

Each CH/π contact of all the hydrocarbon–benzene complexes (**1**–**11**) is characterized by a short contact distance d_1 < 3.0 Å and a bond critical point (see Section 3.3.4). The intermolecular distances (d_1) lie in the range 2.31–2.82 Å (Table 3.2). This in good agreement with the statistical analysis, based on CSD analysis for the crystal structures with a saturated type of C-H bonds (~2.7 Å).[6,7,29,30] In all cases (**1**–**11**), the complex geometry has one C–H group directs toward the centre of the benzene ring (we

shall designate this hydrogen as "ring" hydrogen). The other CH/π contacts lie outside the benzene ring and are located in specific regions defined by the C-C and C-H bonds. In general, the ring C–H hydrogen has the shortest contact distance (d_1) among all the C-H groups facing the π face of benzene (Table 1). Accordingly, the CHX angle (α) associated the ring hydrogen is larger. For the isobutane (**4**) and cyclohexane (**8**) complexes, the α values are very close to 180˚. Interestingly, all the ring hydrogens lie somewhat offset the centre of the benzene ring, d_2 = 0.08–0.23 Å except for the cyclooctane complex. Our finding on the preference of an offset is consistent with the frequency distribution study of hydrogen bond trajectories for the CH···Ph interactions by Ciunik and Desiraju.[31] These authors found that CH···Ph interaction generally favors an offset from the benzene centroid, with 0.3–0.6 being the maximum. For methane–benzene complex (**1**), we found that an asymmetric geometry (**1**) lies almost identical in energy (0.1 kJ mol^{-1}) to the symmetrical C_{3v} geometry (**15**, d_1 = 2.472 Å, d_2 = 0.0 Å and α = 179.3˚, Fig. 3.2) previously reported.[10b] Since the intermolecular potential of this CH/π complex is very flat, it is difficult to determine the preferred geometry with certainty. As with **1**, ethane–benzene complex (**2**, Fig. 3.1) favors an asymmetrical structure with the CH/π contact slightly away from the benzene centroid (d_2 = 0.110 Å and α = 157.2˚). Interestingly, propane–benzene complex (**3**, Fig. 3.1) has 3 sets of CH hydrogens in close contact with the π face of benzene.

How do we account for the structural features of these CH/π complexes? In particular, why does the ring hydrogen points away from the benzene centroid? Inspection of the electrostatic potential map of benzene (Fig. 3.3) indicates that the maximum

negative potential locates approximately 0.5 Å from the centre of the ring. Thus, it is not surprising that the ring hydrogen of each complex favors a molecular geometry outside the centre of the benzene ring. Strong negative potentials are also found in regions outside the ring, in the 6 regions defined by the C-C and C-H bonds (see Fig. 3.3). Fig. 3 plots also the projection points (X, see Scheme 1) of all the CH/π hydrogens for complexes **1**–**11**. It is immediately obvious that all the projection points fall in the regions of strong negative electrostatic potential. It thus appears that the most stable geometry of each CH/π complex favors a maximum overlap of the electropositive C-H hydrogens with the electron rich regions of benzene. In other words, the geometries and directionalities of interaction of the hydrocarbon–benzene complexes are determined mainly by the electrostatic interaction between the interacting molecules.

Our theoretical finding here is supported by analyses of data collected in the Cambridge Structural Database and Brookhaven Protein Data Bank.[9b,29,30] In particular, Ciunik et al.[30] have showed that close intermolecular contacts between alicyclic (such as cyclohexane and cyclopentane) and aromatic rings in a number of crystal structures. Most importantly, multiple CH/π contacts are frequently observed.

Based on our understanding of the geometrical features of the series of hydrocarbon–benzene complexes examined here, we envisage a system of with 5 CH/π interactions is feasible. *Cis*-1,3-dimethylcyclohexane provides one such simple example. In this case, the hydrocarbon has parallel 5 axial C-H bonds and the appropriate dimension to match the negative electrostatic potential of the benzene molecule. Indeed,

geometry optimization [MP2/aug(d,p)-6-311G(d,p)] of such a complex (**16**) yields the predicted geometry, with one C-H bond points close to the centre of benzene (d_2 = 2.497 Å, d_2 = 0.092 Å and α = 179.7˚) and the other four C-H bonds lie on the four regions outside the ring where electrostatic potential are strong. At the CCSD(T)/aug-cc-pVTZ+ZPE+BSSE level, the computed stabilization energy of **16** is −15.8 kJ mol^{-1}, 3.2 kJ mol^{-1} larger than that of cyclohexane–benzene complex (**8**). Remarkably, analysis of the Cambridge Crystal Database (CSD) revealed a crystal structure (Fig. 3.4)[32] with such a geometrical feature. As seen in Fig. 3.4, the substituted phenyl moiety interacts favorably with the dimethylcyclohexane unit via 5 sets of CH/π interactions.

In general, the geometry of the hydrocarbon is hardly changed upon complexation with benzene. Cyclooctane (**10**) and bicyclo[2.2.2]octane (**11**) complexes are the only two exceptions. In **10**, the cyclooctane ring is slightly distorted, with one torsional angle increase from 84 to 114˚, while the six-membered ring of the hydrocarbon is distorted by 17˚ in **11**. In both cases, the change allows a maximum electrostatic fit between the four C-H groups of the cyclic alkane with benzene. As with previous theoretical findings, there is a slight contraction of all the C-H bonds in contact with π face of benzene. The possible origin of this bond shortening will be discussed in Section 3.4.

3.3.2. Interaction Energies

To determine a suitable level of theory for reliable prediction of the interaction energies of the weakly bonded systems studied here, we have performed initially a benchmark study of the interaction energy of the isobutane–benzene complex (**4**) at

various levels of theory. In general, the Hartree-Fock and density functional methods cannot describe this long-range CH/π interaction properly. As a consequence, HF and most DFT methods substantially underestimate the binding energy (Table 3.1). The only notable exception is the modified PW91 method (mPW1PW91) proposed by Adamo and Barone,[33] which yields result close to those of the higher-levels of theory. As dispersion interaction is the main source of attraction in these complexes, MP2 theory gives a much improved result. However, the MP2 value is somewhat overestimated compared to the QCISD(T) and CCSD(T) values (Table 3.1). We note that the effect of triple excitations is particularly important. For instance, on going from CCSD to CCSD(T) (or MP3 to MP4), there is a significant increase of the binding energy by 1.5 kJ mol^{-1}. Not surprisingly, the choice of basis set has a very strong influence on the computed stabilization energy. Previously studies[10b,11a,15c,15e] have shown that a fairly flexible basis set with multiple polarization functions is required for reliable prediction of the binding energy of the weak CH/π complex. Tsuzuki and co-workers have shown that basis set including diffuse polarization functions on both carbon and hydrogen atoms yields result close to that of the complete basis set limit. Here, we have confirmed that the aug(d,p)-6-311G(d,p) basis set gives interaction energy close to those obtained with the larger 6-311++G(3df,2p) and cc-pVQZ basis sets (Table 3.1). Thus, the aug(d,p)-6-311G(d,p) basis set is a practical choice for calculating the interaction energies for large systems.

As evidenced in Table 3.1, the MP2 interaction energies are very sensitive to the effect of BSSE correction. As expected, the BSSE correction is smaller for the larger basis set. Based on benchmark calculations on the methane–benzene complex, we found that the BSSE correction at the CCSD(T) level is similar to that at the MP2 level for a range of

basis sets. A similar finding has been reported by Tsuzuki et al.[10b] This justifies our use of the basis set additivity approximation in calculating the CCSD(T) interaction energies.

To investigate the influence of basis set on the geometries of the CH/π complexes, we have examined the geometry of cyclopropane–benzene complex (**5**) with several basis sets, include aug(d,p)-6-311G(d,p), 6-311+G(2df,p) and cc-pVTZ, at the MP2 level. In addition, optimization include BSSE effect, using the counterpoise-corrected gradient optimization technique,[34] was performed. As seen in Table 3.3, the d_2 and α values vary very little with the size of basis set. The predicted intermolecular distance d_1 is slightly smaller with a larger basis set. On the other hand, counterpoise-corrected optimization leads to a significantly longer d_1 value of 3.026 Å. Previous theoretical studies have shown that the intermolecular potential energy surface is rather flat for the CH/π complexes. Thus, it is not surprising that the calculated interaction energies of **5** employed different basis set are fairly close (Table 3.3). However, the stabilization energy obtained is significantly larger than (by 1.7 kJ mol^{-1}) that derived from the BSSE-uncorrected optimized geometry. Our result here suggests that the MP2/aug(d,p)-6-311G(d,p) level employed for geometry optimization is sufficiently reliable.

The calculated interaction energies of all the hydrocarbon–benzene complexes are summarized in Table 3.4. At the CCSD(T)/aug-cc-pVTZ+ZPE+BSSE level, the computed binding energy for the methane–benzene complex (**1**), a prototypical system with a single CH/π interaction, is –4.5 kJ mol^{-1} (–5.9 kJ mol^{-1} without ZPE correction), in good agreement with the best theoretical estimate of –6.0 kJ mol^{-1} (without ZPE correction).[10b] As evidenced in Table 3.4, all the larger hydrocarbons form a stronger

complex with benzene, with interaction energy two to three times larger than that of the methane complex. The largest binding energies (−15 kJ mol^{-1}) correspond to the systems with four CH/π interaction contributions, namely cyclooctane (**10**) and bicyclo[2.2.2]octane (**11**) complexes. This indicates that the additional CH/π contacts provide further stabilization to the intermolecular complexes. However, the magnitude of the interaction energy is not directly proportional to the number of CH/π interactions. This is perhaps not unexpected as the ring CH/π interaction has greater stabilization energy than those CH/π contacts outside the benzene ring. The CH/π interactions outside the ring are expected to be weaker due to the lower π density. Since *i*-propyl, long-chain alkyl groups and cyclic rings are commonly found in organic and biological systems, the cooperative CH/π interactions should play an essential role in understanding many aspects of organic and biological chemistry. As seen in Table 3.4, there is a gradual increase in the binding energy with the size of the hydrocarbon. Thus, one may expect the stabilization energy to depend on the polarizability of the hydrocarbon. Indeed, a strong correlation (R^2 = 0.95 is found between the interaction energies and calculated polarizabilities [MP2/aug(d,p)-6-311G(d,p)] for the series of hydrocarbon–benzene complexes (Fig. 3.5). As the magnitude of dispersion energy depends on polarizability, the correlation found here confirms that dispersion is the major source of stabilization of the CH/π complexes examined in this chapter. The importance of polarizability is also reflected in the T-shape cyclohexane–benzene complex (**12**) which has one CH/π interaction. Its interaction energy is twice as that of the methane–benzene complex (**1**). Although the scope of this study is limited only to the saturated hydrocarbons, it is important to note also that the strength of CH/π interaction depends on the carbon

hybridization of the C-H bond.[10b,11a,13c,14] The unsaturated C-H bond forms a stronger CH/π bond with an aromatic system.

3.3.3. Spectroscopic Properties

Next, we examine the influence of the cooperative CH/π interactions on the structures, vibrational spectra and proton NMR chemical shifts on the hydrocarbon monomers. Only the bond properties of the ring C-H hydrogen are considered. As evidenced in Table 3.4, a significant C-H bond shortening is observed in all cases, with the largest (0.0043 Å) predicted for cyclooctane complex and the smallest (0.0003 Å) computed for cyclopropane complex. In general, the bond contraction is more pronounced for the larger complexes. This bond shortening may be attributed to the charge polarization (see next Section) upon complex formation. In accord with the bond contraction, the C-H stretching vibration undergoes a significant blue shift upon complexation with benzene. For this reason, Hobza called the CH/π interaction a "blue-shift" hydrogen bond.[2,35] The blue shift in C-H stretching frequencies of CH/π systems has been studied by Hirota et al.[36] The calculated frequency shifts for complexes **1**–**11** range from 4 to 31 cm^{-1} (Table 3.4). Not surprisingly, the extent of the blue shift correlates well with the magnitude of the bond shortening (R^2 = 0.94). A rather large blue shift of 31 cm^{-1} is predicted for the cyclooctane complex (**10**), which represents a potential candidate for future experimental characterization of the CH/π interaction. It is while noting that correction of anharmonicity and use of CP-corrected geometry are likely to yield better results for these weak complexes.[12,35] Nevertheless, our predicted frequency shifts here may serve as a useful guide for future experimental characterization of these complexes in matrix experiment.

Apart from the fact that the new intermolecular modes appear in the vibrational spectra of the complex, the formation of a CH/π interaction is also accompanied by a significant upfield shift of the NMR chemical shift of the reference hydrogen (δ_H) in the hydrocarbon. This shift is due to the effect of diamagnetic field induced by the benzene ring and becomes prominent when the CH hydrogen is close to the centre of benzene. This is essentially the so-called deshielding effect due to the ring current of benzene. Hence, ^{1}H NMR spectroscopy technique was employed in early experimental studies of intermolecular CH/π interaction.[4,37] Here, we have examined the shielding tensor using the gauge-including atomic orbital (GIAO)[21] method at the MP2/6-31G(d) level. $\Delta\delta$ represents the change of proton chemical shift (δ_H) on going from the free CH donor to the CH/π interacting system. As most of these ring protons have a similar distance from the centre of the ring (i.e. similar d_1 and d_2 values, see Table 4.2), their deshielding effects are expected to be comparable. Indeed, the calculated upfield shifts ($\Delta\delta$) are fairly uniform (2.3–3.0) except for the isobutane complex (**4**) (Table 3.4). Our computed NMR shifts suggest that the NMR spectroscopic method is a potential tool to probe the presence of CH/π interactions in the hydrocarbon–benzene complexes.

3.3.4. Topological Properties and Charge Distributions

To gain a better understanding on the nature of the cooperative CH/π interactions of the hydrocarbon–benzene complexes (**1**–**11**), we have examined the topological properties of the electron density using Bader's theory of atoms in molecules (AIM)[23] at

the MP2/aug(d,p)-6-311G(d,p) level. Previously theoretical study by Novoa and Mota have shown that the CH/π interaction can be characterized by a bond path and its associated bond critical point (bcp).[14] For each of the multiple CH/π contacts of the various complexes examined here, there exists a bond path linking the hydrogen atom with one or more carbon atoms of benzene. The calculated topological properties at the bond critical points, namely electron density (ρ), Laplacian of electron density ($\nabla_2\rho$) and ellipicity (ε), are summarized in Table 3.2. The positive sign of the $\nabla_2\rho$ indicates the closed-shell nature of interaction, e.g. hydrogen bond.[38] For all the CH/π contacts, the small ρ and positive $\nabla_2\rho$ values are similar to the characteristic topological properties of a weak hydrogen bond, such as CH···O and OH···π interactions.[14] Significant bond ellipticity (ϵ) is calculated for the ring C-H bond (Table 3.2). This readily confirms the stronger π interaction in the ring C-H bond compared to the other CH/π interactions outside the benzene ring. The stronger CH/π interaction of the ring C-H group for each complex is also reflected in the larger ρ and $\nabla_2\rho$ values compared to those CH/π bonds outside the ring,

The formation of a CH/π bond normally results in shifts of electron density. Although these shifts are relatively small in magnitude, they are useful in providing further insight into the nature of such bonds. Here, we have examined the charge distributions of the complexes **1**–**11** using the NBO analysis, based on the MP2/aug(d,p)-6-311G(d,p) wavefunction. NBO atomic charges of small molecules have recently been demonstrated to agree well with experimental values obtained from X-ray diffraction data.[39] The calculated atomic charges of the carbon and hydrogen of the ring C-H bond

and the magnitude of charge transfer from benzene to the hydrocarbon monomer are given in Table 3.5. In all cases, there is a small amount of charge transfer from benzene to the hydrocarbon in the intermolecular CH/π complexes. This confirms the nature of the soft acid (hydrocarbon)–soft base (benzene) interaction. Interestingly, the trend of charge transfer follows that of the stabilization energy. Both the carbon and hydrogen atoms of the ring C-H bond display strong charges (Table 3.5). Unexpectedly, the ring C-H hydrogen becomes more positive and the adjacent carbon becomes more negative (Table 3.5). In other words, there is a larger degree of charge separation of the C-H bond upon complexation with benzene, which results in an increase in the Coulomb attraction in the C-H bond. As evidenced in Table 3.5, the degree of charge separation parallels to magnitude of bond shortening (Table 3.4). Perhaps, this increase in charge polarization, i.e. charge separation, of the C-H bond is one of the main reasons for the C-H bond shortening in the CH/π complexes. Although all complexes exhibit a small amount of charge transfer, there is an obvious trend in the series: the degree of charge transfer increases with the size of the hydrocarbon (Table 3.4). In addition, we note that the calculated binding energy correlates well with the magnitude of charge transfer. Although the dispersion interaction is the main source of stabilization energy for the CH/π complexes examined here, the charge density analysis suggests that the electrostatic and charge-transfer interactions also contribute to the stabilization energies.

As mentioned in previous section, the geometries of the various hydrocarbon–benzene complexes can be explained by the electrostatic interaction between the interacting molecules. Our argument is further supported by point charge calculations. In these model calculations, the carbon and hydrogen atoms of the benzene

molecule are replaced by point charges, which were obtained from NBO analysis. Full geometry optimizations of the hydrocarbons were then carried out in the presence of the set of point charges. The optimizations readily reproduce the bond contraction of C-H bonds.

3.4 Conclusions

In summary, we have investigated the cooperative behavior of CH/π interactions in several hydrocarbon–benzene complexes using high-level ab initio calculations. Based on the computed interaction energies, structural features, binding properties and bond critical point analysis, it is clear that the multiple CH/π interactions play a complementary role in stabilizing the intermolecular complexes. The CH/π interaction involving the "ring" C-H group is the dominant source of stabilization; while the CH/π interactions outside the benzene ring play a lesser but significant role. Dispersion is confirmed to be the major source of stabilization. The calculated interaction energy correlates with the polarizability of the hydrocarbon. As the size of the hydrocarbon increases, the electrostatic and charge transfer effects play a more prominent role in governing the structures and binding properties of the complexes. To assist further experimental characterization of the CH/π interaction, spectroscopically observable features relative to the unperturbed hydrocarbons are predicted. Given the non-negligible interaction energy (10–15 kJ mol^{-1}) of the multiple CH/π interactions and the fact that cycloalkyl, long-chain alkyl and aromatic functional groups are almost ubiquitous in organic compounds and biomolecules, we believe that the CH/π interaction is even more important than one may

have anticipated in our understanding of conformational behavior of organic molecules, molecular recognition, crystal engineering, protein structures and hydrophobic effect. Since benzene is a common solvent for organic molecules, one might also expect the CH/π interaction to be an important source of solvent-solute interaction. For instance, we have shown recently the reverse of *gauche/trans* equilibrium of 2,2'-dimethyl-2,2'-bi-1,3-dithiolanyl on going from carbon tetrachloride to benzene, which could be explained in terms of the specific benzene-solute interaction via cooperative CH/π interactions.[40] Lastly, we note that the cooperative CH/π interactions should also prevalent in nonpolar and aprotic polar media based on SCRF[41] solvent-effect calculations (mPW1PW91/6-31G(d) level) of several representative systems. The geometries and binding energies of the hydrocarbon–benzene complexes are relatively unperturbed on going from the gas phase to a dielectric medium.

3.5 References

1 Nishio, M.; Hirota, M.; Umezawa, Y. *The CH/π interaction*; Wiley–VCH: New York, 1998.

2 Hobza, P.; Havlas, Z. *Chem. Rev*. **2000**, *100*, 4253.

3 Tarakeshwar, P.; Choi, H. S.; Kim, K. S. *Chem. Rev*. **2000**, *100*, 4145.

4 Nishio, M. *Cryst. Eng. Comm*. **2004**, *6*, 130.

5 Kodama, Y.; Nishihata, K.; Nishio, M.; Nakagawa, N. *Tetrahedron Lett.* **1977**, 2105.

6 Umezawa, Y.; Tsuboyama, S.; Takahashi, H.; Uzawa, J.; Nishio, M. *Tetrahedron* **1999**, *55*, 10047, and references therein.

7 Takahashi, H.; Tsuboyama, S.; Umezawa, Y.; Honda, K.; Nishio, M. *Tetrahedron* **2000**, *56*, 6185, and references therein.

8 (a) Umezawa, Y.; Tsuboyama, S.; Takahashi, H.; Uzawa, J.; Nishio, M. *Bioorg. Med. Chem*. **1999**, *7*, 2021. (b) Umezawa, Y.; Nishio, M. *Bioorg. Med. Chem*. **1998**, *6*, 493. (c) Muraki, M. *Protein Peptide Lett*. **2002**, *9*, 195.

9 (a) Chakrabarti, P.; Samanta, U. J. Mol. Bio. 1995, 251, 9. (b) Brandi, M.; Weiss, M. S.; Jans, A.; Sühnel, J.; Hilgenfeld, R. *J. Mol. Bio*. **2001**, *307*, 357.

10 (a) Tsuzuki, S.; Uchimaru, T.; Mikami. M.; Tanabe, K. *J. Phys. Chem A* **1998**, *103*, 8265. (b) Tsuzuki, S.; Honda, K.; Uchimaru, T.; Mikami, M.; Tanabe, K. *J. Am. Chem. Soc*. **2000**, *122*, 3746. (c) Tsuzuki, S.; Honda, K.; Uchimaru, T.; Mikami, M.; Tanabe, K. *J. Phys. Chem. A* **2002***, 106,* 4423.

11 (a) Tarakeshwar, P.; Choi, H. S.; Kim, K. S. *J. Am. Chem. Soc*. **2001**, *123*, 3323. (b) Lee, E. C.; Hong, B. Y.; Lee, J. Y.; Kim, J. C.; Kim, D.; Kim, Y.; Tarakeshwar, P.; Kim, K. S. *J. Am. Chem. Soc.* **2005**, *127*, 4530.

12 (a) Hobza, P.; Spirko, V.; Selzle, H. L.; Schlag, E. W. *J. Phys. Chem. A* **1998**, *102*, 2501. (b) Hobza, P.; Spirko, V.; Havalas, Z.; Buchhold, K.; Reimann, B.; Barth, H. D.; Bruthschy, B. *Chem. Phys. Lett*. **1999**, *299*, 180. (c) Reimann, B.; Buchhold, K.; Vaupel, S.; Brutschy, B.; Havlas, Z.; Spirko, V.; Hobza, P. *J. Phys. Chem. A* **2001**, *105*, 5560.

13 (a) Takahashi, O.; Kohno, Y.; Iwasaki, S.; Saito, K.; Tomoda, S.; Umezawa, Y.; Nishio, M. *Bull. Chem. Soc. Jpn.* **2001**, *74*, 2421. (b) Takahashi, O.; Kohno, Y.; Saito, K.; Nishio, M. *Chem. Eur. J.* **2003**, *9*, 756. (c) Takahashi, O.; Kohno, Y.; Saito, K. *Chem. Phys. Lett*. **2003**, *378*, 509.

14 Novoa, J. J.; Mota, F. *Chem. Phys. Lett*. **2000**, *318*, 45.

15 (a) Takagi, T.; Tanaka, A.; Matsuo, S.; Maezaki, H.; Tani, M.; Fujiwara, H.; Sasaki, Y. *J Chem. Soc. Perkin Trans. II* **1987**, 1015. (b) Sakaki, S.; Kato, K.; Miyazaki, T.; Musashi, Y.; Ohkubo, K.; Ihara, H.; Hirayama, C. *J. Chem. Soc. Faraday Trans.* **1993**, *89*, 659. (c) Samanta, U.; Chakrabarti, P.; Chandrasekhar, J. *J. Phys. Chem. A* **1998**, *102*, 8964. (d) Oki, M.; Takano, S.; Toyota, S. *Bull. Chem. Soc. Jpn*. **2000**, *73*, 2221. (e) Sinnokrot, M. O.; Valeev, E. F.; Sherrill, C. D. *J. Am. Chem. Soc.* **2002**, *124,* 10887. (f) Sinnokrot, M. O.; Sherrill, C. D. *J. Am. Chem. Soc.* **2004**, *126*, 7690.

16 Sozzani, P.; Comotti, A.; Bracco, S.; Simonutti, R.; *Chem. Commun*. **2004**, 768.

17 Tsuzuki, S.; Honda, K.; Uchimaru, T.; Mikami, M.; Tanabe, K. *J. Phys. Chem. A* **1999**, *103*, 8265.

18 (a) Pople, J. A.; Head-Gordon, M.; Raghavachari, K. *J. Chem. Phys.* **1987**, *87*, 5968. (b) Head-Gordon, M.; Pople, J. A.; Frisch, M. J. *Chem. Phys. Lett*. **1988**, *153*, 503. (c) Scuseria, G. E.; Schaefer, H. F., III, *J. Chem. Phys.* **1989**, *90*, 3700.

19 Boys, S. F.; Bernardi, F. *Mol. Phys*. **1970**, *19*, 553.

20 Scott, A. P.; Radom, L. *J. Phys. Chem*. **1996**, *100*, 16502.

21 Cheeseman, J. R.; Trucks, G. W. Keith, J. A.; Frisch, M. J. *J. Chem. Phys.* **1996**, *104*, 5497.

22 Reed, A. E.; Curtiss, L. A.; Weinhold, F. *Chem. Rev*. **1988**, *88*, 899.

23 (*a*) Bader, R. F. W. *Atoms in Molecules—A Quantum Theory*; Oxford Science Publications: Oxford, **1990**. (*b*) Bader, R. F. W. *Chem. Rev.*, **1991**, *91*, 893.

24 Popelier P. L. A.; Bone, R. G. A. *MORPHY98*; UMIST, Manchester, **1998**.

25 Schaftenaar, G. *MOLDEN* visualization program, Centre for Molecular and Biomolecular Informatics, University of Nijmegen, The Netherlands, 2005.

26 Werner, H.-J.; Knowles, P. J.; et. al. *MOLPRO*, version 2002; University of Birmingham, 2002.

27 Frisch, M. J.; et. al. *Gaussian 98*, Gaussian, Inc., Pittsburgh PA, 1998.

28 Frisch, M. J.; et. al. *Gaussian 03*, Gaussian, Inc., Wallingford CT, 2004.

29 Umezawa, Y.; Tsuboyama, S.; Honda, K.; Uzawa, J.; Nishio, M. *Bull. Chem. Soc. Jpn*. **1998**, *71*, 1207.

30 Ciunik, Z.; Bedrski, S.; Latajka, Z.; Lesczynski, J. *J. Mol. Struct*. **1998**, *442*, 125.

31 Ciunik, Z.; Desiraju, G. R. *Chem. Commun*. **2001**, 703.

32 Schoenholzer, P.; Daly, J. J.; Hennig, M., Private communications (Ref. no. ADOZOI) in Cambridge Structural Database, 2000.

33 Adamo, C.; Barone, V. *J. Chem. Phys.* **1998**, *108*, 664.

34 Simon, S.; Duran, M.; Dannenberg, J. J. *J. Chem. Phys.* **1996**, *105*, 11024.

35 Hobza, P.; Havlas, Z. *Theor. Chem. Acc*. **2002**, *108*, 325.

36 Karatsu, M.; Suezawa, H.; Abe, K.; Hirota, M.; Nishio, M. Bull. *Chem. Soc. Jpn*. **1986**, *59*, 3529.

37 For example, see Ehama, R.; Tsushima, M.; Yuzuri, T.; Suezawa, H.; Sakakibara, K.; Hirota, M. *Bull. Chem. Soc. Jpn*. **1993**, *66*, 814.

38 Koch, U.; Popelier, P. L. A. *J. Phys. Chem*. **1995**, *99*, 9747.

39 Messerschmidt, M.; Wagner, A.; Wong, M. W.; Luger, P. *J. Am. Chem. Soc.* **2002**, *124*, 732.

40 Chen, W.; Lam, Y.; Wong, M. W.; Huang, H.-H.; Liang, E. *J. Phys. Chem. A*. **2003**, *107*, 6714.

41 (a) Wong, M. W.; Frisch, M. J.; Wiberg, K. B. *J. Am. Chem. Soc*. **1991**, *113*, 4776. (b) Wong, M. W.; Wiberg, K. B.; Frisch, M. J. *J. Chem. Phys*. **1991**, *95*, 8991. (c) Wong, M. W.; Wiberg, K. B.; Frisch, M. J. *J. Am. Chem. Soc.* **1992**, *114*, 1645.

3.6 Appendix

Table 3.1 Calculated Interaction Energies (ΔE) of Isobutane–Benzene Complex at Various Levels of Theory[a]

level	ΔE	ΔE[b]	level	ΔE	ΔE[b]
HF/6-31G(d)	–3.3	0.3	MP2/6-31G(d,p)	–14.3	–5.1
SVWN/6-31G(d)	–19.3	–13.0	MP2/6-31+G(d)	–15.7	–5.8
BLYP/6-31G(d)	–2.4	2.2	MP2/6-31++G(d)	-18.8	–6.2
B3LYP/6-31G(d)	–3.5	1.0	MP2/6-31G(2d)	–16.3	–6.8
B3P86/6-31G(d)	–2.1	1.3	MP2/6-311G(d,p)	–15.7	–8.2
PW91PW91/6-31G(d)	–8.3	–3.3	MP2/6-311++G(d,p)	–19.9	–9.2
MPW1PW91/6-31G(d)	–12.6	–9.2	MP2/6-311++G(2df,p)	–16.9	–11.1
MP2/6-31G(d)	–13.6	–4.1	MP2/6-311++G(3df,2p)	–18.1	–12.6
MP3/6-31G(d)	–10.5	–1.5	MP2/aug(d,p)-6-311G(d,p)	–22.7	–12.5
MP4/6-31G(d)	–12.2	–2.8	MP2/aug(d,p)-6-311G(3df,2p)	–21.6	–12.8
QCISD/6-31G(d)	–9.1	–0.6	MP2/cc-pVDZ	–14.7	–7.1
QCISD(T)/6-31G(d)	–11.5	–2.1	MP2/cc-pVTZ	–15.0	–11.7
CCSD/6-31G(d)	–9.2	–0.6	MP2/aug-cc-pVTZ	–18.4	–13.4
CCSD(T)/6-31G(d)	–11.3	–2.1	MP2/cc-pVQZ	–14.6	–13.2

[a] Based on MP2/6-31G (d) optimized geometry except for the HF and DFT methods.

[b] BSSE corrected interaction energies.

Table 3.2 Calculated Structural Parameters (d_1, d_2 and α)[a] and Topological Properties[b] (ρ, $\nabla_2\rho$ and ϵ, in au) at the Bond Critical Point of Various Hydrocarbon–Benzene Complexes (**1**–**11**), Evaluated at the MP2/aug(d,p)-6-311G(d,p) Level

Hydrocarbon	label[c]	d_1	d_2	α	ρ	$\nabla_2\rho$	ϵ
methane (**1**)	1	2.548	0.205	145.5	0.0066	0.0205	7.09
ethane (**2**)	1	2.451	0.110	157.2	0.0074	0.0234	6.51
propane (**3**)	1	2.506	0.150	146.2	0.0070	0.0219	11.8
	2	2.557	2.499	145.8	0.0061	0.0176	2.94
	3	2.629	2.353	140.9	0.0056	0.0163	0.97
isobutane (**4**)	1	2.473	0.170	178.4	0.0075	0.0232	3.73
	2	2.602	2.414	176.2	0.0066	0.0195	1.83
	3	2.602	2.415	176.2	0.0066	0.0195	1.83
cyclopropane (**5**)	1	2.437	0.189	152.8	0.0077	0.0239	4.46
	2	2.618	2.339	145.4	0.0062	0.0176	0.89
	3	2.618	2.339	145.6	0.0062	0.0176	0.89
cyclobutane (**6**)	1	2.361	0.123	165.5	0.0091	0.0285	7.36
	2	2.374	2.575	165.0	0.0076	0.0215	1.70
cyclopentane (**7**)	1	2.402	0.231	161.8	0.0088	0.0269	3.90
	2	2.309	2.945	155.1	0.0059	0.0174	0.91
	3	2.737	2.299	133.5	0.0056	0.0170	0.81
	4	2.512	2.490	153.1	0.0070	0.0200	1.21
cyclohexane (**8**)	1	2.338	0.121	176.1	0.0092	0.0288	4.68
	2	2.567	2.484	172.9	0.0066	0.0182	1.21
	3	2.571	2.481	172.9	0.0066	0.0182	1.21
cycloheptane (**9**)	1	2.377	0.148	162.8	0.0088	0.0275	4.18
	2	2.404	2.580	150.2	0.0073	0.0205	1.63
	3	2.684	2.174	175.4	0.0067	0.0183	0.88
cyclooctane (**10**)	1	2.376	0.000	150.0	0.0084	0.0257	12.04
	2	2.490	2.401	158.1	0.0078	0.0203	1.09
	3	2.504	2.628	167.5	0.0061	0.0158	0.79
	4	2.815	2.293	165.7	0.0054	0.0136	0.43
bicyclooctane (**11**)	1	2.356	0.079	167.9	0.0089	0.0278	5.26

2	2.348	2.711	162.1	0.0074	0.0209	1.53
3	2.578	2.464	152.7	0.0059	0.0165	0.61
4	2.779	2.256	147.5	0.0050	0.0147	0.53

[a] Bond lengths in Å and angles in degrees.

[b] Based on AIM analysis.

[c] See Fig.1 for hydrogen labeling.

Table 3.3 Calculated Structural Parameters (d_1, d_2 and α) and Interaction Energies[a] (ΔE, kJ mol^{-1}) of Cyclopropane–Benzene Complex (**5**) Evaluated at Various Levels of Geometry Optimization

level	d_1	d_2	α	ΔE
MP2/6-31G(d)	2.654	0.277	151.1	–9.0
MP2/aug(d,p)-6-311G(d,p)	2.437	0.189	152.8	–7.9
MP2/6-311+G(2df,p)	2.521	0.145	152.1	–8.8
MP2/cc-pVTZ	2.532	0.159	151.8	–8.7
CP-MP2/6-31G(d)[b]	3.026	0.535	149.5	–10.7

[a] CCSD(T)/aug(d,p)-6-311G(d,p) level including ZPE (MP2/6-31G(d)) and BSSE corrections.

[b] Counterpoise-corrected gradient optimization.

Table 3.4 Calculated Interaction Energies[a] (ΔE, kJ mol^{-1}) and Bond Characteristics (Δd_1, $\Delta\nu$ and $\Delta\delta$) of the Ring C-H Bonds of Various Hydrocarbon–Benzene complexes

hydrocarbon	ΔE	Δd_1[b,c]	$\Delta\nu$[c,d]	$\Delta\delta$[e]
methane (**1**)	–4.4	–0.0011	8.5	2.291
ethane (**2**)	–7.4	–0.0007	11.7	2.673
propane (**3**)	–9.6	–0.0003	10.4	2.534
isobutane (**4**)	–10.2	–0.0010	7.9	2.426
cyclopropane (**5**)	–9.7	–0.0000	4.2	2.749
cyclobutane (**6**)	–11.2	–0.0023	12.7	2.885
cyclopentane (**7**)	–12.7	–0.0021	14.7	2.785
cyclohexane (**8**)	–12.6	–0.0033	15.2	2.919
cycloheptane (**9**)	–13.3	–0.0026	20.3	2.878
cyclooctane (**10**)	–14.2	–0.0043	30.9	2.736
bicyclooctane (**11**)	–14.7	–0.0015	15.7	2.985

[a] CCSD(T)/aug-CC-PVTZ//MP2/aug(d,p)-6-311G (d,p) level including BSSE and ZPE corrections.

[b] Bond distance shortening (Δd_1, Å) upon complex formation.

[c] MP2/6-31G(d) level.

[d] C-H stretching frequency shift ($\Delta\nu$, cm^{-1}) upon complex formation.

[e] Change in ^{1}H NMR chemical shift ($\Delta\delta$, ppm) upon complex formation, evaluated by the GIAO method at the MP2/6-31G (d) level.

Table 3.5 Calculated Atomic Charges (q),[a] Charge Transfer (CT)[a] and Dipole Moments (μ, D) of Various Hydrocarbon–Benzene Complexes[b]

hydrocarbon	q(H)[c]	Δq(H)[c,d]	q(C)[c]	Δq(C)[c,d]	CT[e]	μ[b]
methane (**1**)	0.1950	0.0038	–0.7648	–0.0008	–0.0039	0.27
ethane (**2**)	0.1867	0.0060	–0.5432	–0.0011	–0.0044	0.33
propane (**3**)	0.1877	0.0075	–0.5523	–0.0047	–0.0041	0.38
isobutane (**4**)	0.1878	0.0072	–0.5556	–0.0039	–0.0075	0.40
cyclopropane (**5**)	0.1986	0.0058	–0.3868	–0.0011	–0.0060	0.43
cyclobutane (**6**)	0.1852	0.0070	–0.3639	–0.0031	–0.0081	0.49
cyclopentane (**7**)	0.1838	0.0079	–0.3733	–0.0051	–0.0072	0.49
cyclohexane (**8**)	0.1822	0.0070	–0.3712	–0.0074	–0.0106	0.59
cycloheptane (**9**)	0.1822	0.0081	–0.3666	–0.0086	–0.0099	0.57
cyclooctane (**10**)	0.1871	0.0092	–0.3879	–0.0238	-0.0126	0.61
bicyclo[2.2.2]octane (**11**)	0.1916	0.0038	–0.3823	–0.0082	–0.0110	0.59
dimethylcyclohexane (**12**)	0.1878	0.0099	–0.3876	–0.0080	–0.0105	0.44

[a] Based on NBO analysis.

[b] MP2/aug(d,p)-6-311G (d,p) level.

[c] The "ring" C-H bond of the complex.

[d] Change in atomic charge on going from the monomer to the complex.

[e] Charge transfer from benzene to hydrocarbon in the complex.

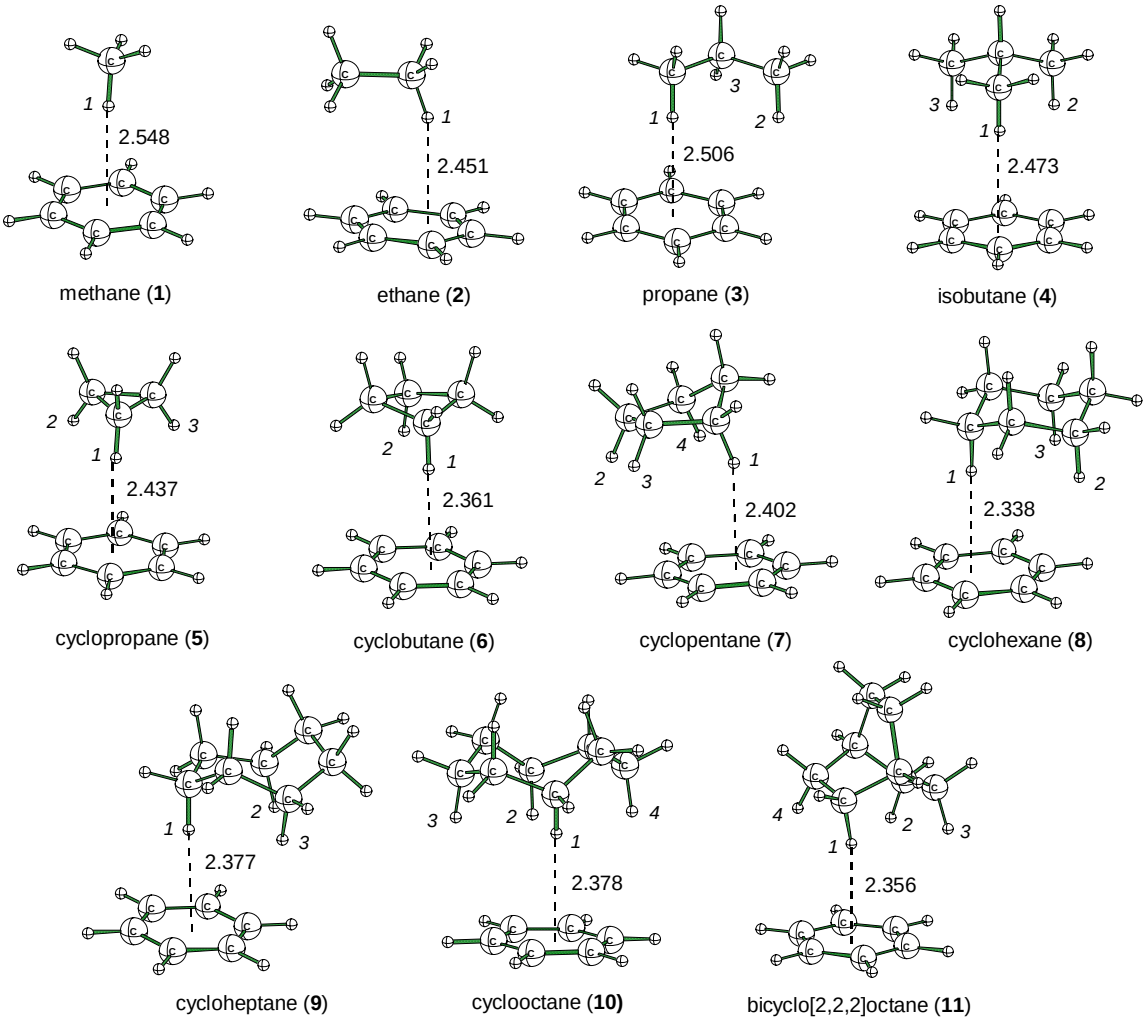

Figure 3.1 Optimized [MP2/aug(d,p)-6-311G(d,p)] geometries of various hydrocarbon–benzene CH/π complexes. The dotted line represents the projection line of the ring C-H hydrogen of the hydrocarbon perpendicular to the molecular plane of benzene.

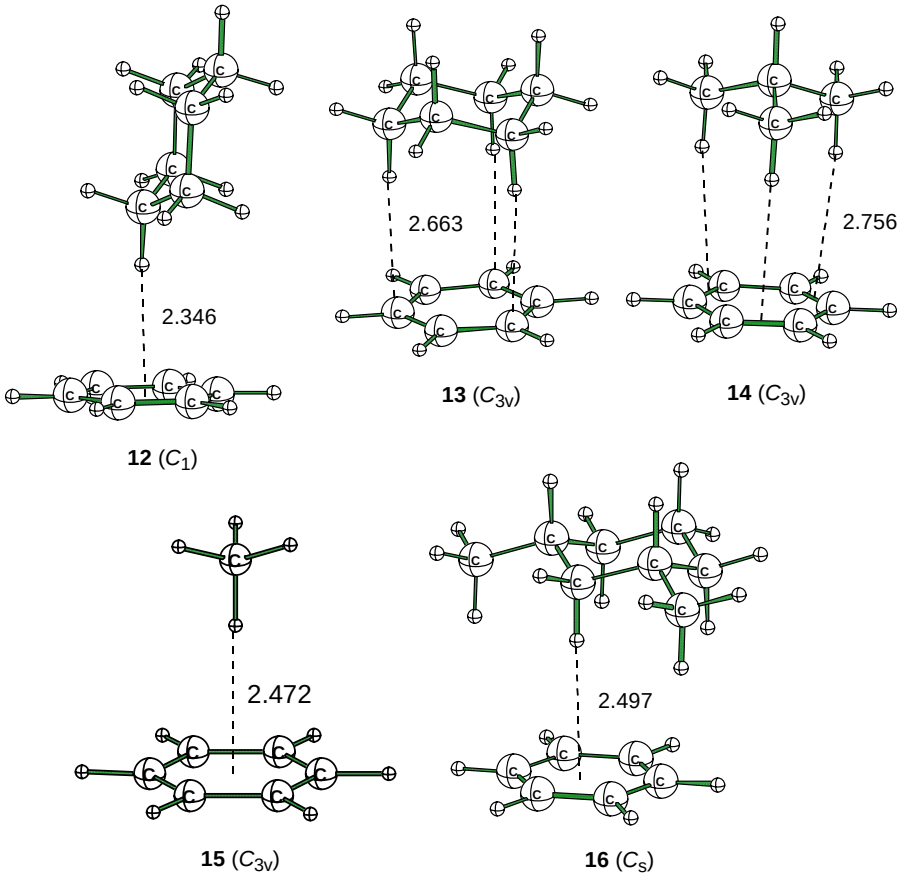

Figure 3.2 Conformations of methane–, isobutane–, cyclohexane– and 1,3-dimethyl-cyclohexane–benzene complexes.

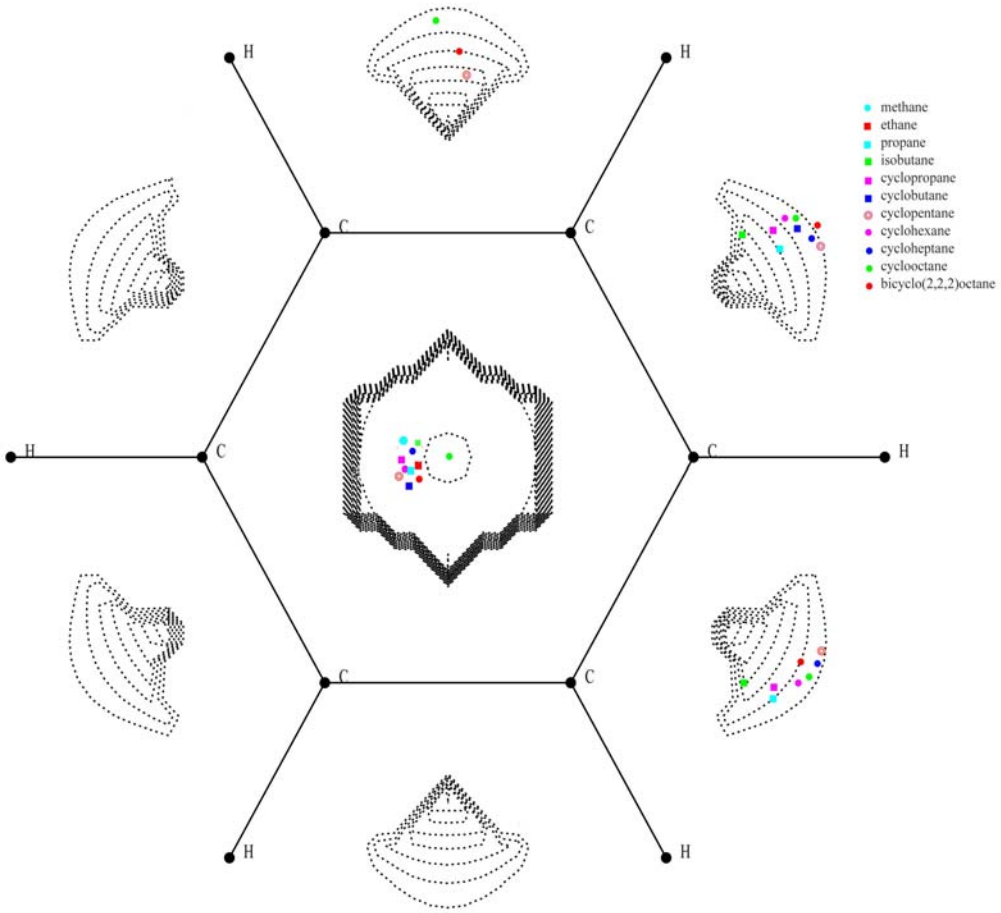

Figure 3.3 Negative electron potential map of benzene in molecular plane. The data points represent the projection points of the C-H hydrogens of various hydrocarbon–benzene complexes.

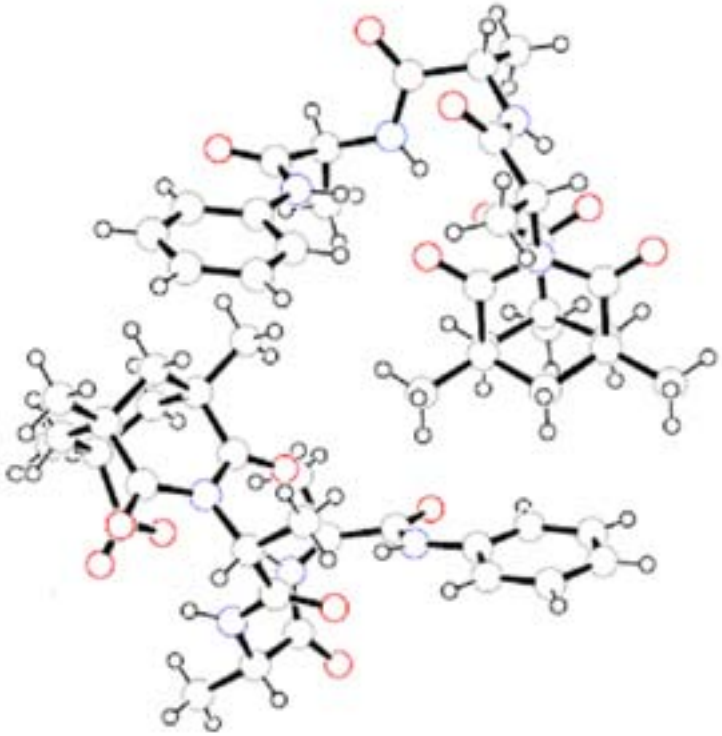

Figure 3.4 X-ray structure of 4-(Dimethylamino)pyridinium *N*-(2-(5-carboxy-1,3,5-trimethyl-cyclohexane-1,3-dicarboximido)propionyl)alanyl-alanine phenyl amide. Part of the molecule was deleted to improve viewing.

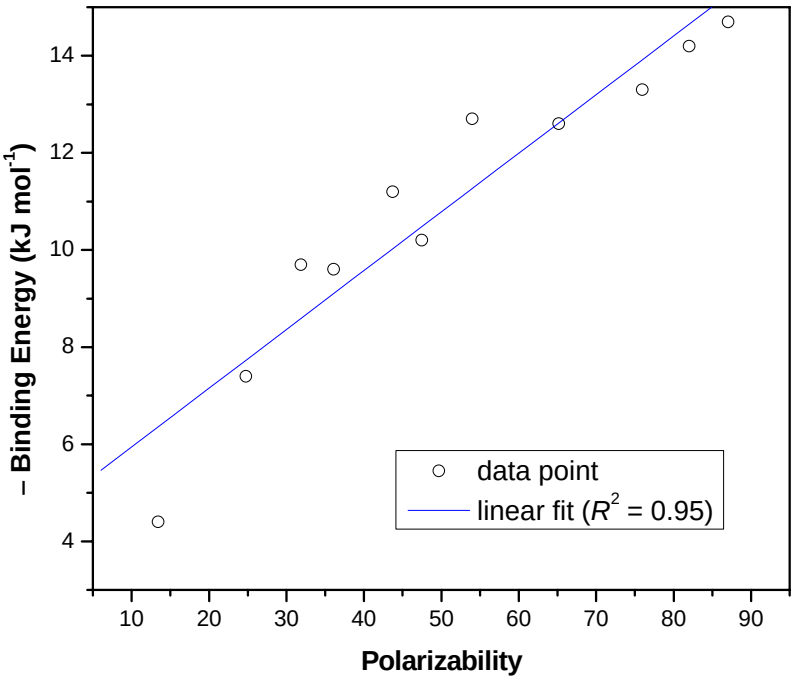

Figure 3.5 Plot of binding energy against polarizability.

Chapter 4 Multiple CH/π Interactions between Benzene and Cyclohexane and Its Heterocyclic Analogues: A Theoretical Study of Substituent Effects

4.1 Introduction

The weak molecular interaction between a nonpolar (or weakly polar) C–H bond and an electron-rich π-system has been recognized to be important in various fields of chemistry and biochemistry. This attractive force is termed the CH/π interaction, [1] which has attracted strong interest [2-4] in recent years. The CH/π interaction was first proposed by Nishio and co-workers to explain the preference of conformations in which bulky and phenyl groups are in close contact.[5] During the last two decades, numerous experimental studies which support the existence of this attraction have been reported.[4] In particular, the short contact between a C–H bond and a π system is observed in large number of crystals of organic molecules[6,7] peptides[8] and proteins.[9,10] It is believed that the CH/π interaction is of importance in understanding many chemical phenomena such as conformational preference, crystal packing, host-guest complexation, and self-organization processes.[4,6,7] The importance of CH/π interaction for structures and properties of biological systems has also been reported.[8-11]

Several theoretical studies of simple benzene complexes have been carried out to evaluate the interaction energy of the CH/π interaction and to shed light on the nature of the interaction.[12-17] In our previous work on cooperative CH/π interactions, we have found

that several C–H protons can be oriented in such as way that multiple CH/π interactions can occur simultaneously with the π face of an aromatic system. However, very little is known about the effect of substituent on the magnitude of multiple CH/π interactions Several experimental studies have demonstrated that electron-donating substituents on the π system and electron-withdrawing substutent on the C–H carbon increase the interaction energy.[18] This is supported by theoretical studies which confirmed that the strength of CH/π interaction is more sensitive to changes in the donor than the acceptor group.[19-22,13b] In this chapter, we have systematically investigated the benzene complexes of cyclohexane, and its heterocyclic analogues, namely $C_5H_{10}O$, $C_4H_8O_2$, $C_3H_6O_3$, $C_5H_{10}S$, $C_4H_8S_2$, $C_3H_6S_3$, $C_5H_{11}N$, $C_4H_{10}N_2$, $C_3H_9N_3$, $C_5H_{11}P$, $C_4H_{10}P_2$, $C_3H_9P_3$, $C_5H_{12}Si$, $C_4H_{12}Si_2$, and $C_3H_{12}Si_3$, using high-level *ab initio* calculations to evaluate the magnitude of substitution effect and the relationship between interaction energy and number of substituent. Up to three heteroatom (N, O, S, Si or P) substitutions were considered. Since the purpose of this study is to investigate the substituent effect on the multiple CH/π interaction, the comparison between CH/π and XH/π is not included. In all cases, only complexes with three axial C–H bonds perpendicular the π face of benzene considered. Cyclohexane–benzene complexes have been examined previously, but it was included in this study for purpose of comparison. The geometrical features, interaction energies, binding properties and topological properties will be examined to gain further insight into the nature of multiple CH/π interactions and the influence of heteroatom substitution on the strength of multiple CH/π complexes.

4.2 Computational Methods

It was well documented that electron correlation is of particular importance for proper description of both geometries and binding energies of CH/π complexes.[2,3,12b,13a,17b] So, the geometry optimization for all multiple CH/π complexes were carried out at the MP2/6-31G(d) level. Frequency analysis was performed at the same level of theory to confirm the optimized structure as a local energy minimum and to evaluate zero-point energy (ZPE) correction. More reliable prediction of interaction (binding) energies were obtained via higher-level single-point calculations at the CCSD(T)[23] level in conjugation with a larger aug(d,p)-6-311G(d,p) basis set, proposed by Tsuzuki et al,[12b,24] via additivity approximation at the MP2 level. In our previous work, we have confirmed that the aug(d,p)-6-311G(d,p) basis set, yielded result very close to that of the cc-pVQZ basis set for the cyclohexane–benzene complex. Correction for basis set superposition error (BSSE), based on the counterpoise method,[25] was included in the calculated interaction energy. The interaction energies reported in the chapter correspond to the CCSD(T)/aug(d,p)-6-311G(d,p) level including zero-point energy (MP2/6-31G(d), scaled by 0.967)[26] and BSSE corrections. All ab initio calculations were performed using the Molpro 2002,[27] Gaussian98,[28] and Gaussian 03[29] programs, while charge density analysis, based on Bader's theory of atoms in molecules (AIM)[30] was carried out using the MORPHY98 program,[31] and the charge transfer were obtained using the natural bond orbital (NBO) approach, based on the MP2/6-31G(d) wavefunction.[32]

4.3 Results and Discussion

4.3.1 Geometries and Binding Energies of the Complexes.

There are several important structural parameters which characterize a CH/π interaction, namely d_1, d_2 and α (see Scheme 1). O is the centre (centroid) of the benzene ring, while X represents the projection point of a C-H hydrogen on the molecular plane of benzene. Thus, d_1 corresponds to the non-bonded intermolecular distance, d_2 represents the distance of the projection point away from the benzene centre (O) and α is the CHX angle. For those structures that the C–H bonds point to the individual carbon atoms of the benzene ring, the d_1 represents the distance between the hydrogen atom of C–H bond and the carbon atom of benzene. The fundamental features of typical CH/π interaction are: the C–H bond points close to the centre of an aromatic ring, and the C–H bond length is shortened upon complexes formation, which leads to a higher C–H stretching frequency.

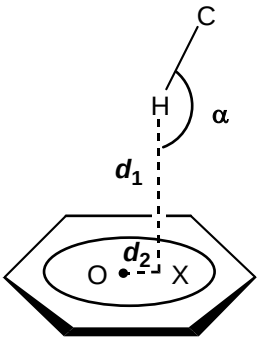

Scheme 1

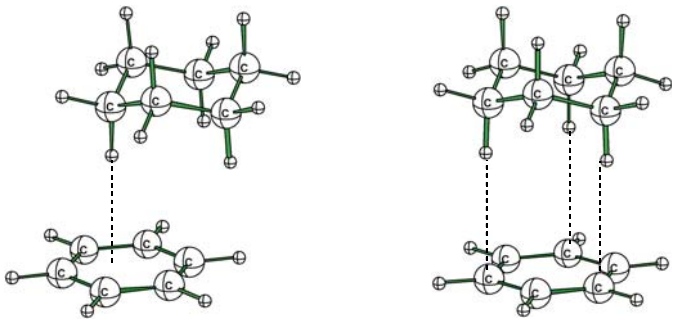

C_c **C_a**

Scheme 2

In this study, we mainly discuss two types of conformers of complexes, one form is derived from asymmetrical cyclohexane-benzene complex with one C–H bond points to the center of benzene (**Cc** conformer) and another conformer corresponding to the

symmetric cyclohexane-benzene complex, which the three sets of C–H bonds point to three separated carbon of benzene ring (**Ca** conformer) (Scheme 2).

In general, the changes in the geometry of the hydrogen bond donor monomer upon complex formation are small. The structural changes accompanying complexation in the oxygen and nitrogen derivatives are larger than those changes in the sulfur and phosphorus analogues, and they are generally smaller still for the derivatives of the silicon. The CH/π angles (α value in **Tables 4.1, and 4.3**) in the complexes of benzene with substituted cyclohexane are still close to linear, with the deviation in most complexes being less than 10º. The CH/π angle in the double oxygen substituted complex **5** (**Figure 4.1**) deviate more significantly from linearity (by 17.1º).

All three parallel C–H bonds are shortened as anticipated in all multiple CH/π complexes. The smallest changes come from the mono-sulfur substituted complexes **9** and **10** (**Figure 4.1**) which was shortened by 0.0003Å and 0.0005Å respectively, while the largest changes come from the tri-oxygen substituted complex **7** and di-oxygen substituted complex **5** (**Figure 4.1**) which was shortened the each C–H bond by 0.043 Å and 0.044 Å, respectively. This contraction of C–H bond in the proton donor upon complexation is also accompanied by an increase in the C–H stretching frequency (5.3-65.6 cm^{-1}) for these complexes. The bond shortening and the blue-shift frequency are the characteristic of an improper hydrogen bond as labeled by Hobza *et al*.[2] In addition, the AIM analysis demonstrated the CH/π interaction fulfills the criteria that proposed by Popelier[33] for the existence of hydrogen bonding.

The remainder of this chapter focuses primarily on the binding energies of the complexes between hetero-substituted cyclohexanes and benzene. Our main goal is to

examine the effect of heteroatom substitution on the binding energy and attempt to understand how these effects change with the number of substituent. Our discussion will begin with the oxygen and sulfur substituted complexes.

4.3.1.1 Oxygen and sulfur-substituted complexes

The optimized geometries of oxygen- and sulfur-substituted complexes are given in **Figure 4.1**. The structural parameters d_1, d_2, and α as well as the electron density parameters are summarized in **Table 4.1**.

As with cyclohexane-benzene complex, all substituted complexes have three sets of CH/π contacts (except for complex **4** with two sets of CH/π contacts). In all cases, the intermolecular distance d_1< 2.9 Å which lies in the range of the typical intermolecular distance (2.6–3.0 Å) of CH/π interaction, suggest the existence of a CH/π interaction between the two components. The binding energies (**2-8**, **Table 4.2**) of the oxygen substituted complexes (**2-8**, **Figure 4.1**) have no significant change compared to the binding energy of cyclohexane-benzene complex (10.9 kJ mol^{-1}). This is not surprised because the main attractive source of CH/π interaction is the dispersion energy. [12-17] The intermolecular distance is the most important parameter corresponded to the binding energy. As seen in **Table 4.1**, the d_1 values of complexes **2-7**, are comparable to those in the cyclohexane-benzene complex **1**. The d_1 value of complex **8**, on the other hand, is shortened about 0.01 Å with the binding energy increase slightly about 1 kJ mol^{-1}.

The binding energies of two mono substituted complexes **2** and **3** (**Figure 4.1**) are almost equivalent, 10.6 and 11.0 kJ mol^{-1}, respectively. Both complexes are **Cc** conformers. The distance between ring proton and benzene ring for the complex **2** is 2.615Å, slightly larger than that of complex **3**, which is 2.584 Å. The increase of distance of complex **2** probably

because of adjacent of oxygen which increases the electron repulsion between the π electron and the lone pairs of the oxygen atom, this may produce the decrease of binding energy. The di-oxygen substituted complexes **4** and **5** are also **Cc** conformers. Complex **4** has slightly shorter distance between the ring proton and benzene, this may result in the complex **4** has binding energy 1 kJ mol^{-1} stronger than complex **5**, although the complex **5** have one additional set CH/π interaction compared to the complex **4**. This indicates that the CH/π interaction of the ring proton is the major contribution in terms of total binding energy. This finding is support by our previous study on hydrocarbon-benzene complexes. The complex **6** has a **Ca** structure. As with the cyclohexane-benzene complex studied in previous chapter, complex **6** and complex **4** are identical in their binding energies. The tri-substituted complex **7** and **8** follow the same trend as their mono- and di- substituted complexes, which have no significant difference in compared to the cyclohexane-benzene complex, as reflected in the structural parameters and in binding energies. We speculated that 1 kJ mol^{-1} difference of two conformations may be due to the complex **7** has a shorten intermolecular distance which results in an increase of electron repulsion between π electron of benzene ring and lone pair electron of two oxygen atoms, because in this complex the two oxygen atoms connected to the ring proton. The all oxygen substituted cyclohexane-benzene complexes do not increase the binding energy appreciably.

The sulfur substituted complexes, on the other hand, increase the binding energy in all three types of substituted complexes. As with cyclohexane-benzene complex, the two mono-sulfur substituted complexes **9** (**Cc** conformer) and **10 (Ca** conformer) have almost identical binding energies. The distance between ring proton and benzene ring of complex **9** is shortened by 0.033 Å compared to that of cyclohexane-benzene complex (**1**, **Figure 4.1**). Correspondingly, there is an increase in the binding energy by 2.4 kJ mol^{-1}.

In previous chapter, we have shown that the CH/π interaction of the ring proton is the major contribution in the total binding energy. The intermolecular distance of complex **10** is shortened by 0.17 Å compared to cyclohexane-benzene complex (**1**, **Figure 4.1**) in two C–H bonds which connected sulfur atom while it is increased by 0.047 Å in one C–H bond which was opposite the sulfur atom. Compared to the shortening of the two C–H bonds, the influence of elongation of one C–H bond should be very small, as a result, the total binding energy also increase by 2.3 kJ mol^{-1}. Both the di-sulfur and tri-sulfur substituted complexes **11** and **12** are **Ca** conformation. The intermolecular distance of complex **11** is shortened by 0.24 Å compared to complex **1** in one C–H bond, which connected to two sulfur atoms, and are shortened by 0.10 Å in two other C–H bonds, which only connected to one sulfur for each of them. These close CH/π contacts are accompanied by a larger interaction energy of 15.6 kJ mol^{-1}. For the tri-sulfur substituted complex **12,** the d_1 shortening are 0.20, 0.21 and 0.22 Å for three sets of C–H bonds in this case. It is characterized a sizable binding energy of 17.8 kJ mol^{-1}. Interestingly, each successive sulfur substitution leads to an increase of ~2.3 kJ mol^{-1} in interaction energy in a uniform manner.

We also investigated the T-shape complexes of mono- and tri-sulfur substituted cyclohexane and benzene. In this conformation, only one C–H bond points to the center of the benzene and the two interacting molecules are close to perpendicular. In the T-shape complexes, the shorter molecules distance d_1 (2.435 Å and 2.339 Å for the mono- and tri-sulfur substituted complexes) leads to a significant increase in binding energies by 2.2 kJ mol^{-1} for the mono-sulfur substituted complex and 6.0 kJ mol^{-1} for the tri-sulfur substituted complex. This result reinforces our previous finding[18] that the ring proton

interaction is the major source of the total binding energy and also indicates that the effect of hetero atom is independent on the conformation of the complex.

4.3.1.2 Nitrogen and phosphorus substituted complexes

The optimized geometries of nitrogen- phosphorus- and silicon-substituted hexane-benzene complexes are shown in Figure 4.2. The structural parameters d_1, d_2, and α as well as the electron density parameters are summarized in **Table 4.3**. As with the oxygen substituted system, all the nitrogen substituted complexes (mono-, di- and tri-nitrogen substituted complexes **13-17**, Figure 4.2) yield essentially the same interaction energies, (~11 kJ mol^{-1} , **Table 4.4**) with deviation less than 1 kJ mol^{-1}. Both of the mono-nitrogen substituted complexes **13** and **14** are **Cc** conformers. The d_1 distances of the ring proton in two complexes differ by only 0.01 Å. This may explain the similar magnitude in binding energy of both complexes. In complex **14 (Cc conformer)**, one nitrogen atom is located at the top of benzene ring, this may slightly increase the repulsion between lone pair electrons of nitrogen atom and π electron of benzene, which may lead to a subtle weaker in stabilization energy in complex **14 (Table 4.4)**. The di-nitrogen substituted complex **15** (**Cc conformer**) has the same structure as complex **14**, which also have one nitrogen located at the top of benzene ring, but probably because of its longer intermolecular distance avoids a stronger repulsion between lone pair of nitrogen and π electron of benzene, thus make a slightly increase in binding energy of complex **15**. The tri-nitrogen substituted complexes **16** has a similar conformer of complex **13**, **14** and **15**, with the ring proton CH/π interaction is the main attractive force. In this complex, the two nitrogen atoms connected to the ring proton, the shorter intermolecular distance (2.556 Å, **Table 4.3**) increases the repulsion between two interacting molecules, which reduces the

stabilization energy of the complex **16**. Complex **17** has a **Ca** conformation. It has a shorter intermolecular distance compared to those in cyclohexane-benzene cmplex (2.840 Å). Accordingly, the binding energy is slightly larger (~11.4 kJ mol^{-1}).

As with the sulfur substituted complexes, the phosphorus substituted complexes (**18-21**, **Figure 4.2**), are characterized by large binding energies and the magnitude depends on the number of phosphorus substitution. The ring proton of mono-phosphorus substituted complex **18 (Cc** conformer), which connected to one phosphorus atom, the d_1 value is shortened by 0.04 Å compared to those in cyclohexane-benzene complex (**1**, **Figure 4.1**), this shortening in intermolecular distance results in a significant increase in binding energy of complex **18** by 2.7 kJ mol^{-1}. This is probably due to the sulfur and phosphorus are larger atoms have greater polarizability compared to those oxygen and nitrogen atom. This increase of polarizability in the sulfur and the phosphorus substituted complexes produces an increase in binding energy. Our previous work has confirmed that the binding energy of CH/π interaction depends on the polarizability of hydrocarbon. The binding energies of di-phosphorus substituted complexes **19 (Ca** conformer**)** and **20** (**Cc** conformer) are almost identical (**Table 4.4**). The d_1 value of ring proton in complex **20**, which connects to two phosphorus atoms, is shortened by 0.07 Å compared to the mono-phosphorus substituted complex **18**. This shortening in C–H bond leads to additional 2.6 kJ mol^{-1} increase in binding energy. The intermolecular distance of complex **19** decreases by 0.15 Å correspond to the cyclohexane-benzene complex and the binding energy of complex increases to 16.1 kJ mol^{-1}. Tri-phosphorus substituted complex **21 (Ca** conformer) causes further shortening in intermolecular distance by 0.024 Å with respect to complex **19** and gain additional 2.5 kJ mol^{-1} in binding energy. In the series complexes

18, **19** and **21**, each phosphorus atom substitution results in an increase in interaction energy of 2.5 kJ mol^{-1}. It is clear that substitution of second row element, sulfur and phosphorus, strengths the multiple CH/π interactions significantly.

4.3.1.3 Silicon substituted complexes

Finally, we examine effect of silicon substitution in cyclohexane-benzene complex. The optimized geometries of silicon-substituted complexes are given in **Figure 4.2** (**22-24**). Structural parameters d_1, d_2, and α as well as the electron density parameters are summarized in **Table 4.3**.

The mono- , di- and tri-silicon substituted complexes **22-24** (**Figure 4.2**), have the same structure with **Cc** conformer. Like the sulfur and phosphorus substituted complexes, the binding energies of three complexes increase as expected (**22-24,Table 4.4**), each of the first and second silicon substituent leads 2.6 and 3.0 kJ mol^{-1} increase in binding energy, the third substitution only introduce 1 kJ mol^{-1} increase in binding energy. The distances of ring proton and benzene ring of three complexes range from 2.540 to 2.597 Å, which have no significant change in comparison with that of cyclohexane-benzene complex, but the binding energy changes significant. This probably because the silicon atom which shows a stronger positive charge than any of other atoms in the substituted complexes leads an increase in electrostatic interaction greatly and finally increases the total interaction energy.

4.3.2 AIM analysis

To gain a better understanding on the nature of the multiple CH/π interactions of the hydrocarbon–benzene complexes and the effects of heteroatom substitution, we have also examined the topological properties of the electron density using Bader's theory of atoms in molecules (AIM) [31]. For each of the multiple CH/π contacts of the various complexes examined here, there exists a bond path linking the hydrogen atom with one carbon atom of benzene. The calculated topological properties at the bond critical points, namely electron density (ρ), Laplacian of electron density ($\nabla_2\rho$), are summarized in **Tables 4.1** and **4.3**. The positive sign of the $\nabla_2\rho$ indicates the closed-shell nature of interaction, e.g. hydrogen bond.[33] For all the CH/π contacts, the small ρ and positive $\nabla_2\rho$ values are similar to the characteristic topological properties of a weak hydrogen bond, such as CH···O and OH···π interactions.[16] As seen in these tables, the sulfur-, phosphorus- and silicon- complexes are characterized by large ρ and $\nabla_2\rho$ values compared to the corresponding oxygen- and nitrogen- complexes. As reflected in the calculated of the binding energies, the oxygen and nitrogen substitution do not increase the binding energies of the multiple CH/π systems, while the sulfur, phosphorus and silicon substitution increase the binding energies significantly.

4.3.3 NBO and Polariability analysis

To obtain further insight into the nature of the effects of heteroatom on cyclohexane-benzene complex, we examine the correlation of the polarizability of the substituted cyclohexane and the total interaction energy. As evidenced in **Figure 4.3**, a reasonable correlation (R^2 = 0.92) is found between the interaction energies and calculated

polarizabilities [MP2/6-31G(d)] for the series of hydrocarbon–benzene complexes. This result confirms that the stabilization energy depends essentially on the polarizability of the hydrocarbon. In addition, we examine the relationship of the calculated charge transfer and interaction energy. Indeed, a very strong correlation (R^2 = 0.97) is found (**Figure 4.4**) between the interaction energies and calculated charge transfer [MP2/6-31G(d,)] for the series of benzene complexes examined. Thus, we can safely conclude that the heteroatom sulfur, phosphorus and silicon connect to the C–H bond in cyclohexane, increase the charge transfer of the interacting molecules and result in an increase in the stabilization energy of the substituted cyclohexane-benzene multiple CH/π interactions.

4.4 Conclusion

In conclusion, we have investigated the effects of heteroatom substitution, namely, N, O, Si, P and S substitution on cyclohexane of cyclohexane-benzene complex using high-level ab initio calculations. The calculated binding energies reveal that oxygen and nitrogen substitution has little effect on the interaction energy, even with the increase the number of heteroatom atom. On the other hand, substitution with the second-row elements Si, P and S leads to significant increase in stabilization energy, with each substitution worth about 2.0–2.5 kJ mol^{-1} increase in interaction energy. The sulfur, phosphorus and silicon substituted complexes are characterized by significant increase in charge transfer between two molecules, subsequently increase the interaction energy significantly. The stabilization energy depends essentially on the polarizability of the substituted hydrogencarbons. The calculated interaction energy (11–19 kJ mol^{-1}) is close to normal hydrogen bond. Considered sulfur, phosphorus and silicon substituted hydrocarbon and

aromatic functional groups are very common in organic molecules and especially abundant in biomolecules, we can expect that the multiple CH/π interactions are extremely important in understanding of many aspects of chemistry, biochemistry and material science.

4.5 References

1 Nishio, M.; Hirota, M.; Umezawa, Y. *The CH/π interaction*; Wiley VCH: New York, 1998.

2 Hobza, P.; Havlas, Z. *Chem. Rev*. **2000**, *100*, 4253.

3 Tarakeshwar, P.; Choi, H. S.; Kim, K. S. *Chem. Rev*. **2000**, *100*, 4145.

4 Nishio, M. *Cryst. Eng. Comm*. **2004**, *6*, 130.

5 Kodma, Y.; Nishihata, K.; Nishio, M.; Nakagawa, N. *Tetrahedron Lett.* **1977**,2105.

6 Umezawa, Y.; Tsuboyama, S.; Takahashi, H.; Uzawa, J.; Nishio, M. *Tetarahedron* **1999**, *55*, 10047, and references therein.

7 Takahashi, H.; Tsuboyama, S.; Umezawa, Y.; Honda, K.; Nishio, M. *Tetarahedron* **2000**, *56*, 6185, and references therein.

8 Umezawa, Y.; Tsuboyama, S.; Takahashi, H.; Uzawa, J.; Nishio, M. *Bioorg. Med. Chem*. **1999**, *7*, 2021, and references therein.

9 Chakrabarti, P.; Samanta, U. *J. Mol. Biol*. **1995**, *251*, 9.

10 Brandi, M.; Weiss, M. S.; Jabs, A.; Suhnel, J.; Hilgenfeld, R. *J. Mol. Biol*. **2001**, *307*, 357.

11 Muraki, M. *Protein Peptide Lett*. **2002**, *9*, 195.

12 (a) Tsuzuki, S.; Uchimaru, T.; Mikami. M.; Tanabe, K. *J. Phys. Chem A* **1998**, *103*, 8265. (b) Tsuzuki, S.; Honda, K.; Uchimaru, T.; Mikami, M.; Tanabe, K. *J. Am. Chem. Soc*. **2000**, *122*, 3746. (c) Tsuzuki, S.; Honda, K.; Uchimaru, T.; Mikami, M.; Tanabe, K. *J. Phys. Chem. A* **2002***, 106,* 4423.

13 (a) Tarakeshwar, P.; Choi, H. S.; Kim, K. S. *J. Am. Chem. Soc*. **2001**, *123*, 3323. (b) Lee, E. C.; Hong, B. Y.; Lee, J. Y.; Kim, J. C.; Kim, D.; Kim, Y.; Tarakeshwar, P.; K, S.; Kim, K. S. *J. Am. Chem. Soc.* **2005**, *127*, 4530.

14 (a) Hobza, P.; Spirko, V.; Selzle, H. L.; Schlag, E. W. *J. Phys. Chem. A* **1998**, *102*, 2501. (b) Hobza, P.; Spirko, V.; Havalas, Z.; Buchhold, K.; Reimann, B.; Barth, H. D.; Bruthschy, B. *Chem. Phys. Lett*. **1999**, *299*, 180. (c) Reimann, B.; Buchhold, K.; Vaupel, S.; Brutschy, B.; Havlas, Z.; Spirko, V.; Hobza, P. *J. Phys. Chem. A* **2001**, *105*, 5560.

15 (a) Takahashi, O.; Kohno, Y.; Iwasaki, S.; Saito, K.; Tomdoa, S.; Umezawa, Y.; Nishio, M. *Bull. Chem. Soc. Jpn.* **2001**, *74*, 2421. (b) Takahashi, O.; Kohno, Y.; Saito, K.; Nishio, M. *Chem. Eur. J.* **2003**, *9*, 756. (c) Takahashi, O.; Kohno, Y.; Saito, K. *Chem. Phys. Lett*. **2003**, *378*, 509.

16 Novoa, J. J.; Mota, F. *Chem. Phys. Lett*. **2000**, *318*, 45.

17 (a) Takagi, T.; Tanaka, A.; Matsuo, S.; Maezaki, H.; Tani, M.; Fujiwara, H.; Sasaki, Y. *J Chem. Soc. Perkin Trans. II* **1987**, 1015. (b) Sakaki, S.; Kato, K.; Miyazaki, T.; Musashi, Y.; Ohkubo, K.; Ihara, H.; Hirayama, C. *J. Chem. Soc. Faraday Trans* **1993**, *89*, 659. (c) Samanta, U.; Chakrabarti, P.; Chandrasekhar, J. *J. Phys. Chem. A* **1998**, *102*, 8964. (d) Oki, M.; Takano, S.; Toyota, S. *Bull. Chem. Soc. Jpn*. **2000**, *73*, 2221. (e) Sinnokrot, M. O.; Valeev, E. F.; Sherrill, C. D. *J. Am. Chem. Soc.* **2002**, *124,* 10887. (f) Sinnokrot, M. O.; Sherrill, C. D. *J. Am. Chem. Soc.* **2004**, *126*, 7690.

18 (a) Karatsu, M.; Suezawa, H.; Abe, K.; Hirota, M.; Nishio, M. *Bull. Chem. Soc. Jpn.* 1**986**, *59*, 3529. (b) Nakai, Y.; Yamamoto, G.; Oki, M. *Chem. Lett*. **1987**, 89.

(c) Nakai, Y.; Inoue, K.; Yamamoto, G.; Oki, M. *Bull. Chem. Soc. Jpn*. **1989**, *62*, 2923. (d) Suezawa, H.; Mori, A.; Sato, M.; Ehama, R.; Akai, I.; Sakakibara, K.; Hirota, M.; Nishio, M.; Kodama, Y. *J. Phys. Org. Chem*. **1993**, *6*, 399. (e) Ehama, R.; Tsushima, M.; Yuzuri, T.; Suezawa, H.; Sakakibara, K.; Hirota, M. *Bull. Chem. Soc. Jpn*. **1993**, *66*, 814. (f) Suezawa, H.; Hashimoto, T.; Tsuchinaga, K.; Yoshida, T.; Yuzuri, T.; Sakakibara, K.; Hirota, M.; Nishio, M. *J. Chem. Soc., Perkin Trans. 2* **2000**, 1243.

19 Gu, Y.L.; Kar, T.; Scheiner, S. *J. Am. Chem. Soc*. **1999**, *121*, 9411.

20 Tsuzuki, S.; Honda, K.; Uchimaru, T.; Mikami, M.; Tanabe, K. *J. Phys. Chem. A* **2002**, *106*, 4423.

21 Takahashi, O.; Kohno, Y.; Saito, K. *Chem. Phys. Lett*. **2003**, *378*, 509.

22 Sinnokrot, M. S.; Sherrill, C. D. *J. Am. Chem. Soc*. **2004**, *126,* 7609.

23 (a) Pople, J. A.; Head-Gordon, M.; Raghavachari, K. *J. Chem. Phys.* **1987**, *87*, 5968. (b) Head-Gordon, M.; Pople, J. A.; Frisch, M. J. *Chem. Phys. Lett*. **1988**, *153*, 503. (c) Scuseria, G. E.; Schaefer, H. F., III, *J. Chem. Phys.* **1989**, *90*, 3700.

24 Tsuzuki, S.; Honda, K.; Uchimaru, T.; Mikami, M.; Tanabe, K. *J. Phys. Chem. A* **1999**, *103*, 8265.

25 Boys, S. F.; Bernardi, F. *Mol. Phys*. **1970**, *19*, 553.

26 Scott, A. P.; Radom, L. *J. Phys. Chem*. **1996**, *100*, 16502.

27 Werner, H.-J.; Knowles, P. J.; Schütz, J. M.; Lindh, R.; Celani, P.; Korona, T.; Rauhut, G.; Manby, F. R.; Amos, R. D.; Bernhardsson, A.; Berning, A.; Cooper, D. L.; Deegan, M. J. O.; Dobbyn, A. J.; Eckert, F.; Hampel, C.; Hetzer, G.; Lloyd, A. W.; McNicholas, S. J.; Meyer, W.; Mura, M. E.; Nicklaß, A.; Palmieri, P.; Pitzer,

R.; Schumann, U.; Stoll, H.; Stone, A. J.; Tarroni, R.; Thorsteinsson, T. *MOLPRO*, version 2002; University of Birmingham, 2002.

28 Frisch, M. J.; Trucks, G. W.; Schlegel, H. B.; Scuseria, G. E.; Robb, M. A.; Cheeseman, J. R.; Montgomery, Jr., J. A.; Vreven, T.; Kudin, K. N.; Burant, J. C.; Millam, J. M.; Iyengar, S. S.; Tomasi, J.; Barone, V.; Mennucci, B.; Cossi, M.; Scalmani, G.; Rega, N.; Petersson, G. A.; Nakatsuji, H.; Hada, M.; Ehara, M.; Toyota, K.; Fukuda, R.; Hasegawa J.; Ishida, M.; Nakajima, T.; Honda, Y.; Kitao, O.; Nakai, H.; Klene, M.; Li, X.; Knox, J. E.; Hratchian, H. P.; Cross, J. B.; Adamo, C.; Jaramillo, J.; Gomperts, R.; Stratmann, R. E.; Yazyev, O.; Austin, A.; Cammi, J., R.; Pomelli, C.; Ochterski, J. W.; Ayala, P. Y.; Morokuma, K.; Voth, G. A.; Salvador, P.; Dannenberg, J. J.; Zakrzewski, V. G.; Dapprich, S.; Daniels, A. D.; Strain, M. C.; Farkas, O.; Malick D. K.; Rabuck, A. D.; Raghavachari, K.; Foresman, J. B., Ortiz, J. V.; Cui Q.; Baboul, A. G.; Clifford S.; Cioslowski, J., Stefanov, B. B.; Liu, G.; Liashenko, A. Piskorz, P.; Komaromi, I.; Martin, R. L.; Fox, D. J.; Keith, T.; Al-Laham, M. A.; Peng, C. Y.; Nanayakkara, A.; Challacombe, M.; Gill, P. M. W.; Johnson, B.; Chen, W.; Wong, M. W.; Gonzalez, C.; Pople, J. A. *Gaussian 03*, Gaussian, Inc., Wallingford CT, 2004.

29 Frisch, M. J.; Trucks, G. W.; Schlegel, H. B.; Scuseria, G. E.; Robb, M. A.; Cheeseman, J. R.; Montgomery, Jr., J. A.; Vreven, T.; Kudin, K. N.; Burant, J. C.; Millam, J. M.; Iyengar, S. S.; Tomasi, J.; Barone, V.; Mennucci, B.; Cossi, M.; Scalmani, G.; Rega, N.; Petersson, G. A.; Nakatsuji, H.; Hada, M.; Ehara, M.; Toyota, K.; Fukuda, R.; Hasegawa J.; Ishida, M.; Nakajima, T.; Honda, Y.; Kitao, O.; Nakai, H.; Klene, M.; Li, X.; Knox, J. E.; Hratchian, H. P.; Cross, J. B.; Adamo, C.; Jaramillo, J.; Gomperts, R.; Stratmann, R. E.; Yazyev, O.; Austin, A.;

Cammi, J., R.; Pomelli, C.; Ochterski, J. W.; Ayala, P. Y.; Morokuma, K.; Voth, G. A.; Salvador, P.; Dannenberg, J. J.; Zakrzewski, V. G.; Dapprich, S.; Daniels, A. D.; Strain, M. C.; Farkas, O.; Malick D. K.; Rabuck, A. D.; Raghavachari, K.; Foresman, J. B., Ortiz, J. V.; Cui Q.; Baboul, A. G.; Clifford S.; Cioslowski, J., Stefanov, B. B.; Liu, G.; Liashenko, A. Piskorz, P.; Komaromi, I.; Martin, R. L.; Fox, D. J.; Keith, T.; Al-Laham, M. A.; Peng, C. Y.; Nanayakkara, A.; Challacombe, M.; Gill, P. M. W.; Johnson, B.; Chen, W.; Wong, M. W.; Gonzalez, C.; Pople, J. A. *Gaussian 03*, Gaussian, Inc., Wallingford CT, 2004.

30 (*a*) Bader, R. F. W. *Atoms in Molecules—A Quantum Theory*; Oxford Science Publications: Oxford, **1990**. (*b*) Bader, R. F. W. *Chem. Rev.*, **1991**, *91*, 893.

31 Popelier P. L. A.; Bone, R. G. A. *MORPHY98*; UMIST, Manchester, **1998**.

32 Reed, A. E.; Curtiss, L. A.; Weinhold, F. *Chem. Rev*. **1988**, *88*, 899

33 Koch, U.; Popelier, P. L. A. *J. Phys. Chem*. **1995**, *99*, 9747.

4.6 Appendix

Table 4.1 Calculated Structural Parameters (d_1, d_2 and α)[a] and Topological Properties[b] (ρ, $\nabla_2\rho$, in au) at the Bond Critical Point of Various Cyclohexane–benzene Complex and its Oxygen and Sulfur analogues (**1**–**12**), Evaluated at the MP2/6-31G(d) Level

hydrocarbon	label	d_1	d_2	α	ρ	$\nabla_2\rho$
C_6H_{12} (**1**)	1	2.578	0.260	179.8	0.0068	0.0222
	2	2.697	2.386	175.4	0.0049	0.0140
	3	2.700	2.386	175.3	0.0048	0.0139
$C_6H_{10}O$ (**2**)	1	2.615	0.346	169.5	0.0067	0.0215
	2	2.653	2.282	171.6	0.0057	0.0168
	3	2.964	2.159	169.3	0.0038	0.0104
$C_6H_{10}O$ (**3**)	1	2.584	0.311	179.8	0.0069	0.0225
	2	2.746	2.348	173.1	0.0047	0.0132
	3	2.750	2.347	173.1	0.0047	0.0132
$C_6H_8O_2$ (**4**)	1	2.569	0.264	162.8	0.0072	0.0229
	2	2.687	2.336	162.1	0.0052	0.0148
$C_6H_8O_2$ (**5**)	1	2.589	0.365	172.5	0.0069	0.0227
	2	2.848	2.057	171.9	0.0049	0.0136
	3	2.841	2.046	172.0	0.0050	0.0139
$C_6H_8O_2$ (**6**)	1	2.842			0.0062	0.0176
	2	2.849			0.0062	0.0178
	3	2.899			0.0051	0.0143
$C_6H_6O_3$ (**7**)	1	2.567	0.373	172.9	0.0074	0.0238
	2	2.875	2.013	170.9	0.0047	0.0131
	3	2.853	2.009	171.0	0.0049	0.0139
$C_6H_6O_3$ (**8**)	1	2.838			0.0060	0.0176

	2	2.838			0.0061	0.0176
	3	2.853			0.0061	0.0176
$C_6H_{10}S$ (**9**)	1	2.545	0.451	173.7	0.0079	0.0255
	2	2.837	2.147	170.5	0.0046	0.0131
	3	2.508	2.425	173.5	0.0062	0.0229
$C_6H_{10}S$ (**10**)	1	2.671			0.0080	0.0239
	2	2.897			0.0054	0.0157
	3	2.672			0.0080	0.0239
$C_6H_8S_2$ (**11**)	1	2.602			0.0091	0.0269
	2	2.739			0.0071	0.0210
	3	2.739			0.0071	0.0210
$C_6H_6S_3$ (**12**)	1	2.624			0.0088	0.0259
	2	2.632			0.0086	0.0254
	3	2.638			0.0085	0.0251

[a] Bond lengths in Å and angles in degrees.

[b] Based on AIM analysis.

[c] See Fig 4.1 for hydrogen labeling.

Table 4.2 Calculated Binding Energies and Bond Characteristics of Various Oxygen- and Sulfur-Substituted CH/π complexes

Conformer[a]	BE[b]	Δd_1[c,d]	$\Delta\nu$[d,e]	Dipole[d,f]	CT[d,g]
1	–10.9	-0.0033	23.6	0.65	0.0078
2	–10.6	-0.0028	20.9	2.24	0.0076
3	–11.0	-0.0038	48.3	1.98	0.0076
4	–11.2	-0.0044	65.6	2.73	0.0078
5	–10.2	-0.0038	54.3	3.06	0.0074
6	–11.4	-0.0017	22.9	3.01	0.0079
7	–11.0	-0.0043	52.4	3.31	0.0085
8	–11.9	-0.0020	25.2	3.40	0.0083
9	–13.3	-0.0025	18.0	2.17	0.0086
10	–13.2	-0.0012	6.2	2.34	0.0094
11	–15.6	-0.0015	14.6	3.07	0.0111
12	–17.8	-0.0012	14.1	3.57	0.0138

[a] See Figure 4.1 for various complexes.

[b] Binding energies (BE, kJ mol^{-1}) evaluated at CCSD(T)/aug(d,p)-6-311G**+ZPE+BSSE level.

[c] bond distance shortening (Δd_1, Å)) upon complex formation.

[d] MP2/6-31G(d) level.

[e] C-H stretching frequency shift ($\Delta\nu$, cm^{-1}) upon complex formation.

[f] Dipole moments in D.

[g] Charge transfer (CT, e), based on NBO analysis, upon complex formation.

Table 4.3 Calculated Structural Parameters (d_1, d_2 and α)[a] and Topological Properties[b] (ρ, $\nabla_2\rho$, in au) at the Bond Critical Point of Various benzene Complexes of Nitrogen, Phosphorus and Silicon analogues of cyclohexane (**13**–**24**), Evaluated at the MP2/6-31G(d) Level

hydrocarbon	label	d_1	d_2	α	ρ	$\nabla_2\rho$
$C_6H_{11}N$ （**13**）	1	2.585	0.289	178.8	0.0068	0.0223
	2	2.674	2.368	175.6	0.0050	0.0146
	3	2.685	2.366	175.4	0.0050	0.0146
$C_6H_{11}N$ （**14**）	1	2.575	0.335	175.1	0.0070	0.0231
	2	2.663	2.292	174.1	0.0055	0.0159
	3	2.810	2.285	172.7	0.0044	0.0125
C_6H10N_2（**15**）	1	2.583	0.365	176.4	0.0070	0.0230
	2	2.654	2.258	174.7	0.0056	0.0164
	3	2.771	2.273	173.9	0.0046	0.0134
$C_6H_9N_3$（**16**）	1	2.556	0.369	178.5	0.0074	0.0242
	2	2.716	2.163	174.3	0.0054	0.0158
	3	2.703	2.161	174.5	0.0055	0.0162
$C_6H_9N_3$ （**17**）	1	2.792			0.0064	0.0192
	2	2.778			0.0066	0.0197
	3	2.775			0.0066	0.0198
$C_6H_{11}P$ （**18**）	1	2.537	0.335	168.1	0.0075	0.0248
	2	2.863	2.306	169.0	0.0040	0.0112
	3	2.423	2.674	169.8	0.0057	0.0174
$C_6H_{10}P_2$（**19**）	1	2.693			0.0082	0.0246
	2	2.861			0.0063	0.0185
	3	2.813			0.0064	0.0186
$C_6H_{10}P_2$（**20**）	1	2.469	0.444	174.7	0.0089	0.0290
	2	2.503	2.627	177.0	0.0053	0.0157
	3	2.507	2.623	177.0	0.0053	0.0157

$C_6H_9P_3$ （**21**）	1	2.669			0.0079	0.0238
	2	2.669			0.0079	0.0238
	3	2.669			0.0079	0.0238
$C_6H_{12}Si$ （**22**）	1	2.597	0.376	168.9	0.0069	0.0225
	2	2.444	2.832	172.0	0.0048	0.0145
	3	2.749	2.305	173.8	0.0047	0.0134
$C_6H_{12}Si_2$（**23**）	1	2.540	0.465	170.9	0.0079	0.0257
	2	2.440	2.845	177.1	0.0048	0.0145
	3	2.443	2.843	177.2	0.0048	0.0145
$C_6H_{12}Si_3$ (**24**)	1	2.573	0.587	174.7	0.0080	0.0256
	2	2.446	2.652	178.2	0.0057	0.0175
	3	2.449	2.649	178.1	0.0057	0.0175

[a] Bond lengths in Å and angles in degrees.

[b] Based on AIM analysis.

[c] See Fig 4.2 for hydrogen labeling.

Table 4.4 Calculated Binding Energies and Bond Characteristics of Various Nitrogen-, Phosphorus- and Silicon-Substituted CH/π complexes

CH/π complex[a]	BE[b]	Δd_1[c,d]	$\Delta\nu$[d,e]	Dipole[d,f]	CT[d,g]
13	–11.2	-0.0028	21.0	1.43	0.0081
14	–10.6	-0.0029	22.2	1.06	0.0081
15	–11.1	-0.0028	20.0	1.49	0.0085
16	–10.5	-0.0022	19.3	1.34	0.0089
17	–11.4	-0.0010	5.8	1.22	0.0090
18	–13.6	-0.0025	21.8	1.50	0.0093
19	–16.1	-0.0015	12.2	1.72	0.0121
20	–16.2	-0.0026	25.5	1.39	0.0116
21	–18.6	-0.0010	8.3	1.31	0.0135
22	–13.5	-0.0020	15.0	1.21	0.0096
23	–16.5	-0.0016	13.4	1.58	0.0119
24	–17.5	-0.0013	8.5	2.18	0.0130

[a] See Figure 4.2 for various complexes.

[b] Binding energies (BE, kJ mol^{-1}) evaluated at CCSD(T)/aug(d,p)-6-311G**+ZPE+BSSE level.

[c] bond distance shortening (Δd_1, Å)) upon complex formation.

[d] MP2/6-31G (d) level.

[e] C-H stretching frequency shift ($\Delta\nu$, cm^{-1}) upon complex formation.

[f] Dipole moments in D.

[g] Charge transfer (CT, e), based on NBO analysis, upon complex formation.

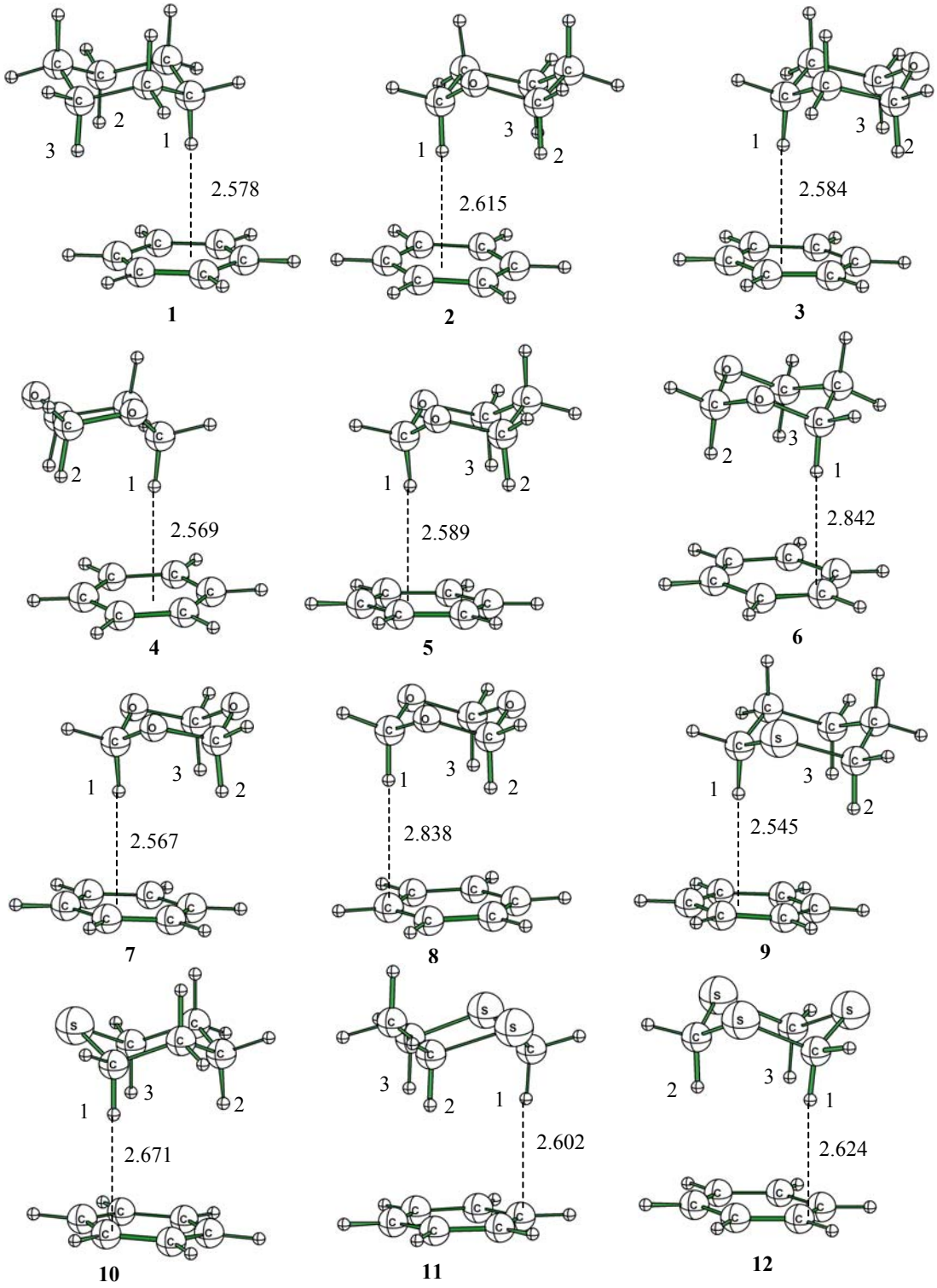

Figure 4.1 Optimized (MP2/6-31G (d)) geometries of various oxygen-, sulfur-substituted hydrocarbon-benzene CH/π complexes. Only the ring CH/π interaction (in dash line) is shown.

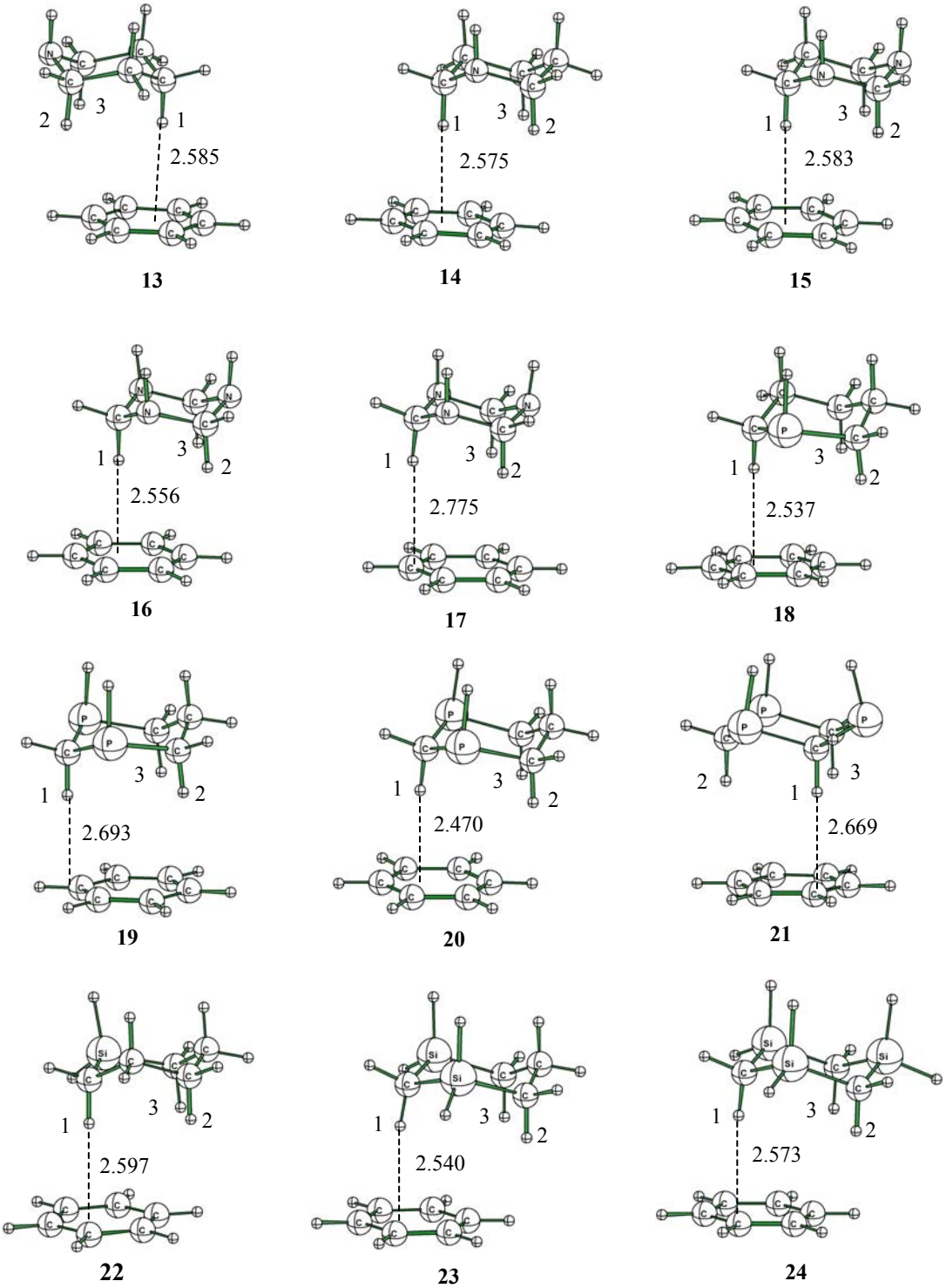

Figure 4.2 Optimized (MP2/6-31G (d)) geometries of various nitrogen-, phosphorus- and silicon-substituted hydrocarbon–benzene CH/π complexes. Only the ring CH/π interaction (in dash line) is shown.

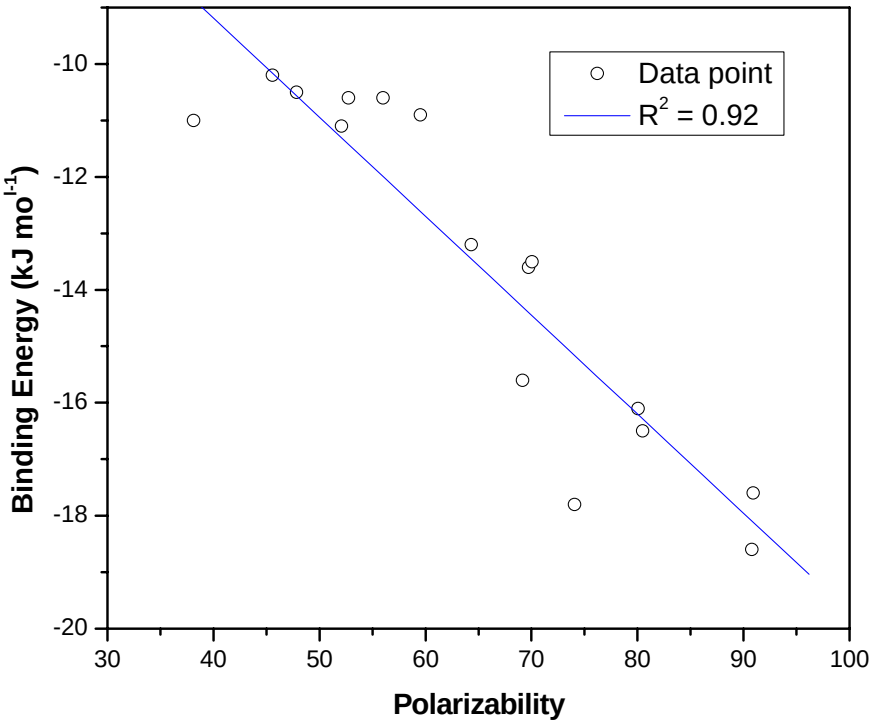

Figure 4.3 Plot of binding energy against polarizability.

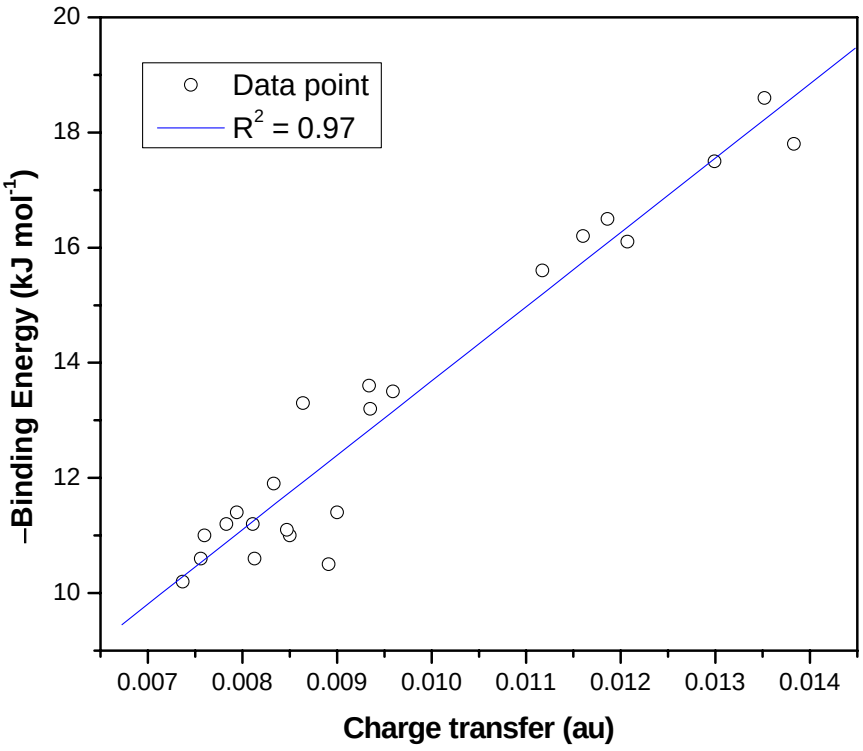

Figure 4.4 Plot of binding energy against charge transfer.

Chapter 5 A Theoretical Study of Cooperative XH/π (X= C or N) Interactions in Proline and Phenylalanine Complex

5.1 Introduction

Hydrogen bonding plays a key role in structures and functions of proteins, including features such as overall folding, local architecture, protein-ligand recognition, enzymatic activity, protein hydration and molecular dynamics.[1] For a long time, research has focused mainly on hydrogen bonds X–H···Y with both X and Y are electronegative atoms (mostly O and N). The structural aspects of these classic hydrogen bonds in proteins are well studied, and have been reviewed by Baker and Hubbard.[2] In structural biology, some of the 'non-conventional' hydrogen bonds have recently been shown to be of great importance, in particular the variants CH···O,[3] and O/NH···π. Surveys of earlier structural biology literature have been given for the special case NH···π [4] and CH···O, [5] for "weak polar interaction" in a wide sense [6] and for the whole field of non-conventional hydrogen bond.[7] Hydrogen bond between donor X–H and the π electron cloud of an aromatic moiety (called XH/π hydrogen bonds) was discovered by Wulf et al [8] and are today well documented for organic structure chemistry.[9] The geometry of XH/π hydrogen bond is very soft, even softer than that of conventional hydrogen bonds, allowing large lateral displacements of the donor, and strong bending of the hydrogen bond angle without much of change in energy.[10] In fact, X–H may point at the center area of an aromatic ring, at particular C–C bonds, or even at individual C atom.[11]

The polar C–H groups also can form intermolecular interactions with aromatic groups.[12] For instance, in a recent study, [13] Weiss and co-workers found 3×10^5 CH/π contacts in a database of 1000 proteins, which means that about three-quarters of all Trp and one half of all Tyr and Phe residues participate in these interactions in the interior of proteins. This finding supports previous suggestions about the relevant contribution of CH/π interactions to the folding of protein[14] and reinforces their significant structural and functional roles in biomacromolecules and supramolecular chemistry.

The intermolecular interaction of the natural amino acids is of special interest because it determines the functional specificity of proteins and polypeptides.[15] Proline has a very special conformation among 20 natural amino acids. [15] Its nitrogen atom is bonded to the aliphatic side chain forming the five membered pyrrolidine ring. This cyclic conformation may interact with aromatic ring forming a strong complex by cooperative XH/π interaction. In addition, the high polar NH bond will also contribute a significantly stronger NH/π interaction. To gain a better insight into the role of CH/π and NH/π interaction in proteins, in this chapter, we present a high-level *ab initio* study of the benzene complexes of pyrrolidine-2-carbaldehyd (PCA), cyclopentanecarbaldehyde (CCA) and proline as well as proline-phenylalanine complex. We investigate the magnitude of interaction energies in the amino acid complexes and the directionality of such complexes.

5.2 Computational Methods

Dispersion interaction is an important factor for the proper description of both the geometries and binding energies of the weak hydrogen bond CH/π and NH/π complexes.[16-21] Our previous work has demonstrated that both Hartree–Fock (HF) and

density functional theory (DFT) methods underestimate the binding energies of the CH/π related complexes. Thus geometry optimization of all the complexes examined here were carried out at the MP2/6-31G (d) level. Frequency analysis was also performed at the same level of theory to confirm the optimized structure as a local energy minimum and to evaluate zero-point energy (ZPE) correction (scaled by 0.967).[22] Previous theoretical studies have established undoubtedly that a large basis set including multiple polarization functions and appropriate electron correlation are necessary to accurately evaluate the interaction energies of XH/π complexes.[16-20] Thus, more reliable prediction of binding energies were obtained via higher-level single-point calculations at the CCSD(T) level in conjugation with a large aug(d,p)-6-311G(d,p) basis set, proposed by Tsuzuki et al.[18,21] Correction for basis set superposition error (BSSE), based on the counterpoise method,[23] was including in the final calculated binding energy. Charge density analysis, based on Bader's theory of atoms in molecules (AIM) [24] was carried out using the Morphy98 program.[25] All other calculations were performed using the Molpro2002[26] and Gaussian 98 programs. [27]

5.3 Results and discussion

5.3.1 PCA-benzene and CCA-benzene complexes

5.3.1.1 Geometry parameters and Electron properties

There are several important structural parameters which characterize a XH/π interaction, namely d_1, d_2 and α (see Scheme 3.1). O is the centre (centroid) of the aromatic ring, while X represents the projection point of a C–H hydrogen on the molecular plane of aromatic ring. Thus, d_1 corresponds to the non-bonded intermolecular

distance, d_2 represents the distance of the projection point away from the benzene centre (O) and α is the CHX angle. Based on previous experimental and theoretical studies,[11,29] the characteristic properties of a typical XH/π interaction are: (1) the intermolecular distance d_1 is in the range 2.6–3.0 Å, (2) the C–H bond points close to the centre of an aromatic ring, and (3) the CHX angle (α) is close to linearity, and (4) the C–H bond length is shorten upon complexation, which leads to a higher C–H stretching frequency.

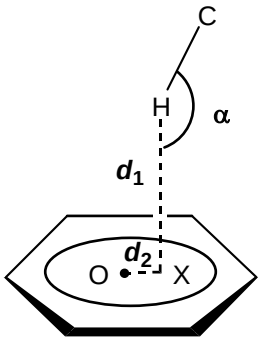

We begin our discussion on the benzene complex of a simple model system of proline, pyrrolidine-2-carbaldehyd (PCA) and cyclopentanecarbaldehyde (CCA). We found two stable conformations for each complex. The optimized geometries of two conformations of the PCA– and CCA–benzene complexes are shown in **Fig 5.1** (**1-4**). Selected structural parameters, d_1, d_2 and α, are listed in **Table 5.1**. All conformations of each complex favor multiple XH/π contacts. This clearly demonstrates that several X–H groups can interact with the π face of benzene in a cooperatively manner.

Each NH or CH/π contact of all the complexes (**1**–**4**) is characterized by a short contact distance d_1 < 3.0 Å and a bond critical point (see below). The intermolecular distances (d_1) lie in the range of 2.36–2.40 Å for NH/π and 2.55–2.84 Å for CH/π (**Table 5.1**). This is in good agreement with the statistical analysis, based on both Cambridge

Crystallographic Database (CSD) analysis for the crystal structures with a saturated type of C–H bonds (~2.7 Å) [29-32] and Brookhaven Protein Data Bank (PDB) (~2.5 Å).[11] In all cases (**1**–**4**), the complex geometry has one C–H or N–H group directs toward the centre of the benzene ring (we shall designate this hydrogen as "ring" hydrogen). The other CH/π contacts lie outside the benzene ring and are located in specific regions defined by the C–C and C–H bonds. In general, the ring C–H or N–H hydrogen has the shortest contact distance (d_1) among all the C–H groups facing the π face of benzene (**Table 5.1**). Accordingly, the XHO angle (α) associated the ring hydrogen is larger. The angle between XH and aromatic ring varied from 134.8 to 171.2°, this suggests that the XH/π interaction could adopt a slightly bent orientation in contrast to the classic hydrogen bond which only prefers a linear orientation. In other words, the XH/π interaction has a max flexible directionality than normal hydrogen bond.

All the ring hydrogens lie somewhat offset the centre of the benzene ring, d_2 is around 0.40 Å, which map well with the electrostatic potential of benzene in our previous chapter. It thus appears that the most stable geometry of each XH/π complex favors a maximum overlap of the electropositive X–H hydrogens with the electron rich regions of benzene. Hence, we conclude that the geometries and directionalities of interaction of the XH/π complexes are determined mainly by electrostatic interaction between the interacting molecules.

To gain a better understanding on the nature of the cooperative XH/π interactions of the model complexes (**Figure 5.1**), we have examined the topological properties of the electron density using Bader's theory of atoms in molecules (AIM) [24] at the MP2/6-31G

(d,p) level. Previous theoretical study by Novoa and Mota have shown that the XH/π interaction can be characterized by a bond path and its associated bond critical point (bcp).[33] For each of the multiple XH/π contacts of the various complexes examined here, there exists a bond path linking the hydrogen atom with one or more carbon atoms of benzene. The calculated topological properties at the bond critical points, namely electron density (ρ) and Laplacian of electron density ($\nabla_2\rho$), are summarized in **Table 5.1**. The positive sign of the $\nabla_2\rho$ indicates the closed-shell nature of interaction, e.g. hydrogen bond.[34] For all the CH/π contacts, the small ρ and positive $\nabla_2\rho$ values are similar to the characteristic topological properties of a weak hydrogen bond, such as CH···O and OH···π interactions.[33] There is the stronger π interaction in the ring C–H or N–H bond compared to the other XH/π interactions outside the benzene ring which reflected in the larger ρ and $\nabla_2\rho$ values compared to those XH/π bonds outside the ring.

The electron densities (ρ) at each bcp vary from 0.0034 to 0.0097 au and the laplacian of electron density ($\nabla_2\rho$) at bcp vary from 0.0108 to 0.0340. These values are consisent with the criteria proposed by Popelier [35] for the existence of hydrogen bonding. The typical range for hydrogen bonding is between 0.002 and 0.034 au for ρ value. In conclusion, the CH/π as well as NH/π interactions exhibit the characteristic of a typical hydrogen bond.

5.3.1.2 Interaction energy of PCA-benzene and CCA-benzene complexes.

The interaction energies of the two conformations of PCA–benzene complex are almost equivalent at the CCSD(T)-aug-(d,p)-6311G(d,p) level and the binding energies are 19.5 and 19.9 kJ mol^{-1}, (**Table 5.2**) respectively. These values are very close to the

hydrogen bond energy of water dimer [28] (20 kJ mol^{-1}). This result indicates that there is strong attractive interaction between π face of benzene ring and PCA. Given the fact that the benzene is a prototype aromatic system and a very common organic solvent, we believe that such interaction may compete with classic hydrogen bond in solvation of the biological molecules. The larger interaction energy can be explained by the cooperative multiple XH/π interaction. In this model system, by using the AIM theory, one unit of NH/π and three units of CH/π interactions were identified.

The interaction energies (binding energy) were also calculated at the MP2 method using various basis sets to evaluate the basis set effect. The binding energies calculated at the 6-311+G (d, p) basis set are greater than those calculated at the 6-31G (d) basis set. For both conformations, the binding energy increases by 6 to 7 kJ/mol. This result indicates that both diffuse and polarization functions are very important for the calculation of XH/π interaction. Our best results were calculated at the aug(C, H)-6-311G** basis set proposed by S, Tsuzuki,[19,22] this augmented basis set evaluates dispersion energy (which is believed to be the most important contribution of XH/π interaction) more efficiently than the standard basis set. We also calculated binding energy at aug-(C,H,N)-6-311G** basis set, which included the augmented basis set for the nitrogen atom. The calculated binding energies are almost identical with those augmented only carbon and hydrogen atoms. This is perhaps not surprising because in this complex, the electron donor is π face of benzene ring, so the inclusion of diffuse function on the nitrogen atom has very little effect on the binding energy of the system. This result also suggests that if the complexes are composed of pyridine, furan or thiophone molecules instead of benzene as the electron

donor, the inclusion of diffuse function for nitrogen, sulfur or oxygen atoms may lead to a significant increase in the interaction energy.

The calculated binding energies of CCA and benzene complex are summarized in **Table 5.3**. CCA is a carbon analogue of PCA. In other words, the NH group of the PCA molecule was replaced by the CH_2 group in CCA molecule. The purpose of studying this model system is to evaluate the difference between NH/π and CH/π interaction. The interaction energies of the two conformers are almost identical at CCSD (T)-aug-(d, p)-6-311G (d,p) level and the binding energies are 15.7 and 15.4 kJ mol^{-1} for two different conformers, respectively. These values are slightly lower than that of hydrogen bond of water dimer.[29] The result suggests that even without NH/π interaction, the CH/π interaction energy is not neglecable. Compared to the interaction energies PCA–benzene complex (**Table 5.2**), the interaction energies of the CCA–benzene complexes are smaller as expected for various levels of theory considered by 3-5 kJ mol^{-1}. This can be readily explained by lower acidity of C–H bond in CCA than that acidity of N–H bond in the PCA.

5.3.2 Proline-benzene and proline-phenylalanine complex

5.3.2.1 Geometrical parameters and Electron properties

The optimized geometries of different conformations of proline-benzene and proline-phenalanine complexes are shown in **Figure 5.2** (**p1-p8**) and **Figure 5.3** (**pp1-pp6**).

Except for **p3**, all other conformations of proline-benzene complexes favor multiple XH/π contacts. This clearly demonstrates that XH/π interaction has a strong tendency to maximization of intermolecular interactions.[11] The structural parameters, d_1,

d_2 and α, and electron density properties ρ and $\nabla_2\rho$ of proline-benzene complexes are listed in **Table 5.4**

Except for the **p3** conformation, all other complexes have three sets of bond critical points (bcp). The electron densities (ρ) at each bcp vary from 0.0041 to 0.0103 AU and the Laplacian of electron density ($\nabla_2\rho$) at each bcp vary from 0.0129 to 0.0363. These values are slightly higher than those reported in **Table 5.1**. These bond properties are consistent with the binding energy differences between proline–benzene and PCA–benzene as well as CCA–benzene complexes. **Table 5.4** also presented that the interaction distances between X–H hydrogen and the aromatic ring (d_1 value) are in the range from 2.304 to 2.798 Å , which are shorter compared to those at PCA and CCA complexes. (**Table 5.1**). This shortening provides evidence to that the electrostatic interaction is an important part in the XH/π interaction. The angle between XH and aromatic ring vary from 130.3 to 174.3°, similar to the PCA– and CCA–benzene complexes (**Table 5.1**).

The structural parameters, d_1, d_2 and α, and electron properties ρ and $\nabla_2\rho$ of proline-phenylalanine complexes are listed in **Table 5.5**. In all the conformations of proline-phenylalanine complex, cooperative XH/π interactions exist (**Table 5.4**). The electron density (ρ) of ring hydrogen at **pp2**, **pp4**, and **pp6** are 0.0112, 0.0110 and 0.0091 au, these values are as large as the electron density (ρ) of ring hydrogen at **pp1**, **pp3**, and **pp5**, (0.0109, 0.0109 and 0.0111, respectively). This means that the α C–H group of the proline ring can compete with high polar N–H to form a very strong CH/π interaction and allow N–H group to form a substantial stronger classic NH/N hydrogen bond to maximize the intermolecular interactions.

5.3.2.2 Interaction energy of Proline-benzene and Proline-phenylalanine complex

The interaction energies of various conformations (**Figure 5.2 p1-p8**) of proline-benzene complex are given in **Table 5.5.** The interaction energies of conformation **p1**, **p2**, **p5** and **p7** are 22.6, 19.4, 19.4 and 22.3 kJ mol^{-1} respectively. These values are close to the interaction of water dimer.[28] Again, this clearly indicates that the interaction energy between aromatic ring and proline complex is strong enough for stabilization of biological molecules. The relatively large interaction energy can be explained by the cooperative XH/π interactions. Like it was in the PCA–benzene, by using the AIM theory, one unit of NH/π and two units of CH/π interactions were identified. Compared to PCA–benzene complex, the binding energy is larger by 3.1 kJ/mol. This can be explained by the increase of the polarizability of proline molecule since one OH group was added compared to the PCA molecule. This also implies that the electrostatic interaction is an important part in terms of total interaction energy. The interaction energies of conformation **p4**, **p6** and **p8** are 15.0, 15.2 and 16.0 $kJmol^{-1}$ respectively which are slightly weaker than that of water dimer. In these three conformations, only the multiple CH/π interactions involved, without any NH/π interaction. Compared to CCA–benzene complex, the binding energies of conformations **p4**, **p6** and **p8** of proline–benzene complex are slightly increase due to increase of the polarizability of proline as same as **p1**, **p2**, **p5** and **p7** respect to the PCA–benzene complex. The **p3** conformation of proline-benzene complex has a very special structure which the C–H bond of the α carbon of proline points to the center of benzene ring with a T-shape geometry. The C=O bond of proline is parallel to benzene plane and

form a π–π interaction. This is in good agreement with the PDB analysis results that the interactions between proline and aromatic ring have a tendency to maximizing of intermolecular interactions to form a face to face conformation.[11] This conformation may be formed easily in real situation due to its highly favorable orientation in polypeptides. The interaction energies for proline-phenylalanine complex at Aug(C, H)-6-311G** level are summarized in **Table 5.7**.

The interaction energies of proline–phenalanine complex are substantially greater than the proline–benzene complex. In this case, the binding energies are higher than that interaction energy of water dimer.[28] The larger binding energy can be explained in terms of the one additional NH/N intermolecular interaction involving in all conformations. However, these NH/N interactions are different in different conformations. In the conformations **pp1**, **pp3** and **pp5**, the NH bond of phenylalanine act as a hydrogen donor and the lone pair electron of nitrogen of proline act as the hydrogen bond acceptor, while in the conformations **pp2** and **pp4**, the NH bond of proline act as a hydrogen donor and the lone pair electron of nitrogen of phenylalanine molecule. The **pp1**, **pp3** and **pp5** have similar conformations which involve one NH/N, one NH/π and two sets of CH/π interactions. The only difference between **pp3** and **pp5** is that phenylalanine bonded different proline conformations. In **pp3** complex, the proline has a conformation with an OH/N intermolecular interaction, but in **pp5** complex, there is no any intramolecular interaction. The **pp2** and **pp4** conformations have similar structures which involve one unit of NH/N and three units of CH/π interactions. In these two conformations, the α C–H bond form a very strong CH/π interaction compared to that in **pp1**, **pp3** and **pp5** complexes. This strong CH/π interaction complex can compete with the complex which

involves NH/π interaction to form more favorable polypeptides. The interaction energy of conformation **pp6** is significantly larger, because of the additional one NH/O and CH /O interactions. Again, this result is in accord with the PDB analysis that the N-H has a strong preference for stronger classic hydrogen binging.[11]

5.4 Conclusions

In conclusion, multiple bond critical points (bcp) were located between aromatic molecule and various model systems including amino acid. These results confirm the existence multiple XH/π (including CH/π and NH/π in this study) hydrogen bonds.

The interaction energies between aromatic molecules and amino acids are considerable stronger than the typical hydrogen bond (e.g. water dimer). The calculated binding energy of proline-phenylalanine is up to 49 kJ mol^{-1}. This attractive interaction is stronger enough to stabilize the polypeptides as well as proteins. And this internal force in the biological molecules may compete with the aquatic hydrogen bond in terms of structure conversion and consequently change the properties of molecules.

The geometries of the CH/π or NH/π interaction in all complexes have a strong tendency to maximize multiple interactions. This result clearly reveals that the electrostatic interaction is the governing factor in the geometry of XH/π interaction.

5.5 References

1. Jeffrey, G. A.; Saenger, W. *Hydrogen Bonding in Biological Structures*; Springer-Verlag: Berlin, **1991**.
2. Baker, E. N.; Hubbard, R. E. *Prog. Biophys. Mol. Biol*. **1984**, *44*, 97.
3. (a) Steiner, T.; Saenger, W. *J. Am. Chem. Soc*. **1993**, *115*, 4540. (b) Derewenda, Z. S.; Lee, L.; Derewends, U. *J. Mol. Biol*. **1995**, *252*, 248. (c) Auffinger, P.; Westhof, E. *Biophys. J*. **1996**. *71*, 940. (d) Fabiola, G. F.; Krishnaswamy, S.; Nagarajan, V.; Pattabhi, V. *Acta Crystallog. Sect. D*. **1997**, *53*, 316. (e) Ghosh, A.; Bansal, M. *Acta Crystallog. Sect. D*. **1999**, *55*, 481.
4. Perutz, M. F. *Phil. Trans. Roy. Soc. Ser. A* **1993**, *345*, 105.
5. Wahl, M.; Sundralingam, M. *Trands Biochem. Sci*. **1997**, *22*, 97.
6. Burley, S. K.; Petsko, G. A. *Advan. Protein Chem.* **1988**, *39*, 125.
7. Desiraju, G. R.; Steiner, T. The Weak Hydrogen Bond in Structure Chemistry and Biology; Oxford University Press: Oxford, **1999**.
8. Wulf, O. R.; Liddel, U.; Hendricks, S. B. *J. Am. Chem. Soc*. **1936**, *58*, 2287.
9. Malone, J. F.; Murray, C. M.; Charlton, M. H.; Docherty, R.; Lavery, A. J. *J. Chem. Soc. Faraday Trans*. **1997**, *93*, 3429.
10. (a) Levitt, M.; Perutz, M. F. *J. Mol. Biol*. **1988**, *201*, 751. (b) Rodham, D. A.; Susuki, S.; Suenram, R. D.; Lovas, F. J.; Dasgupta, S.; Goddard, W. A.; Blake, G. A. *Nature*. **1993**, *362*, 735. (c) Worth, G. A.; Wade, R. C. *J. Phys. Chem*. **1995**, *99*, 17473.
11. Steiner, T.; Koellner, G. *J. Mol. Biol*. **2001**, *305*, 535.
12. (a) Steiner, T.; Starikov, E. B.; Amado, A. M.; Teixeiradias, J.J. C. *J. Chem. Soc. Perkin Trans. 2*, **1995**. 1321. (b) Nishio, M.; Umezawa, Y.; Hirota, M.;

Takeuchi, Y. *Tetrahedron* **1995**, *51*, 8665. (c) Nishio, M.; Hirota, M.; Umezawa, Y. *The CH/π interaction*; Wiley VCH: New York, **1998**. (d) Nishio, M. *Cryst. Eng. Comm*. **2004**, *6*, 130.

13. Brandl, M.; Weiss, M. S.; Jabs, A.; Sühnel, J.; Hilgenfeld, R. *J. Mol. Biol*, **2001**, 307. 357.

14. Burley, S. K.; Petsko, G. A. *J. Am. Chem. Soc*. **1986**, *108*, 7995.

15. Stepanian, S. G.; Treva, I. D.; Radchenko, E. D.; Adamowicz, L. *J. Phys. Chem. A* **2001**, *105*, 10664.

16. Hobza, P.; Havlas, Z. *Chem. Rev*. **2000**, *100*, 4253.

17. Tarakeshwar, P.; Choi, H. S.; Kim, K. S. *Chem. Rev*. **2000**, *100*, 4145.

18. Tsuzuki, S.; Honda, K.; Uchimaru, T.; Mikami, M.; Tanabe, K. *J. Am. Chem. Soc*. **2000**, *122*, 3746.

19. Tarakeshwar, P.; Choi, H. S.; Kim, K. S. *J. Am. Chem. Soc*. **2001**, *123*, 3323.

20. Sinnokrot, M. O.; Valeev, E. F.; Sherrill, C. D. *J. Am. Chem. Soc.* **2002**, *124,* 10887.

21. Tsuzuki, S.; Honda, K.; Uchimaru, T.; Mikami, M.; Tanabe, K. *J. Phys. Chem. A* **1999**, *103*, 8265.

22. Boys, S. F.; Bernardi, F. *Mol. Phys*. **1970**, *19*, 553.

23. Scott, A. P.; Radom, L. *J. Phys. Chem*. **1996**, *100*, 16502.

24. (*a*) Bader, R. F. W. *Atoms in Molecules—A Quantum Theory*; Oxford Science Publications: Oxford, **1990**. (*b*) Bader, R. F. W. *Chem. Rev.* **1991**, *91*, 893.

25. Popelier P. L. A.; Bone, R. G. A. *MORPHY98*; UMIST, Manchester, **1998**.

26. Werner, H.-J.; Knowles, P. J.; Schütz, J. M.; Lindh, R.; Celani, P.; Korona, T.; Rauhut, G.; Manby, F. R.; Amos, R. D.; Bernhardsson, A.; Berning, A.; Cooper,

D. L.; Deegan, M. J. O.; Dobbyn, A. J.; Eckert, F.; Hampel, C.; Hetzer, G.; Lloyd, A. W.; McNicholas, S. J.; Meyer, W.; Mura, M. E.; Nicklaß, A.; Palmieri, P.; Pitzer, R.; Schumann, U.; Stoll, H.; Stone, A. J.; Tarroni, R.; Thorsteinsson, T. *MOLPRO*, version 2002; University of Birmingham, **2002**.

27. Frisch, M. J.; Trucks, G. W.; Schlegel, H. B.; Scuseria, G. E.; Robb, M. A.; Cheeseman, J. R.; Zakrzewski, V. G.; Montgomery, Jr, J. A.; Stratmann, R. E.; Burant, J. C.; Dapprich, S.; Millam, J. M.; Daniels, A. D.; Kudin, K. N.; Strain, M. C.; Farkas, O.; Tomasi, J.; Barone, V.; Cossi, M.; Cammi, R.; Mennucci, B.; Pomelli, C.; Adamo, C.; Clifford, S.; Ochterski, J.; Petersson, G. A.; Ayala, P. Y.; Cui, Q.; Morokuma, K.; Malick, D. K.; Rabuck, A. D.; Raghavachari, K.; Foresman, J. B.; Cioslowski, J.; Ortiz, J. V.; Baboul, A. G.; Stefanov, B. B.; Liu, G.; Liashenko, A.; Piskorz, P.; Komaromi, I.; Gomperts, R.; Martin, R. L.; Fox, D. J.; Keith, T.; Al-Laham, M. A.; Peng, C. Y.; Nanayakkara, A.; Gonzalez, C.; Challacombe, M.; Gill, P. M. W.; Johnson, B.; Chen, W.; Wong, M. W.; Andres, J. L.; Gonzalez, C.; Head-Gordon, M.; Replogle, E. S.; Pople, J. A. *Gaussian 98*, Gaussian, Inc., Pittsburgh PA, **1998**.

28. (a) Gu, Y.; Kas, T.; Scheiner, S. *J. Am. Chem. Soc.* **1999**, *121*, 9411. (b) Feyereisen, M. W.;Feller, D.; Dixon, D. A. *J. Phys. Chem*. **1996**, *100*, 2993.

29. Ciunik, Z.; Berski, S.; Latajka, Z.; Leszczyński, J. *J. Mol. Struct*. **1988**, *442*, 125.

30. Umezawa, Y.; Tsuboyama, S.; Takahashi, H.; Uzawa, J.; Nishio, M. *Tetraheron* **1999**, *55*, 10047, and references therein

31. Takahashi, H.; Tsuboyama, S.; Umezawa, Y.; Honda, K.; Nishio, M. *Teahedron* **2000**, *56*, 6185, and references therein.

32. Umezawa, Y.; Tsuboyama, S.; Honda, K.; Uzawa, J.; Nishio, M. *Bull. Chem. Soc. Jpn*. **1998**, *71*, 1207

33. Novoa, J. J.; Mota, F. *Chem. Phys. Lett*. **2000**, *318*, 45.

34. Koch, U.; Popelier, P. L. A. *J. Phys. Chem*. **1995**, *99*, 9747.

5.6 Appendix

Table 5.1. Calculated Structural Parameters (d_1, d_2 and α)[a] and Topological Properties[b] (ρ, and $\nabla_2\rho$ in au) at the Bond Critical Point of PCA–, CCA–Benzene Complexes (**1**–**4**), Evaluated at the MP2/6-31G (d) Level

	label[c]	d_1	d_2	α	ρ	$\nabla_2\rho$
(**1**)	1	2.399	0.396	163.9	0.0090	0.0310
	2	2.755	2.659	154.4	0.0037	0.0113
	3	2.749	1.973	139.6	0.0061	0.0180
	4	2.836	2.011	145.0	0.0052	0.0156
(**2**)	1	2.355	0.393	171.2	0.0097	0.0340
	2	2.619	2.404	156.6	0.0056	0.0166
	3	2.788	2.806	141.8	0.0034	0.0108
	4	2.839	2.031	134.8	0.0052	0.0159
(3)	1	2.643	0.366	149.9	0.0064	0.0204
	2	2.538	2.892	161.1	0.0041	0.0124
	3	2.833	2.165	151.8	0.0046	0.0136
	4	2.740	2.075	141.5	0.0058	0.0173
(4)	1	2.600	0.369	160.3	0.0069	0.0220
	2	2.658	2.415	154.8	0.0052	0.0156
	3	2.554	2.934	150.5	0.0041	0.0125
	4	2.783	2.133	139.3	0.0053	0.0162

[a] Bond lengths in Å and angles in degrees.

[b] Based on AIM analysis.

[c] See **Fig 5.1** for hydrogen labeling.

Table 5.2
Binding energy of PCA–benzene

	conformation1	conformation2
MP2/6-31G*	-12.5	-12.4
MP2/6-311+G**	-18.6	-19.0
Aug-(C,H)-MP2/6-311G**	-23.7	-24.4
Aug-(C,H,N)-MP2/6-311G**	-23.8	-24.5
CCSD(T)/6-31G*	-8.3	-7.8
Aug-(C,H)-CCSD(T)/6-311G**	-19.5	-19.9

Table 5.3
Binding energy of CCA–benzene

	conformation1	conformation2
MP2/6-31g*	-7.9	-8.1
MP2/6-311+G**	-14.9	-14.6
Aug-(C,H)-MP2/6-311G**	-19.5	-19.0
CCSD(T)/6-31G*	-4.1	-4.5
Aug-(C,H)-CCSD(T)/6-311G**	-15.7	-15.4

Table 5.4. Calculated Structural Parameters (d_1, d_2 and α)[a] and Topological Properties[b] (ρ and $\nabla_2\rho$ in au) at the Bond Critical Point of Proline-Benzene Complexes (**p1-p8**), Evaluated at the MP2/6-31G (d) Level

	label[c]	d_1	d_2	α	ρ	$\nabla_2\rho$
proline-benzene (**p1**)	1	2.304	0.036	172.2	0.0103	0.0363
	2	2.791	2.002	138.2	0.0058	0.0179
	3	2.587	2.426	160.4	0.0057	0.0170
(**p2**)	1	2.349	0.408	172.0	0.0099	0.0346
	2	2.627	2.331	160.5	0.0058	0.0171
	3	2.782	2.012	139.4	0.0058	0.0178
(**p3**)	4	2.414	0.018	147.4	0.0082	0.0227
π-π interaction					0.0064	0.0217
(**p4**)	1	2.707	0.268	155.0	0.0057	0.0178
	2	2.740	2.075	141.5	0.0058	0.0178
	3	2.635	2.822	155.9	0.0041	0.0129
(**p5**)	1	2.339	0.384	174.3	0.0099	0.0348
	2	2.795	1.987	141.4	0.0058	0.0180
	3	2.632	2.352	162.8	0.0057	0.0167
(**p6**)	1	2.459	0.122	158.5	0.0069	0.0249
	2	2.415	2.889	146.8	0.0050	0.0153
	3	2.709	2.397	130.3	0.0055	0.0179
(**p7**)	1	2.573	0.385	162.8	0.0097	0.0334
	2	2.798	2.030	144.5	0.0054	0.0161
	3	2.680	1.988	143.4	0.0066	0.0200
(**p8**)	1	2.573	0.148	153.4	0.0058	0.0197
	2	2.392	2.705	148.9	0.0063	0.0195
	3	2.541	2.332	137.4	0.0073	0.0236

[a] Bond lengths in Å and angles in degrees.

[b] Based on AIM analysis.

[c] See **Fig 5.2** for hydrogen labeling.

Table 5.5
Binding energy of proline…benzene

	p1	p2	p3	p4	p5	p6	p7	p8
MP2/6-31G*	-16.0	-12.3	-8.1	-6.0	-12.5	-6.2	-16.3	-7.8
Aug-(C,H)-MP2/6-311G**	-27.5	-23.9	-20.0	-19.5	-23.8	-19.5	-26.9	-20.3
CCSD(T)/6-31G*	-11.1	-7.8	-3.7	-2.5	-8.1	-1.9	-11.7	-3.5
CCSD(T)/Aug-(C,H)-6-311G**	-22.6	-19.4	-15.6	-15.0	-19.4	-15.2	-22.3	-16.0

Table 5.6. Calculated Structural Parameters (d_1, d_2 and α)[a] and Topological Properties[b] (ρ, and $\nabla_2\rho$ in au) at the Bond Critical Point of Proline-Phenylalanine Complexes (**pp1-pp6**), Evaluated at the MP2/6-31G (d) Level

Proline-phenylalanine	label[c]	d_1	d_2	α	ρ	$\nabla_2\rho$
pp1	1	2.154	0.082	166.7	0.0109	0.0411
	2	2.886	2.548	154.3	0.0039	0.0115
	3	2.650		133.9	0.0074	0.0273
	4	2.168		165.2	0.0225	0.0618
pp2	1	2.210	0.018	167.7	0.0112	0.0404
	2	2.167		141.7	0.0216	0.0654
	3	2.629		163.6	0.0077	0.0262
pp3	1	2.155	0.082	166.7	0.0109	0.0411
	2	2.885	2.545	154.4	0.0039	0.0115
	3	2.650		133.9	0.0074	0.0273
	4	2.168		165.2	0.0225	0.0618
pp4	1	2.229	0.228	165.5	0.0110	0.0390
	2	2.159		141.3	0.0219	0.0665
	3	2.641		165.1	0.0075	0.0256
pp5	1	2.149	0.000	170.4	0.0111	0.0413
	2	2.874	2.604	154.1	0.0038	0.0115
	3	2.520		144.9	0.0118	0.0358
pp6	1	2.509	0.537	157.8	0.0091	0.0289
	2	2.743	1.990	142.2	0.0058	0.0203
	3	2.481		123.4	0.0130	0.0415
	4	2.686	2.873	143.2	0.0043	0.0135
	5	2.641	2.289	157.0	0.0065	0.0199
	6	2.490		119.5	0.0098	0.0334

[a] Bond lengths in Å and angles in degrees, for classic hydrogen bond X-H…Y, d_1 represents hydrogen distance $d_{H...Y}$ and the α represents the hydrogen bond angle .

[b] Based on AIM analysis.

[c] See **Fig 5.3** for hydrogen labeling.

Table 5.7
Binding energy of proline…phenylalanine

	pp1	pp2	pp3	pp4	pp5	pp6
MP2/6-31G*	-29.1	-30.2	-29.1	-30.0	-18.6	-42.1
Aug-(C,H)-MP2/6-311G**	-43.7	-43.6	-43.6	-43.2	-35.7	-55.5
CCSD(T)/6-31G*	-22.7	-23.4	-21.9	-22.5	-14.6	-35.6
CCSD(T)/Aug-(C,H)-6-311G**	-37.3	-36.8	-36.4	-35.7	-31.7	-49.0

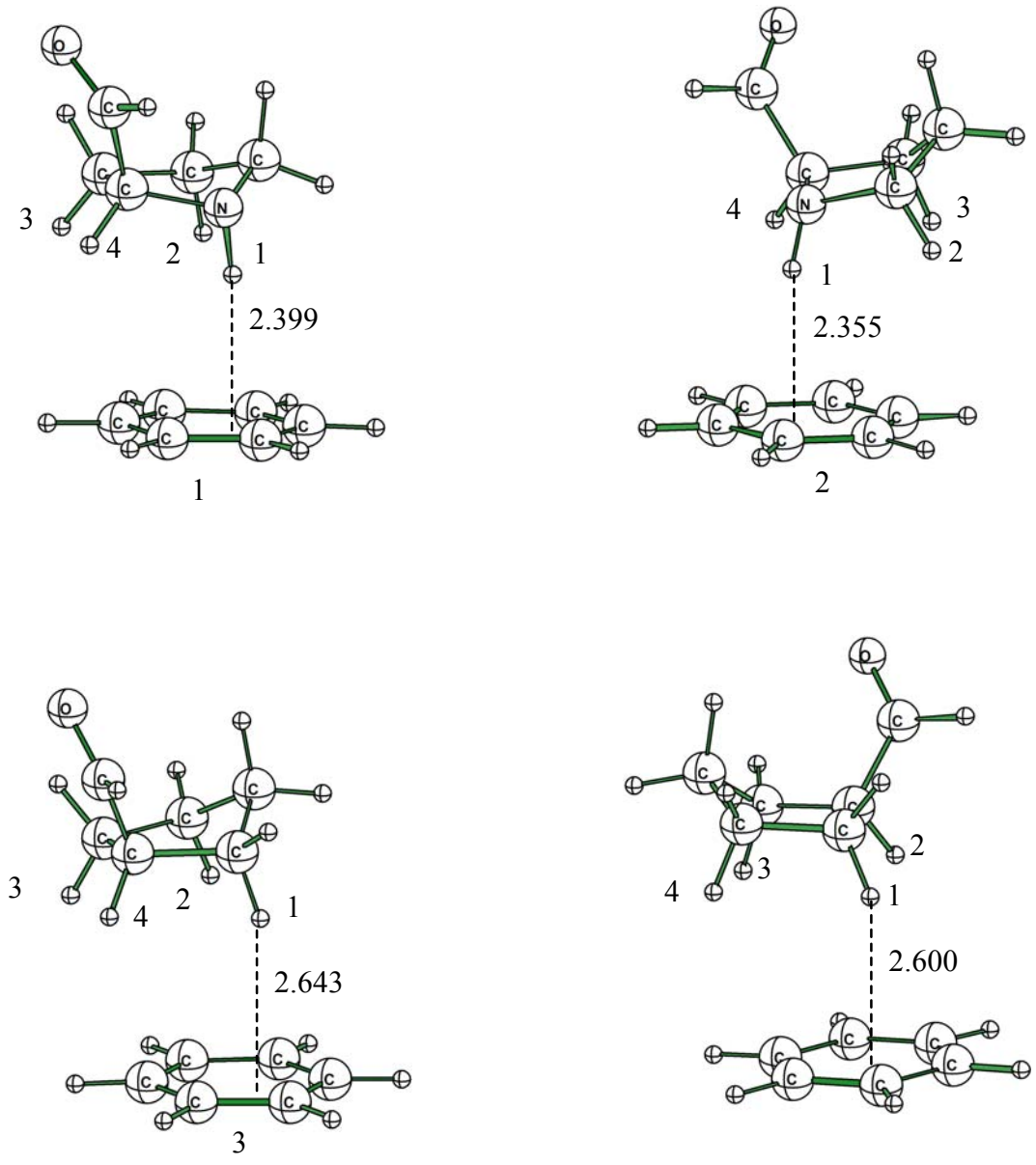

Figure 5.1 Optimized (MP2/6-31G (d)) geometries PCA– and CCA–benzene complexes. Bond distance in Å. The dotted line represents the projection line of the ring X–H (X = C or N) hydrogen of the hydrocarbon perpendicular to the molecular plane of benzene.

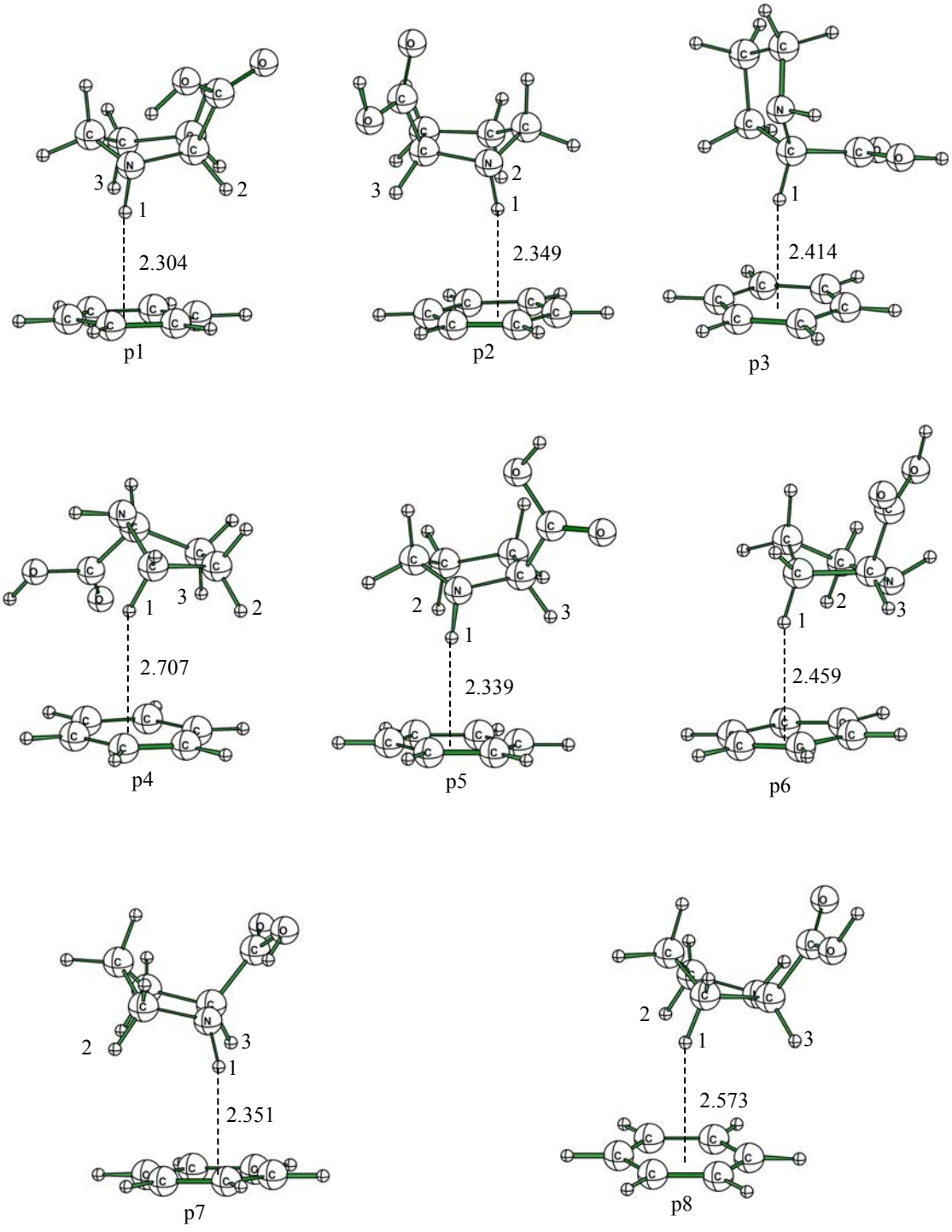

Figure 5.2 Optimized (MP2/6-31G (d)) geometries of proline-benzene complexes. Bond distance in Å. The dotted line represents the projection line of the ring X–H (X = C or N) hydrogen of the hydrocarbon perpendicular to the molecular plane of benzene.

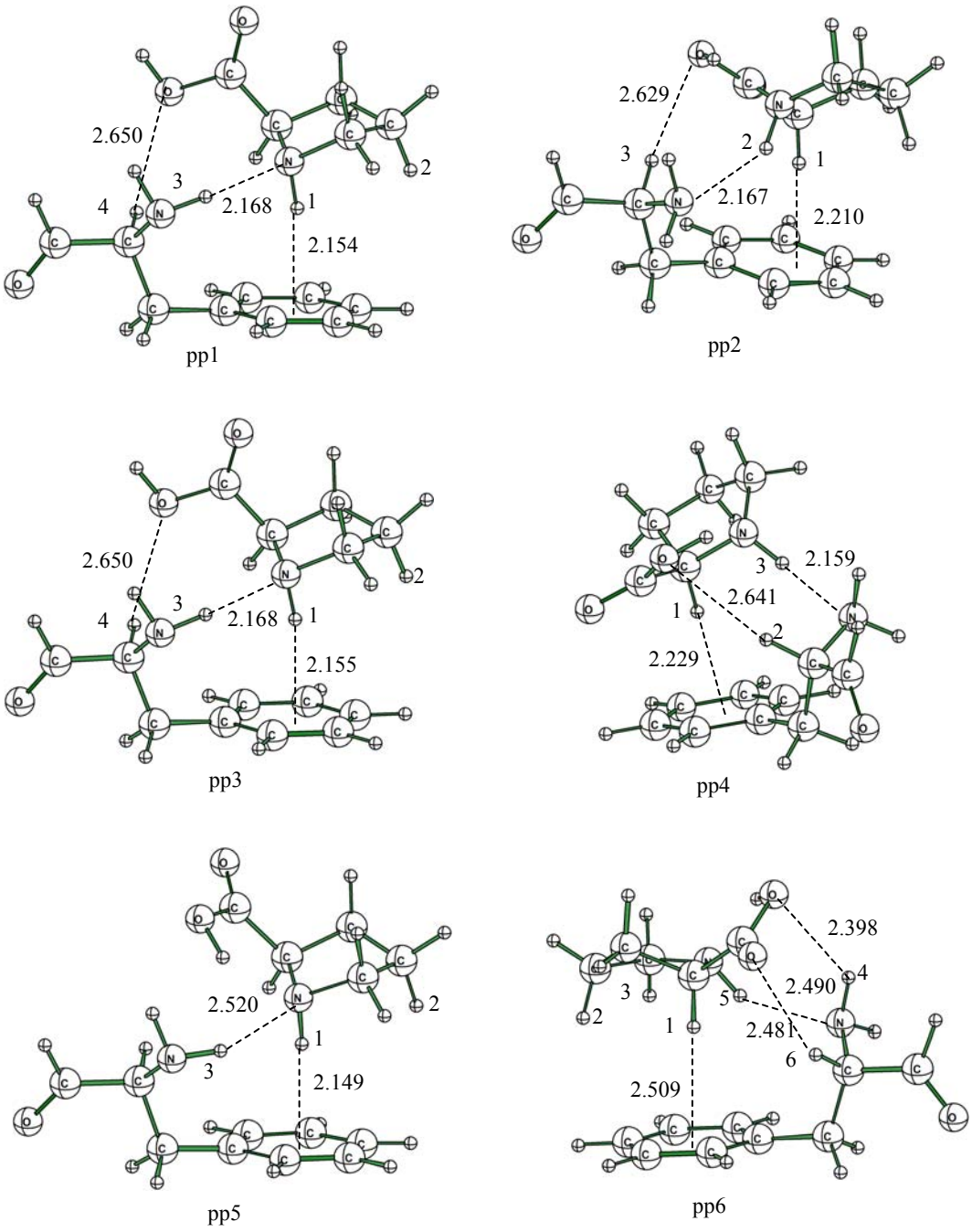

Figure 5.3 Optimized (MP2/6-31G (d)) geometries of proline-phenylalanine complexes. Bond distance in Å. The dotted line represents both hydrogen bond distance and the projection line of the ring C-H hydrogen of the hydrocarbon perpendicular to the molecular plane of benzene.

Chapter 6 A Conformational study of disubstituted ethanes XCH_2CH_2Y (X, Y= OMe, NMe_2, SMe and PMe_2) : The role of intramolecular CH···X (X= O, N, S and P) interactions

6.1 Introduction

The importance of hydrogen bond has made it an attractive topic of research for many decades. Much knowledge has been acquired about its fundamental properties from both experimental and theoretical perspectives.[1,2] In its standard definition, a hydrogen bond results from the approach of a proton donor molecule to an acceptor, forming a bridge of the X–H···Y connectivity. The X atom is normally thought to be very electronegative, e.g. O or N, as is the acceptor atom Y, which must contain at least one lone pair of electrons by which to form the bridge. Since the early 1960s, crystallographic and spectroscopic studies have shown that C–H groups could act as proton donors in a Hydrogen bond system.[3] It was not until 1982 that the first appearance of a thorough and conclusive survey of the CH···X hydrogen bonds surfaced.[4] Support was provided on the basis of crystal correlation studies and spectroscopic examinations. The concept of CH···X hydrogen bonds is now well documented,[2,5] in particular the CH···N,[6] CH···O,[7] and CH···π [8] interactions, which have been the focus of a number of investigations. Special attention has also been given to the interactions involving acceptors with less electronegativity atoms, such as CH···S,[9] CH···Hal (Hal= F, Cl, Br),[10,11] CH···Se,[12,13] and even CH···C[14-18] interactions.

Recently, the CH···O hydrogen bond has attracted strong attention from researchers in chemists and biochemists because of its potential capacity in stabilizing structures of molecules and molecular assemblies.[19-20] In 1992, Hiroatsu et al have reported the important of an intramolecular 1,5-CH···O interaction for determining the conformational stabilities of 1,2-dimethoxyethane (DME) in an argon matrix.[21] Since that work was reported, a considerable number of theoretical studies have been published, which deal with the conformational properties of this molecule with special attention given to this intriguing interaction.[22-29] These theoretical studies have demonstrated the importance of this interaction in the conformational stabilization of single molecules, in agreement with the experimental results by the gas-phase electron diffraction[30] and IR spectroscopy.[31-33] In 1997, on the basis of infrared spectroscopic studies, Hiroatsu et al have reported that a conformer of 1-methoxy-2-(methylthio)ethane (MMTE), which is stabilized by an intramolecular 1,5-CH···O interaction.[34] The characteristics of this interaction is similar with that of in the DME since MMTE is an analogous compound of 1,2-dimethoxyethane (DME). On the basis of the comparison of the results for MMTE and DME, the authors claimed that the 1,5-CH···O is strong in MMTE rather than in DME. Quantum chemical calculations have shown that the formation of CH···X (X = O, N, S, P and π) hydrogen bond shorten the C–H bond in some molecular system.[35,36] The contraction of the C–H bond leads to a blue-shift of stretching vibrational frequency of this bond. This blue-shifting hydrogen bond has received much attention from theoreticians.[35-39] The infrared and Raman spectroscopic observations of blue-shifted CH···O hydrogen bond have been reported in recent years.[40] Late on 2003, Hiroatsu et al have successful in observing a blue-shifted infrared band for a gauche conformer of 1-methoxy-2-(dimethylamino)ethane (MDAE),[41] which is the first experimental evidence

for the intramolecular CH···O interaction. Most of these works focus mainly on the intermolecular CH···O interaction. To the best of our knowledge, there are very few investigations on other types of intramolecular CH···X interaction. To gain further insight into the role of the CH···X (X = O, N, S and P) intramolecular interactions in the conformational properities of a series of molecules, we have systematically investigated the *gauche/trans* conformational equilibrium of disubstituted ethane XCH_2CH_2Y (X, Y = NMe_2, PMe_2, OMe or SMe) using high-level G3(MP2) theory. In particular we attempt to estimate the magnitude of the CH···X intramolecular interaction and their influence on the conformational preference.

6.2 Computational Methods

Since XCH_2CH_2Y are flexible molecules, a systematic conformation search, via a dihedral driver, was carried out initially using Spartan program[42] at HF/6-31G* level to locate all possible conformers of XCH_2CH_2Y molecules. Subsequently, we selected the most stable *gauche* conformers which involve 1,5-CH···X or 1,5-CH···Y interaction as well as the most stable *trans* form. The energy difference between the *gauche* and *trans* forms were examined at several levels of theory, namely HF/6-31G*, B3LYP/6-31G*, MP2(full)/6-31G* and a modified G3(MP2)[43] theory, in which uses the MP2(full)/6-31G* zero-point energy (ZPE) correction to replace the standard HF/6-31G* ZPE, since our studies have shown that the trend of the HF/6-31G* geometries is not consistent with the MP2/6-31G* results. Solvent effect calculations were performed in a polar medium using the self-consistent reaction field (SCRF)[44] solvation models, based on the Onsager's reaction field theory.[45] For all solvent calculations, geometries were optimized at the

B3LYP/6-31G* level. All *ab initio* calculations are performed by using the GAUSSIAN 98 program,[46] while electron density analysis, based on Bader's theory of atoms in molecules (AIM)[47] was carried out using the MORPHY98 program.[48]

6.3 Results and Discussion

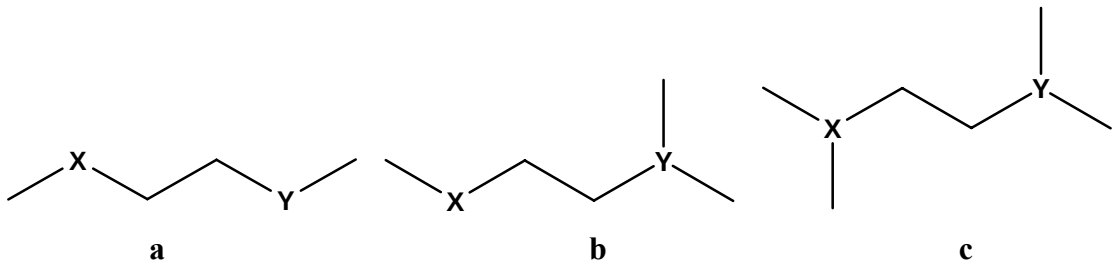

Scheme 1. Possible structures of XCH_2CH_2Y molecules

Scheme 1 shows the possible structures of disubstituted ethanes.The structure **a** represents the molecules **OO, SS** and **OS,** the structure **b** represents the molecules **ON, OP, NS** and **SP,** and the structure **c** represents the molecules **NN, PP and NP.** The energy differences of the *gauche* conformers and *trans* conformer of **X**CH2CH2**Y** molecules calculated at RHF/6-31G*, B3LYP/6-31G*, MP2/6-31G* and G3(MP2) levels are given in **Table 6.1**, and the optimized structures of *gauche* and *trans* conformers are depicted in **Figures 6.1-6.4**. Let us firstly discuss the four molecules with identical substituents, namely **OO, NN, SS** and **PP**. In all four cases, only the 1,5-(X)CH···X interaction is feasible.

6.3.1 Relative energies and geometry properties of disubstituted ethanes

As evidenced in **Table 6.1**, the *trans* form is the preferred conformer of **OO** at all calculated levels of theory. This result is in good agreement with previous experimental studies[21,34] and theoretical investigations.[22-29] The experimentalists found that *gauche* form with the 1,5-CH···O intramolecular interaction is the second most stable conformation in the gas phase and the calculated energy difference between two conformations (2.1 kJ mol^{-1}) agrees well with our G3(MP2) value of 2.4 kJ mol^{-1}. The distance between one of the methoxyl hydrogen and the oxygen atom is 2.453 Å, which is significantly shorter than the sum of van der Waals radii (2.700 Å for CH···O).[49] It is obvious that an attractive intramolecular 1,5-CH···O interaction occurs between this non-bonded atoms which significantly stabilizes this gauche conformation. For comparison the *gauche/trans* energy difference in hexane is 6.1 kJ mol^{-1}. Unlike the 'normal' hydrogen bond with the X–H (X= O and N) bond elongated upon the hydrogen bond formation, the CH···O interaction, on the contrary, contracts the C–H bond which leads to an increase the C–H stretching frequency. As a consequence, a blue-shift to high wave number is observed. The geometrical parameters of CH···X interaction, the change of C–H stretch frequency and the electron density properties of CH···X interaction are summarized in **Table 6.2**. As seen in **Table 6.2**, the C–H bond is shortened by 0.0063 Å in the *gauche* form compared to that in the trans form. This in C–H bond shortening results in an increase of C–H stretching vibrational frequency by 47 cm^{-1}.

In distinct contrast to **OO**, as evidenced in **Table 6.1**, at the HF method, the *trans* form (trans-**NN, Figure 6.1**) is the most stable conformer in the gas phase, and the *gauche* form (gauche-**NN**, **Figure 6.1**) is the most stable conformer in the DFT and MP2 methods.

This result is in consistent with the previous theoretical finding.[50] In this case, there are two sets of equivalent intramolecular CH···N interactions in the *gauche* form, which suggests that the stabilization energy contributed from two sets of (N)CH···N interactions. Perhaps this is the major reason for the preference of the *gauche* form in **NN**. The distance between interacting hydrogen atoms and nitrogen atoms are 2.601Å, which is significantly shorten than the sum of van der Waals radii (2.750Å for CH···N). Both C–H bonds in *gauche* form are shortened by 0.0013 Å, and the corresponding C–H stretching frequency shows a blue shift of 13 cm^{-1}.

As we mentioned in introduction, the less electronegativity atom such as sulfur and phosphorus can also act as the hydrogen bond acceptor. As a sulfur analogue of **OO**, for **SS**, the *trans* form is slightly favored in gas phase in gas phase. It is interesting to note that *gauche/trans* energy differences vary little from HF to G3(MP2), within 2.2 kJ mol^{-1}. This result may imply that the SCH···S interaction is insensitive to the computational method employed. The distance of hydrogen and the sulfur atoms is 2.794 Å, correspond to the sum of van der Waals radium (2.900 Å for CH···S). The C–H bond is contracted by 0.0019 Å and the corresponding blue shift of C–H stretching frequency is 16 cm^{-1}.

As with in the **SS**, the **PP** also favors a *trans* conformer**.** However, the magnitude of energy differences is small compared to those in **SS**, especially in MP2 and G3(MP2) theory. It seems that the electron correlation appears to be critically important for proper description of the PCH···P interaction. The distance of two phosphorus atoms in *gauche* form (3.562 Å) of **PP** is longer than the sulfur analogue **SS** (3.330 Å). This suggests that there is strong steric repulsion between two sulfur atoms. The distance of interacting

hydrogen and the phosphorus atoms is 2.955 Å, which is close to the sum of van der Waals radii (2.950 Å for CH···P), which indicates a weaker PCH···P interaction. Accordingly, the C–H bond shortening is small (0.0010 Å) and the blue shift of C–H stretching frequency is just 10 cm^{-1}.

Next we discuss the mixed systems, with both (Y)CH···X and (X)CH···Y intramolecular interactions may are feasible.

We first discuss the **OS**. As evidenced from **Table 6.1**, the *gauche* (gauche'**-OS**, **Figure 6.2**) conformer is the preferred conformation in the gas phase. This result confirms the experimental observation that the *gauche* form is the most stable conformation by IR spectroscopy.[36] The comparison of the relative energy of **OS** (all negative) and **OO** (all positive) indicates that the (S)CH···O interaction might be stronger than the (O)CH···O interaction. This result further support by our AIM calculation(**Table 6.2**), which shows that the value of electron density of ρ at bond critical point in (S)CH···O is bigger than that in O)CH···O interaction. The substituent group (SMe or OMe) bonded to the C–H bond may influence the strength of the 1,5-CH···O interaction. We also calculated another possible *gauche* conformation of **SS** (gauche"**-OS**, **Figure 6.2**). In this *gauche* form, the 1,5-CH···S interaction exits, as evidenced in **Table 6.1**. However, this form is less stable than the *trans* form. This might attribute to the less electronegativity of sulfur atom, which reduces the strengthen of the CH···X intramolecular interaction. The interaction distance between hydrogen and oxygen in **OS** is 2.438 Å, which is slightly shorter than that in the **OO**. This significantly shorter hydrogen bonding distance also implies that the SCH···O interaction is stronger than that OCH···O interaction. The C–H bond is shortened by 0.0048 Å in gauche form 1 (gauche'**-OS**, **Figure6.2**), and the corresponding blue shift of

C–H bond stretching frequency is 35 cm $^{-1}$. The CH···S distance is 2.745 Å in the second *gauche* form (gauche"**-OS**, **Figure 6.2**), which is slightly shorter than that in **SS**. The shorter interacting distance suggests that the OCH···S interaction in the **OS** is probably stronger than that of the SCH···S interaction in **SS**. The C–H bond is shortened by 0.0021 Å in this conformer and the blue shift is 16 cm $^{-1}$.

For **ON**, the *gauche* form is slightly favored in all correlated methods, and the G3(MP2) energy difference is just 0.3 kJ mol^{-1}. Our calculated result is consistent with the first experimental evidence based on matrix-isolation infrared spectroscopy.[41] The authors claimed that the most stable conformation of ON is *gauche* form (gauche'**-ON**, **Figure 6.2**) with an intramolecular (N)CH···O hydrogen bond formed, with the *gauche* form is more stable than the *trans* form (trans**-ON**, **Figure 6.2**) by 0.54 kJ mol^{-1}. The greater stability of the *gauche* form can be explained by the formation of this intramolecular interaction. In this molecule, there is another possible *gauche* form (gauche"**-ON**, **Figure 6.2**) with an intramolecular (O)CH···N interaction. As shown in **Table 6.1**, this conformer is less favorable. One may speculate whether it is because the interaction of (O)CH···N is weaker than that of (N)CH···O or because the stronger repulsion of two heavy atoms in the second *gauche* form. Given the fact that the energy difference of the two gauche forms is about 4 kJ mol^{-1}, and based on the previous theoretical study of weak hydrogen bond complexes[51] which has been demonstrated that the strengths of (O)CH···N and (N)CH···O interactions are similar in magnitude, we can safely conclude that the energy difference of two gauche forms is due to the repulsion effect of two heavy atoms which is higher in the second *gauche* form (gauche"**-ON**, **Figure 6.2**) than that in the first gauche form (gauche'**-ON**, **Figure 6.2**). The distances of two heavy atoms in two *gauche* forms are

3.094 Å and 3.112 Å respectively, which strongly support our explanation. The CH···O distance is 2.323 Å in the *gauche* form 1 (gauche'**-ON**, **Figure 6.2**), which is significantly shorter than that in the *gauche* form of **OO** and **OS**. This shortest CH···O interacting distance indicates that this *gauche* form should have strongest intramolecular CH···O interaction among all the molecules studied here. The C–H bond is shortened by 0.0049 Å in this *gauche* form and the corresponding blue shift is of 38 cm $^{-1}$, which agrees well with the experiment observation[41] which measured a blue shift of about 35 cm $^{-1}$ due to the intramolecular (N)CH···O interaction. The CH···N distance in gauche form 2 (gauche"**-ON**, **Figure 6.2**) is 2.483 Å , which is shortened tremendously than that in **NN (**2.601 Å), it should be concluded that the OCH···N intramolecualr interaction in **ON** is stronger than that NCH···N interaction in **NN**. However, as we mentioned above, based on the relative energies, such conformation is unfavorable in **ON**. Clearly, this result reflects that the intramolecular interaction is not the only factor to determine the molecular conformation. The C–H bond is shortened by 0.0065 Å in this *gauche* form and the blue shift is of 45 cm $^{-1}$. It seems that the change of C–H bond length corresponds well to the magnitude of C–H stretching blue frequency.

In **OP**, the *gauche* form (gauche'**-OP**, **Figure 6.2**) is the most stable conformation. It is important to consider the **OP** which is the phosphorus analogue of **ON**. In all calculated levels, the *gauche/trans* energy differences are slightly more negative than those for the **ON**. One possible interpretation of this *gauche* preference would be that the substituted phosphorus atom produces a stronger intramolecular (P)CH···O interaction in **OP** than (N)CH···O interaction in **ON**. Alternatively, the repulsion between oxygen and phosphorus of the **OP** molecule is smaller than those in **ON**. The distances between two

heavy atoms are 3.090 Å and 3.112 Å in **OP** and **ON,** respectively. The partial charge of phosphorus is positive in **OP**. The shorter distance between two heavy atoms, on the other hand, increases the stablity of the *gauche* form of **OP**. The (P)CH···O distance in gauche form of **OP** is 2.542 Å, which is longer than that in **ON**. This long interacting distance suggests that the intramolecular interaction in **OP** is weaker than that in **ON**. The C–H bond is shortened by 0.0025 Å and the resulting blue shift of C–H stretching frequency is 28 cm^{-1}, which both are slightly smaller than those in **ON**. Another possible *gauche* form of **OP** (gauche"**-OP**, **Figure 6.2**) has an intramolecular (O)CH···P interaction. It is less favorable. The substantial longer interacting distance indicates (2.922 Å) that the intramolecular (O)CH···P interaction is weaker in the **OP**.

For **NS**, the *gauche* (gauche'**-NS**, **Figure 6.3**) and trans (trans**-NS**, **Figure 6.3**) forms are very close in energy at the G3(MP2) level. In this *gauche* form, the (S)CH···N interaction has an interaction distance of 2.501 Å corresponding to the van der Waals separation of 2.750 Å. Compared to second gauche form of the **ON** molecule (gauche"**-ON**, **Figure 6.2**), which involves an (O)CH···N interaction, this distance is slightly longer by 0.018 Å. Given the fact that sulfur atom has a large van der Waals radius, we can conclude that the (S)CH···N interaction in **NS** is slightly stronger than the (O)CH···N interaction in **ON**. In other words, the sulfur substitution, which is bonded to the C–H bond, may influence the strength of the CH···N interaction. The comparison of the relative energy of **NS** (negative) and the relative energy of second *gauche* form of ON (positive) also support the argument mentioned above. The C–H bond in **NS** is contracted by 0.0028 Å and the C–H frequency blue shift is 27 cm^{-1}. In **NS**, an analogous intramolecular interaction is expected between one of NMe2 hydrogen and the sulfur atom (gauche"-**NS**,

Figure 6.3). In this case, the (N)CH···S distance is 2.805 Å , the longer interacting distance suggests that the interaction is weaker than the corresponding (S)CH···N interaction. The calculated relative energy of two gauche forms is 6.8 kJ mol^{-1} at G3(MP2) level.

In **NP**, the *gauche* form (gauche**-NP**, **Figure 6.3**) is the most stable conformer in gas phase. The G3(MP2) relative energy is 3.1 kJ mol^{-1}, which is the largest *gauche* preference among the all molecules examined in this study. The distance of (P)CH···N in NP molecule is 2.680 Å slightly longer than (N)CH···N distance of 2.601 Å (gauche**-NN**, **Figure 6.1**) in **NN**. Based on the relative energies of **NP** and **NN**, we can conclude the intramolecular (P)CH···N interaction in **NP** is slightly stronger than the (N)CH···N in **NN**. The C–H bond is contracted by 0.0023 Å and the frequency blue shift is 25 cm^{-1}. In **NP**, there exists another type of *gauche* conformer which involves (N)CH···P intramolecular interaction. However, there is not a stable species on the potential energy surface.

For **SP**, the *trans* (trans**-SP**, **Figure 6.3**) conformer is the most stable form. Both *gauche* conformers which involve intramolecular interaction of (S,P)CH···(S,P), are substantial weak compared to those of (S,P)CH···O,N interactions in related molecules. This can be attributed to the less electronegativity of sulfur and phosphorus atoms as hydrogen bond acceptors. So, the molecule shows a trans preference. The *gauche* form with (S)CH···P intramolecular interaction (gauche"**-SP**, **Figure 6.3**) is slightly more favorable than the *gauche* form with (P)CH···S intramolecular interaction (gauche'**-SP**, **Figure 6.3**) by 1.9 kJ mol^{-1} at G3(MP2) level. The first conformer (gauche"**-SP**) has a shorter interacting distance compared to the second *gauche* form by 0.05 Å. The shorter

interacting distance reflects slightly stronger of (S)CH···P interaction than that (P)CH···S interaction. This result further support by our AIM analysis.(see **Table 6.2**)

6.3.2 General trend of CH···X (X = O, N, S and P) intramolecular interactions

On the basis of results discussed above, the CH···X intramolecular interaction plays an important role in stabilizing the *gauche* conformer of disubstituted ethanes. In particular, the systems with one first-row atom (e.g. O or N) and one second-row atom (e.g. S or P), namely OS, OP, NS, NP favour a gauche conformation. Interestingly, the *gauche/trans* energy differences for the phosphorus containing systems are more negative compared to the sulfur analogous. This result may imply that the (P)CH···X is stronger than corresponding (S)CH···X interaction. The systems with two identical hetero atoms (e.g. **OO, NN, SS, PP**) favour a trans conformation except the **NN**, which has two sets of intramolecular (N) CH···N hydrogen bond stabilizing the *gauche* conformer. Due to the high electronegativity of both oxygen and nitrogen atoms, both intramolecular interaction of (N)CH···O and (O)CH···N stabilize the gauche conformers significant. As a result, the molecule **ON** prefers to a *gauche* conformation. But, due to the stereic repulsion of oxygen and nitrogen atoms, the second *gauche* is slightly less stable than *trans* form. Because of the weaker hydrogen accepting ability of sulfur and phosphorus atoms, not surprising, like as in the SS and PP molecules, the weak intramolecular interaction of (S,P) CH···(S,P) is the major reason of the unfavorable of *gauche* form of SP molecule. The hydrogen bond distances of all possible *gauche* conformers studied here are shorter than the sum of van der Waals radii with respective atoms. In all the *gauche* conformers, the

C–H bonds which interact with the hetero atoms are contracted and the C–H stretching frequencies undergo a blue shift.

6.3.3 Energy of intramolecular CH···X (X= O, N, S and P) interaction and Topological parameters

The interaction energy of intramolecular CH···X interaction can be roughly estimated as a difference in energy between the *gauche* conformer which involves the relevant interaction and one that does not. The latter is a conformer in which the methyl group containing the C–H proton donor is rotated away from the acceptor X atom. The direction of the rotation of the methyl group is opposite to that in the interaction-involved conformer, with the conformer of other part of the molecule being the same as that of the interaction-involved conformer. The estimated interaction energies (ΔE) of the 1,5-CH···X interaction of the ten molecules, are summarized in Table 2. As mentioned above, the ON system has the shortest interacting distance. As a result, the intramolecular interaction (N)CH···O has the strongest interaction energy (**6.3** kJ mol^{-1}) among all ten molecules studied here. The estimated interaction energies of other molecules which involve the (X)CH···O and (X)CH···N are almost identical (**5.0** kJ mol^{-1}). Those systems involve (X)CH···S and (X)CH···P show a positive value, which probably due to the sulfur and phosphorus are weak hydrogen bond acceptors and the increase of repulsion between two heavy atoms as sulfur and phosphorus are large in size. To gain a better understanding on the nature of the intramolecular CH···X interaction, we have examined the topological properties of the electron density using Bader's theory of atoms in molecules (AIM) [47] at the MP2/6-31G* level. Previously theoretical study by Popelier et al[48] has shown that the CH···X interaction can be characterized by a bond path and its associated bond critical

point (bcp). For each of intramolecular CH···X contact of the various molecules examined here, there exists a bond path linking the hydrogen atom with one hetero atoms of other part of the same molecule. The calculated topological properties at the bond critical points, namely electron density (ρ) and Laplacian of electron density ($\nabla_2\rho$), are summarized in **Table 6.2**. The positive sign of the $\nabla_2\rho$ indicates the closed-shell nature of interaction, as in the case of the 'normal' hydrogen bond.[52] For all the intramolecular CH···X contacts, the small ρ and positive $\nabla_2\rho$ values are similar to the characteristic topological properties of a weak hydrogen bond.

The geometrical parameters of the optimized *gauche* conformers of all molecules studied here are also summarized in **Table 6.2**. In all cases the C–H bond is shortened than that the corresponding relative form and the C–H stretching frequency is increased compared to the *trans* form. Not surprisingly, the extent of the C–H blue shift correlates well with the magnitude of the bond shortening (R^2 = 0.95, **Figure 6.4**).

6.3.4 Solvent effect

Solvent effect calculations were performed in a polar medium using the self-consistent reaction field (SCRF)[44] solvation model. For all SCRF (ε=40) calculations, geometries were optimized at the B3LYP/6-31G* level. The gas-phase dipole moments, *gauche/trans* energy differences both in the gas phase and in solvent are given in Table 3. As expected, the relative energies in all systems examined here become either more negative or less positive which indicates that the greater stabilization of the gauche form in polar solvent. However, the change is rather small. This result is not surprised because

that the difference in dipole moment between the *gauche* form and *trans* form is quite small in all cases. Nevertheless, the small solvent effect is sufficient to alter the conformational preference of several molecules, for example, **OO**.

6.4 Conclusions

The gauche/trans conformational equilibrium of a series of XCH_2CH_2Y (X, Y = NMe_2, PMe_2, OMe and SMe) molecules were studied by ab *initio* and DFT methods. The relevant intramolecular CH···X (X = O, N, S and P) interaction was examined by G3(MP2) level. The calculations show that intramolcular CH···X interaction stabilizes the gauche conformation significantly. The estimated CH···O and CH···N interaction energies are in the range 4-6 kJ mol^{-1}. Systems with mixed hetero atoms, such as OS, ON, OP, NS and NP prefer a *gauche* conformer. The repulsion between heavy atoms also contributes to the conformational preference. Due to the small difference in dipole moment between *gauche* and *trans* forms, the calculated solvent effect is generally small. All the intramolecular CH···X (X = O, N, S and P) interactions are confirmed to be hydrogen bonding in nature based on AIM analysis.

6.5 References

1 Jeffrey, G. A.; Saenger, W. *Hydrogen Bonding in Biological Structures*; Springer-Verlag: Berlin, 1991.

2 Scheiner, S. *Hydrogen Bonding: A Theoretical Perspectiv*e; Oxford University Press: New York, 1997.

3 (a) Pimentel, C. G.; McClellan, A. L. *The hydrogen bond*; W. H. Freeman and Co.: San Francisco, 1960; (b) Allerhand, A.; Schleyer, P. v. R. *J. Am. Chem. Soc.* **1963**, *85*, 1715. (c) Creswell, C. J.; Allred, A. L. *J. Am. Chem. Soc.* **1963**, *85*, 1723. (d) Sutor, J. D. *J. Chem. Soc*. **1963**, 1105.

4 Taylor, R.; Kennard, O. *J. Am. Chem. Soc.* **1982**, *104*, 5063.

5 Cappelli, A.; Giorgi, G.; Anzini, M.; Vomero, S.; Ristori, S.; Rossi, C.; Donati, A. *Chem. Eur. J*. **2004**, *10*, 3177 and references therein.

6 Wetmore, S. D.; Schofield, R.; Smith, D. M.; Radom, L. *J. Phys. Chem. A* **2001**, *105*, 8718, and references therein.

7 Desiraju, G. R. *Chem. Commun*, **2005**, 2995, and references therein.

8 Nishio, M. *CrystEngComm*, **2004**, *6*, 130, and references therein.

9 (a) Novoa, J. J.; Rovira, M. C.; Rovira, C. Veciana, J.; Tarres, J. *Adv. Mater.* **1995**, *7*, 233. (b) Surange, S. S.;Kumaran, G.; Rajappa, S.; Pal, D.; Chakrabarti, P. *Hel*V. *Chim. Acta* **1997**, *80*, 2329. (c) Ueno, T.; Inohara, M.; Ueyama, N.; Nakamura, A.*Bull. Chem. Soc. Jpn* **1997**, 1077. (d) Pedireddi, V. R.; Chatterjee,S Ranganathan, A.; Rao, C. N. R. *J. Am. Chem. Soc.* **1997**, *119*, 10 867. (e) Potrzebowski, M. J.; Michalska, M.; Koziol, A. E.; Kazmierski, S.; Lis, T.; Pluskowski, J.; Ciesielski, W. *J. Org. Chem.* **1998**, *63*, 4209.

10 Weiss, H. C.; Boese, R.; Smith, H. L.; Haley, M. M. *J. Chem. Soc., Chem. Commun.* **1997**, 2403.

11 (a) Davis, S. R.; Andrews, L. *J. Am. Chem. Soc.* **1987**, *109*, 4768. (b) Shimoni. L.; Carrell, H. L.; Glusker, J. P.; Coombs, M. M. *J. Am. Chem. Soc.* **1994**, *116*, 8162. (c) Aakeroÿ, C. B.; Seddon, K. R. *Z. Naturforsch.* **1996**, *B48*, 1023. (d) James, S. L.; Verspui, G.; Spek, A. L.; van Koten, G. *J. Chem. Soc., Chem. Commun.* **1996**, 1309. (e) Howard, J. A. K.; Hoy, V. J.; O¢Hagan, D.; Smith,G. T. *Tetrahedron* **1996**, *52*, 12 613. (f) Weiss, H. C.; Boese, R.; Smith, H. L.; Haley, M. M.; *J. Chem. Soc., Chem. Commun.* **1997**, 2403. (g) Thalladi, V. R.; Weiss, H. C.; Blåser, D.; Boese, R.; Nangia, A.; Desiraju, G. R. *J. Am. Chem. Soc.* **1998**, *120*, 8702. (h) Grepioni, F.; Cojazzi, G.; Draper, S. M.; Scully, N.; Braga, D. *Organometallics* **1998**,*17*, 296. (i) Spaniel, T.; Gols, H.; Scholz, J. *Angew. Chem., Int. Ed. Engl.* **1998**, *37*, 1862. (j) Aakeroÿ, C. B.; Evans, T. A.; Seddon, K. R.; Palinko, I. *New J. Chem.* **1999**, *3*, 145. (k) Bats, J. W.; Parsch, J.; Engels, J. W. *Acta Crystallogr. C* **2000**, *56*, 201. (l) Ma, B. Q.; Gao, S.; Yi, T.; Yan, C. H.; Xu, G. X. *Inorg. Chem. Commun*. **2000**, *3*, 93. (m) Freytag, M.; Jones, P. G. *Chem. Commun*. **2000**, 277.

12 Narayanan, S. J.; Sridevi, B.; Chandrashekar, T. K.; Vij, A.; Roy, R. *Angew. Chem. Int. Ed. Eng.* **1998**, *37*, 3394.

13 (a) Iwaoka, M.; Tomoda, S. *J. Am. Chem. Soc.* **1994**, *116*, 4463. (b) Iwaoka, M.; Komatsu, H.; Tomoda, S. *Bull. Chem. Soc. Jpn.* **1996**, *69*,1825.

14 (a) Mueller-Westerhoff, U. T.; Nazzal, A.; Prössdorf. *J. Am. Chem. Soc.* **1981**, *103*, 7678. (b) Mueller-Westerhoff, U. T. *Angew. Chem., Int. Ed. Engl.* **1986**, *25*,

702. (c) Arduengo, A. J., III.; Gamper, S. F.; Tamm, M.; Calabrese, J. C.; Davidson, F.; Craig, H. A. *J. Am. Chem. Soc.* **1995**, *117*, 572. (d) Platts, J. A.; Howard, S. T.; Wozniak, K. *J. Chem. Soc., Chem. Commun.* **1996**, 63. (e) Platts, J. A.; Howard, S. T.; *J. Chem. Soc., Perkin Trans. 2* **1997**, 2241.

15 (a) Legon, A. C.; Wallwork, A. L. *J. Chem. Soc., Chem. Commun.***1989**, 588. (b) Legon, A. C.; Wallwork, A. L. *J. Chem. Soc., Faraday Trans.* **1992**, *88*, 1.

16 Nguyen, M. T.; Coussens, B.; Vanquickenborne, L. G.; Gerber, S.; Huber, H. *Chem. Phys. Lett.* **1990**, *167*, 227.

17 Legon, A. C.; Wallwork, A. L.; Warner, H. E. *Chem. Phys. Lett.* **1992**, *191*, 97.

18 Komasa, J.; Szalewicz, K.; Leszczynski, J. *Chem. Phys. Lett.* **1998**, *285*, 449.

19 Scheiner, S. *Advances in Molecular Structure Research*; Hargittai, M., Hargittai, I., Eds.; JAI Press: Stamford, CT, **2000**, *6*, 159.

20 Hobza, P.; Havlas, Z. *Chem*. *Phys*. *Lett.* **1999***, 303*, 407.

21 Yoshida, H.; Kaneko, I.; Matsuura, H.; Ogawa, Y.; Tasumi, M. *Chem*. *Phys*. *Lett*. **1992**, *196*, 601.

22 Tsuzuki, S.; Uchimaru, T.; Tanabe, K.; Hirano, T. *J*. *Phys*. *Chem*. **1993**, *97*, 1346.

23 R. L. Jaffe.; G. D. Smith.; D. Y. Yoon. *J. Phys. Chem.* **1993**, *97*, 12745.

24 G. D. Smith.; R. L. Jaffe.; D. Y. Yoon. *J. Phys. Chem.* **1993**, *97*, 12752.

25 G. D. Smith.; R. L. Jaffe.; D. Y. Yoon. *J. Am. Chem. Soc.* **1995**, *117*, 530.

26 F. Müller-Plathe.; W. F. Gunsteren. *Macromolecules.* **1994**, *27*, 6040.

27 H. Liu.; F. Müller-Plathe.; W. F. Gunsteren. *J. Chem.Phys.* **1995**, *102*, 1722.

28 O. Engkvist.; P.-O. Åstrand.; G. Karlstrom. *J. Phys. Chem.* **1996**, *100*, 6950.

29 D. J. Williams.; K. B. Hall. *J. Phys. Chem.* **1996**, *100*, 8224.

30 Astrup, E. E. *Acta Chem*. *Scand*., *Ser*. *A* **1979**, *33*, 655.

31 Yoshida, H.; Tanaka, T.; Matsuura, H. *Chem*. *Lett*. **1996**, 637.

32 T. Steiner. *Chem. Commun*. **1997**, 727.

33 Harada, T.; Yoshida, H.; Ohno, K. ; Matsuura, H.; Zhang, J.; Iwaoka, M.; Tomoda, S. *J. Phys. Chem. A*. **2001**. *105*. 4517.

34 Yoshida, H.; Harada, T.; Ohno, K. Matsuura, H. *Chem. Commun*. **1997**, 2213.

35 Hobza, P.; Havlas, Z. *Chem. Rev*. **2000**, *100*, 4253.

36 Yoshida, H.; Harada, T.; Ohno, K.; Matsuura, H. *Chem*. *Phys*. *Lett*. **2002**, *365*, 453.

37 Scheiner, S.; Kar, T. *J. Phys. Chem. A*. **2002**. *106*. 1784.

38 Li, X.; Liu, L.; Schlegel, H. B. *J. Am. Chem. Soc.* **2002**, *124*, 9639.

39 Alabugin, I. V.; Manoharan, M.; Peabody, S.; Weinhold, F. *J. Am. Chem. Soc.* **2003**, *125*, 5973.

40 Delanoye, S. N.; Herrebout, W. A.; van der Veken, B. J. *J. Am. Chem. Soc.* **2002**, *124*, 11854, and references therein.

41 Matsuura, H.; Yoshida, H.; Harada.; Hieda, M.;Yamanaka, S. Y.; Harada, T.; Kei, S. Y.; Ohno, K. *J. Am. Chem. Soc.* **2003**, *125*, 13910.

42 SPARTAN 5. Wavefunction Inc., Irvine, CA 1997.

43 Curtiss, L. A.; Raghavachari, K.; Redfern, P. C.; Rassolov, V.; Pople, J. A. *J. Chem. Phys.* **1999**, *110*, 4703.

44 Onsager, L. *J. Am. Chem. Soc*. **1936**, *58*, 1486.

45 (a) Tapia, O.; Goscinski, O. *Mol. Phys*. **1975**, *29*, 1653. (b) Wong, M. W.; Frisch, M. J.; Wiberg, K. B. *J. Am. Chem. Soc*. **1991**, *113*, 4776. (c) Wong, M. W.;

Wiberg, K. B.; Frisch, M. J. *J. Chem. Phys*. **1991**, *95*, 8991. (d) Wong, M. W.; Wiberg, K. B.; Frisch, M. J. *J. Am. Chem. Soc*. **1992**, *114*, 1645.

46 Frisch, M. J.; Trucks, G. W.; Schlegel, H. B.; Scuseria, G. E.; Robb, M. A.; Cheeseman, J. R.; Zakrzewski, V. G.; Montgomery, Jr, J. A.; Stratmann, R. E.; Burant, J. C.; Dapprich, S.; Millam, J. M.; Daniels, A. D.; Kudin, K. N.; Strain, M. C.; Farkas, O.; Tomasi, J.; Barone, V.; Cossi, M.; Cammi, R.; Mennucci, B.; Pomelli, C.; Adamo, C.; Clifford, S.; Ochterski, J.; Petersson, G. A.; Ayala, P. Y.; Cui, Q.; Morokuma, K.; Malick, D. K.; Rabuck, A. D.; Raghavachari, K.; Foresman, J. B.; Cioslowski, J.; Ortiz, J. V.; Baboul, A. G.; Stefanov, B. B.; Liu, G.; Liashenko, A.; Piskorz, P.; Komaromi, I.; Gomperts, R.; Martin, R. L.; Fox, D. J.; Keith, T.; Al-Laham, M. A.; Peng, C. Y.; Nanayakkara, A.; Gonzalez, C.; Challacombe, M.; Gill, P. M. W.; Johnson, B.; Chen, W.; Wong, M. W.; Andres, J. L.; Gonzalez, C.; Head-Gordon, M.; Replogle, E. S.; Pople, J. A. *Gaussian 98*, Gaussian, Inc., Pittsburgh PA, 1998.

47 (a) Bader, R. F. W. Atoms in Molecules–*A Quqntum Theory*; Oxford Science Publications: Oxford, **1999**. (b) Bader, R. F. W. *Chem. Rev*. **1991**, *91*, 893.

48 Popelier, P. L. A.; Bone, R. G. A. *MORPHY98*; UMIST, Manchester, **1998.**

49 Bondi, A. *J. Phys. Chem.* **1964**, 68, 441.

50 Tian, A. M.; Wu, D.Y.; Ren, Y.; Wang, X.; Wong, N.B.; Li, W-K. *J. Mol. Struct*. (Theochem), **1999**, *363*, 171.

51 Hartmann, M.; Wetmore, S. D.; Radom, L. *J. Phys. Chem. A* **2001**, *105*. 4470.

52 (a) Kock, U. ; Popelier, P. L. A. *J. Phys. Chem.* **1995**, *99*, 9747. (b) Popelier, P. L. A. *J. Phys. Chem. A* **1998**, *102*, 1873.

6.6 Appendix

Table 6.1 Calculated gauche/trans energy difference (kJ mol^{-1}) of disubstituted ethanes XCH_2CH_2Y (X, Y= NMe_2, PMe_2, OMe, SMe)

Species	HF/6-31G*	B3LYP/6-31G*	MP2(Full)	G3(MP2)
ON*[b]	1.7	-2.4	-3.6	-0.3
ON**[c]	8.8	3.8	1.6	4.0
OS*	-0.5	-2.3	-3.1	-0.6
OS**	13.2	10.8	11.5	10.6
OP*	-2.7	-3.4	-5.6	-2.6
OP**	4.9	12.1	11.2	12.7
NS*	1.7	0.0	-2.4	-0.2
NS**	11.0	8.3	7.8	6.6
NP*	-1.4	-1.6	-6.3	-3.1
SP*	7.3	5.8	3.5	2.3
SP**	11.5	8.1	5.5	4.2
OO	6.9	1.3	0.3	2.4
NN	1.3	-0.3	-5.7	-1.6
SS	8.8	8.6	7.5	6.6
PP	9.0	7.4	4.0	3.8

[a] Energies are given in kJ mol^{-1}.

[b] One asterisk represents that the first atom is the hydrogen bond acceptor.

[c] Two asterisk represent that the second atom is the hydrogen bond acceptor

Table 6.2 Calculated CH···X bonding properties of the gauche/trans forms of disubstituted ethanes XCH_2CH_2Y (X, Y= NMe_2, PMe_2, OMe, SMe)

Species	d(H···Y)[a]	d(X···Y)[a]	Δ(C–H)[a]	ρ(H···Y)[b]	$\nabla_2\rho$ (H···Y)[b]	Δυ[c]	ΔE[d]
OO	2.453	3.034	-0.0048	0.0117	0.0429	34.8	-4.6
OS*[e]	2.438	3.227	-0.0063	0.0122	0.0441	46.8	-5.0
SS	2.794	3.330	-0.0019	0.0091	0.0322	15.6	1.9
OS**[f]	2.745	3.589	-0.0021	0.0097	0.0341	15.7	
NN	2.606	2.884	-0.0013	0.0103	0.0401	13.4	-4.5
NP*	2.680	3.186	-0.0023	0.0096	0.0309	25.4	-4.5
NS*	2.501	3.327	-0.0028	0.0130	0.0395	27.2	-4.6
ON**	2.483	3.094	-0.0065	0.0137	0.0410	45.3	
ON*	2.323	3.112	-0.0049	0.0151	0.0522	38.0	-6.3
OP*	2.542	3.090	-0.0025	0.0097	0.0363	27.9	-5.6
NS**	2.805	3.637	-0.0025	0.0097	0.0346	24.2	
SP*	2.897	3.525	-0.0012	0.0076	0.0264	4.7	0.6
SP**	2.843	3.620	-0.0021	0.0094	0.0279	17.5	
OP**	2.922	3.265	-0.0027	0.0080	0.0245	19.1	
PP	2.955	3.562	-0.0010	0.0059	0.0177	9.5	1.5

[a] Distance is given in Å, based on MP2/6-31G* geometry.

[b] ρ and $\nabla_2\rho$ are given in au, based on MP2/6-31G* wavefunction.

[c] $\Delta\upsilon$ is given in cm $^{-1,}$ based on the MP2/6-31G* frequency.

[d] ΔE is given in kJ mol^{-1}, based on modified G3(MP2) method.

[e] One asterisk represents that the first atom is the hydrogen bond acceptor.

[f] Two asterisk represent that the second atom is the hydrogen bond acceptor.

Table 6.3 Calculated dipole moments (D) and *gauche/trans* energy difference (kJ mol^{-1}) of disubstituted ethanes XCH_2CH_2Y (X, Y = NMe_2, PMe_2, OMe, SMe) in solution[a]

Species	Dipole[b]	$\delta\Delta E$[c]	ΔE[d]
OO*	1.56	-2.7	-0.3
OS*	2.12	-0.8	-1.4
OS**	1.45	1.0	11.6
ON*	0.95	-0.3	-0.6
ON**	1.66	-0.9	3.1
OP*	1.36	-0.2	-2.8
OP**	1.89	-0.9	11.8
NN*	0.66	0.0	-1.6
NS*	2.27	-1.3	-1.5
NS**	1.91	-0.5	6.1
NP*	1.55	-0.7	-3.8
SP*	1.45	-0.4	1.9
SP**	2.42	-1.4	2.8
SS*	1.86	-1.1	5.5
PP*	2.04	-1.6	2.2

[a] based on B3LYP/6-31G* SCRF (ε=40) calculation.

[b] based on B3LYP/6-31G* calculation.

[c] $\delta\Delta E=\Delta E_s - \Delta E_g$

[d] relative energy of *gauche/trans* conformation estimated at G3(MP2) level in solution.

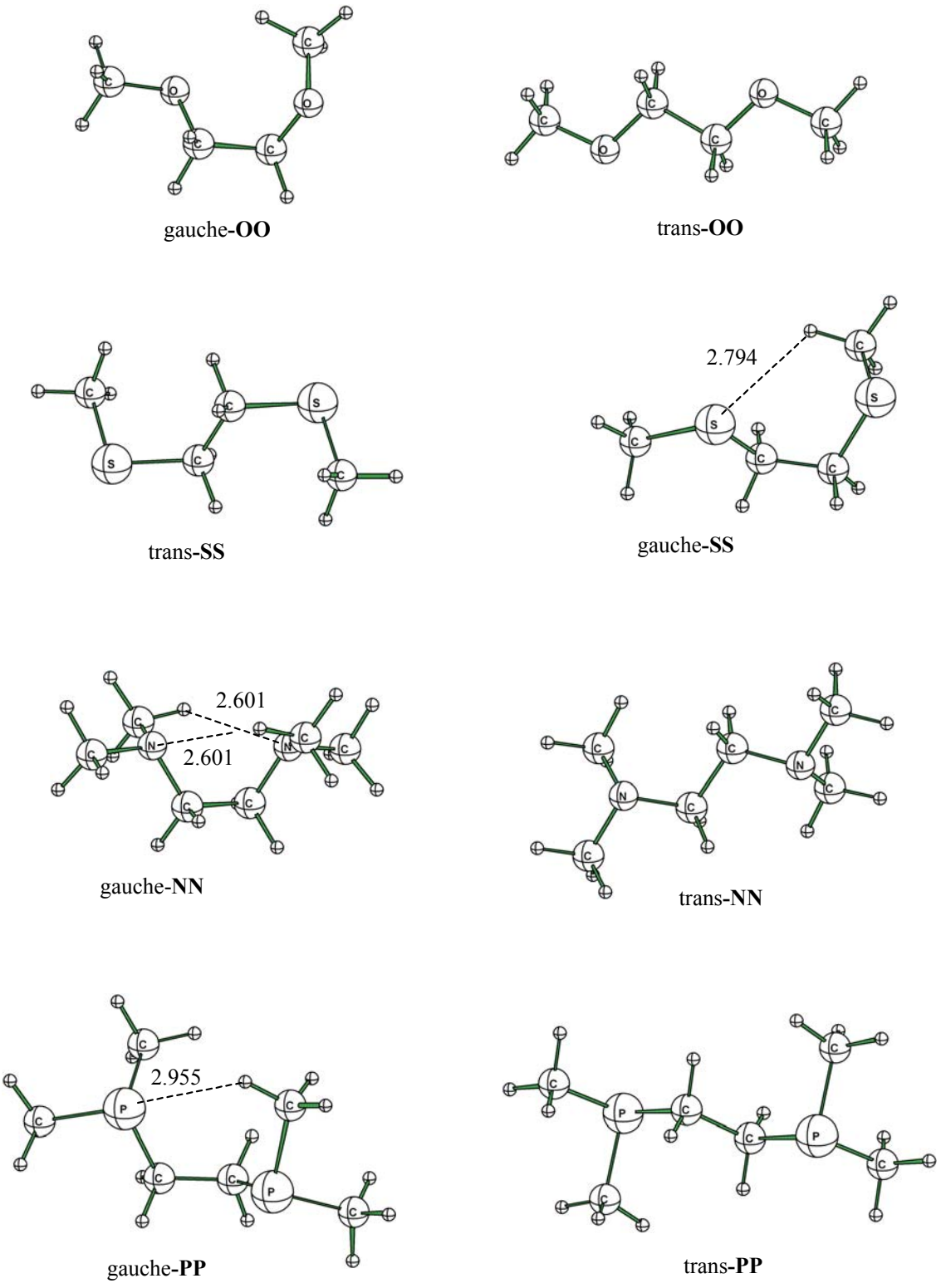

Figure 6.1 Optimized (MP2/6-31G*) geometries of molecules OO, OS and ON. Bond distances in Å.

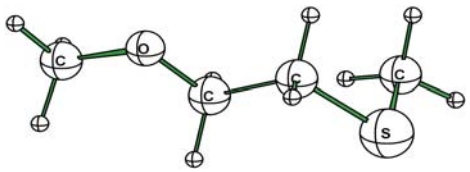

trans-**OS**

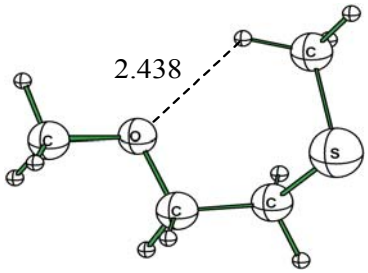

gauche'-**OS**

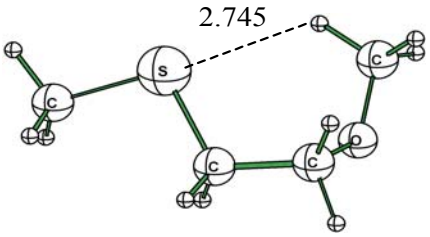

gauche"-**OS**

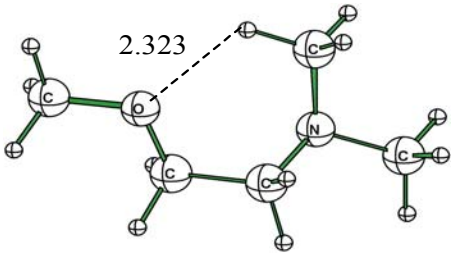

gauche'-**ON**

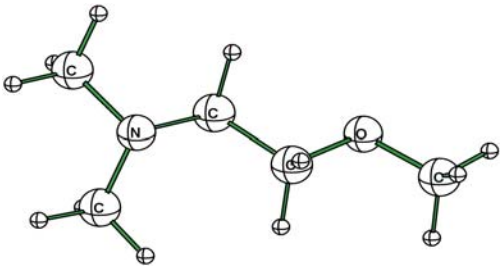

trans-**ON**

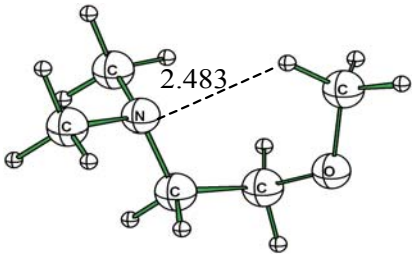

gauche"-**ON**

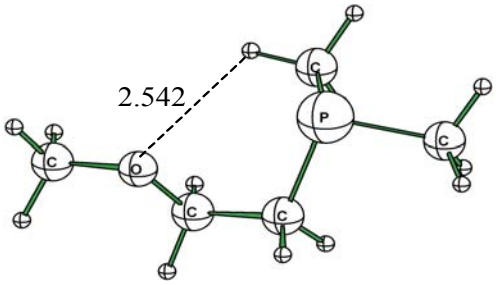

gauche'-**OP**

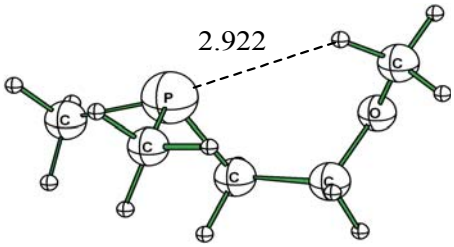

gauche"-**OP**

Figure 6.2 Optimized (MP2/6-31G*) geometries of molecules **OS, ON and OP**. Bond distances in Å.

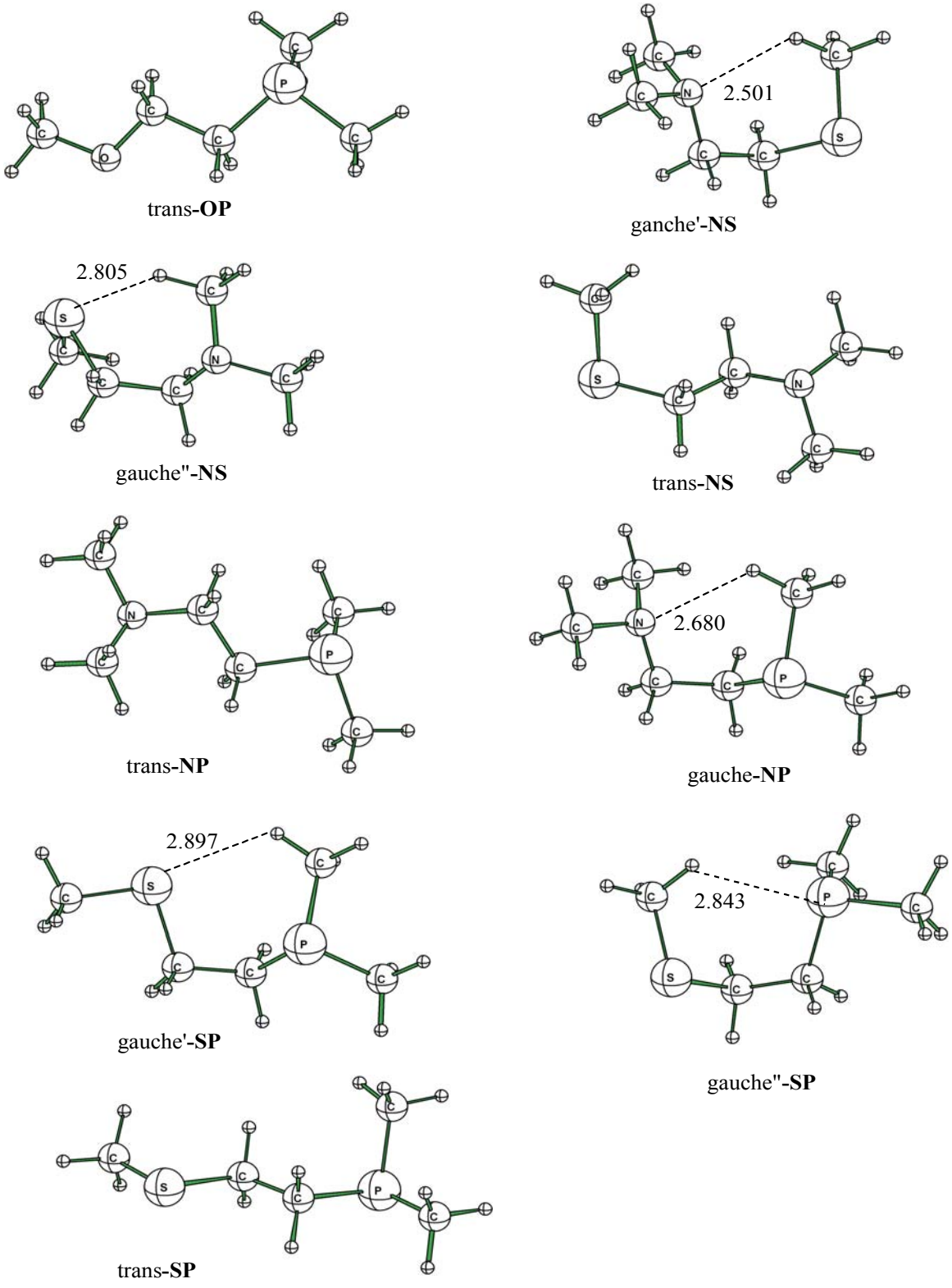

Figure 6.3 Optimized (MP2/6-31G*) geometries of molecules **OP, NS, NP and SP.** Bond distances in Å.

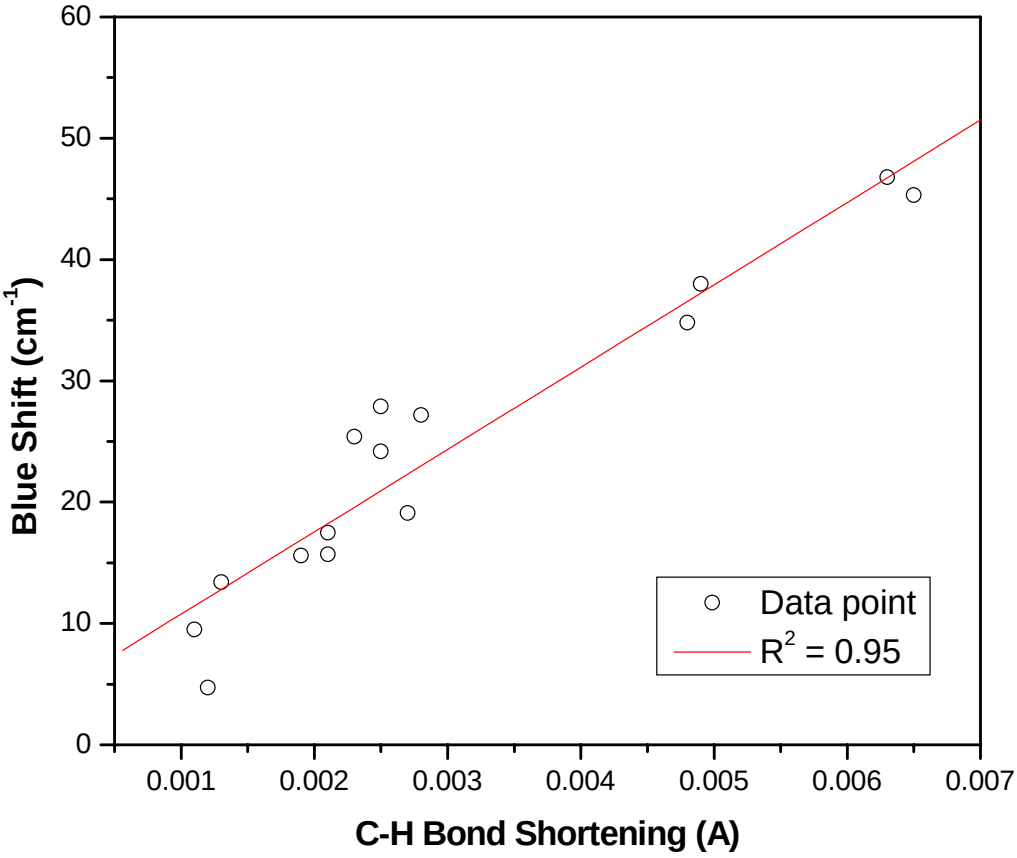

Figure 6.4 Correlation plot between C-H bond shortening and vibrational frequency shift for the gauche forms of disubstituted ethanes.

Chapter 7

Conformations of 4,4-Bisphenylsulfonyl-*N*,*N*-dimethylbutylamine: Interplay of Intramolecular C–H···N, C–H···O and π···π Interactions

7.1 Introduction

During the past decades, the weak hydrogen bonding involving a hydrogen atom bound to a carbon atom (C–H) as hydrogen donor has attracted strong interest from the scientific community. These weak interactions are found to play essential roles in molecular recognition, properties of condensed phases, solid state reactions, crystal engineering and structures of biomolecules.[1-4] The concept of C–H···X (X = electronegative element or π acceptor) hydrogen bonds is now well documented.[5] In particular, the C–H···N,[6] C–H···O,[7] and C–H···π [3,8] interactions have been the subject of numerous experimental and theoretical investigations. Further advancement in this area is attributed to the development of new experimental techniques and the refinement of theoretical calculations which allow a more accurate description of these subtle weaker interactions.

X-ray diffraction studies have provided strong evidence for the existence of weak intermolecular and intramolecular C–H···X hydrogen bonds in solids. On the other hand, detection of these weak hydrogen bonds in solution represents a major challenge as they

are weaker than the typical solvent-solute interactions and the thermal effects in liquid. A few elegant experimental studies have shown convincingly that C–H···O hydrogen bonds can persist in solution.[9,10] This type of intermolecular force is crucial in understanding the structures and functions of molecules with biological and pharmaceutical interest.[11] More recently, Fox and co-workers have demonstrated the persistence of an intramolecular C–H···N bond in solution on the basis of ^{1}H NMR chemical shift experiments.[12] Furthermore, Arunima and Kurur have employed a cross-correlated method to establish the existence of a C–H···N hydrogen bond in a diphenyl disulfone compound, 4,4-bisphenylsulfonyl-*N,N*-dimethylbutylamine (BPSDMBA).[13] For a similar methyl derivative, 4,4-bisphenylsulfonyl-2,*N,N*-trimethylbutylamine (BPSTMBA), both X-ray[14] and ^{1}H NMR[15] studies by Sammes et al have shown unequivocally the existence of an intramolecular C–H···N hydrogen bond. In this chapter, we examined in detail the role of the weak C–H···N hydrogen bond in the conformational stability of BPSDMBA and BPSDTMA in the gas phase and in solution. In addition, we attempted to provide an estimate the bond strength of this weak C–H···N intramolecular hydrogen bond using the topological analysis based on the Bader's theory of atoms in molecules (AIM). Unexpectedly, we found that C–H···O and π-π interactions also play an important role in governing the conformational stability of these disulfone compounds.

7.2 Computational Methods

Conformational search at HF/3-21G level was carried out using the SPARTAN program[16] to locate all possible conformers of BPSDMBA. The unique conformers were

fully optimized using the hybrid DFT method B3LYP [17,18] together with the 6-31+G* basis set. Higher-level relative energies were obtained through single-point calculations at the MP2 level in conjunction with a larger 6-311+G** basis set based on the B3LYP/6-31+G* optimized geometries. The MP2 theory is important for reliable prediction of the relative energies of BPSDMBA conformers as several conformers are stabilized by π-π interaction.[19] The effect of solvation was examined by Onsager's self-consistent reaction field (SCRF) theory.[20] For the solvent effect calculations, energies were obtained at the B3LYP/6-311+G**//B3LYP/6-31+G* level in a dielectric medium of ε = 40. In addition, we have investigated a series of intermolecular $AH^{\cdots}NH_3$ (AH = proton donor) complexes which involve a $C–H^{\cdots}N$ hydrogen bond. Their structures and binding properties were examined at the B3LYP/6-31+G* level. The computed interaction energies of these intermolecular complexes were corrected by the basis set superposition error (BSSE), based on the counterpoise method.[21] Charge density analysis, based on Bader's theory of atoms in molecules (AIM),[22] was carried out using the MORPHY98 program.[23] NMR chemical shift calculations were performed using the gauge-independent atomic orbital (GIAO) method.[24] All ab initio and DFT calculations were performed using the Gaussian 03 suite of program.[25]

7.3 Results and Discussion

7.3.1 Conformational Analysis of BPSDMBA

We are not aware of any theoretical study on BPSDMBA [molecular formula: $Ne_2CH_2CH_2CH_2CH(SO_2Ph)_2$]. To locate all possible conformers of BPSDMBA, a

systematic conformational search, via a dihedral driver, was carried out initially at the HF/3-21G level. All the unique conformers were then fully optimized at the B3LYP/6-31+G* level. The benchmark calculations of **a** indicate that the DFT optimized structure is in good agreement with MP2/6-311+G** and QCISD/6-31G* geometries. Our conformational analysis led to 17 unique conformers of BPSDMBA (**a** – **q**). Their calculated relative energies (MP2/6-311+G**) are given in Table 1 and the optimized geometries of selected conformers are shown in Figure 7.1. All the BPSDMBA conformers are stabilized by the non-conventional C–H···X (X = N or O) type of internal hydrogen bonding interactions. The C–H···X contact distances are summarized in Table 7.1 and Figure 7.1. The calculated C–H···X bond distances and angles are consistent with the geometry criteria of a hydrogen bond proposed by Steiner and Saenger,[26] e.g. C–H···O distance ≤ 2.70 Å and C–H···O angle > 90° for C–H···O hydrogen bond. Of the 17 conformations, the 4 most stable conformers (**a** – **d**) exhibit an intramolecular C–H···N hydrogen bond between the dimethylamino nitrogen and the central methine hydrogen. Conformer **b** has a shorter C–H···N contact distance of 2.251 Å, while the H···N interaction distances of other three conformers fall in a narrow range of 2.36 – 2.38 Å. These interacting distances are significantly less than the sum of their van der Waal radii (2.70 Å).[27] In these conformers, the C–H···N interaction forms part of a stable arrangement of six-membered ring. The side chain has curled round to allow the intramolecular interaction. Conformer **a** is the most stable conformer of BPSDMBA. The calculated structure is in excellent agreement with the X-ray structure of the methyl analogue (BPSTMBA),[14] which is characterized by an intramolecular hydrogen bond (C–H···N distance = 2.34 Å). The methane C–H stretching vibrational frequencies in **a** – **d** are

~24 cm^{-1} lower than those in conformers without the intramolecular C–H···N hydrogen bond. Interestingly, the parallel orientation of the two phenyl rings observed in the crystal structure of BPSTMBA is readily reproduced in the optimized geometry of conformer **a**. The inter-plane distance between the two phenyl rings is 3.20 Å, close to those observed in organic molecular crystals of benzene, 3.3 – 3.6 Å .[28] This suggests that the π-π interaction contributes significantly to the stability of **a**. Furthermore, this stacking form is expected to be favored compared to other conformations in crystal packing environment.

Somewhat unexpectedly, the sulfonyl oxygens interact with neighbouring methylene, *N*-methyl or phenyl hydrogen via the C–H···O interaction (Figure 7.1). In fact, multiple C–H···O close contacts are found in all the BPSDMBA conformers except **d.** The C–H···O interacting distances in BPSDMBA are in the range 2.35 – 2.87 Å (Table 7.1). Interestingly, a C–H···π type of interaction is also observed in conformers **d** and **h**. In these cases, the C–H hydrogen points towards the mid point of a C=C bond of the phenyl ring (Figure 7.1). In summary, various weak types of intramolecular force play an important role in the governing the conformational stability of the BPSDMBA. However, it is difficult to assess the relative importance of these interactions. The most stable conformation (**a**) is stabilized by three types of molecular force: C–H···N, C–H···O and π-π interactions.

Since several of the lowest energy conformations lie close in energy, we expect solvation may influence the relative stability of these conformers. In particular, many conformations are characterized by a fairly large dipole moment of 7.3–8.3 D (Table 7.1).

It is also intriguing to know how solvation affects the stability of the weak intramolecular C–H···N and C–H···O interactions in BPSDMBA. Hence, we have examined the structures and relative stability of the BPSDMBA conformers using the SCRF continuum model[20] in a dielectric medium of ε = 40 (representing an aprotic polar medium). The calculated solvation energy [$\delta\Delta E = \Delta E$ (ε = 40) – ΔE (ε = 1)] are given in Table 7.1. Introduction of a solvent effect has small effect on the calculated geometries (Table 7.1). As one might have expected, the polar conformers have a large change of $\delta\Delta E$ (~10 kJ mol^{-1}). Thus, the order of conformational stability changes significantly in the presence of a polar medium. However, conformer **c** remains the lowest energy structure of BPSDMBA. Most importantly, the weak intramolecular C–H···N, C–H···O and π-π interactions are found to prevail in solution. In fact, the C–H···N interaction distance decreases slightly in all cases (Table 7.1).

7.3.2 Structural Parameters and ^{1}H Chemical Shifts of BPSDMBA

The presence of intramolecular C–H···N hydrogen bonding in BPSDMBA was established indirectly by cross-correlated method in solution.[13] On the other hand, there were direct X-ray crystallographical and ^{1}H NMR spectroscopic evidences for the methyl analogue, 4,4-bisphenylsulfonyl-2,*N*,*N*-trimethylbutylamine (BPSTMBA).[14,15] The additional methyl group in BPSTMBA was introduced to the side chain to reduce the conformational mobility of the molecule. To provide a direct comparison with experiment, we have investigated also the structure and ^{1}H NMR chemical shifts of BPSTMBA at the B3LYP/6-31+G* level. The computed results are summarized in Table 7.2. The

calculated the C–H···N structural parameters of BPSTMBA are in good accord with the X-ray structure,[14] with the calculated C–H···N distance within 0.06 Å of the experimental value and the C–H···N angle within 2.6°. The computed ^{1}H chemical shift (6.6 ppm) of the disulfone methine proton agrees well the experimental value (6.2 ppm).[15] Furthermore, the observed downfield shift (2.2 ppm) with respect to a carbon reference compound is readily reproduced by our GIAO calculations (2.5 ppm). In summary, our calculated results confirm the existence of the intramolecular C–H···N hydrogen bond in both BPSDMBA and BPSTMBA.

7.3.3 Topological Analysis of the C–H···N interaction in BPSDMBA

Apart from the geometry criteria mentioned above, there are other means of characterizing the C–H···N interaction. One such approach is based on quantum theory of "atoms in molecules" (AIM).[22] This theory allows one to identify and characterize a bonding interaction between atoms through an analysis of the charge density ρ. The AIM analysis has been successfully employed to characterize hydrogen bonds and non-covalent interactions in a variety of molecular complexes. In particular, Koch and Popelier have proposed a set of criteria to characterize the weak C–H···O hydrogen bonds.[29] Here, we have applied the three most important criteria of Koch and Popelier to examine the nature of the intramolecular C–H···N interaction in the BPSDMBA conformers **a**–**d**. Firstly, the charge density contour plot of **a** (Figure 7.2) clearly shows the correct topology for a hydrogen bond. There exists a bond critical point (bcp) between the two interacting hydrogen and nitrogen atoms. In addition, the characteristic flat hydrogen bond

interatomic surface is observed, a pattern that has been reported previously.[29] Secondly, the charge density evaluated at the bond critical point (ρ = 0.0153 – 0.0194) is an order of magnitude smaller than those found for a covalent bond. In fact, the ρ values observed here are similar to those of the intermolecular C–H···N hydrogen-bonded systems (see Section 3.4). Thirdly, the Laplacian of the charge density ($\nabla_2\rho$) evaluated at the bcp is positive, consistent with those calculated for a typical hydrogen bond. This is in distinct contrast to the negative $\nabla_2\rho$ value of a typical covalent bond. In summary, the intramolecular C–H···N interaction between the methine hydrogen and the nitrogen atom in BPSDMBA exhibits the characteristic charge density topology of a typical weak hydrogen bond.

7.3.4 The strength of intramolecular C–H···N hydrogen bond in BPSDMBA

To shed light on the strength of the intramolecular C–H···N hydrogen bond in BPSDMBA, we have studied the binding properties of a series of AH···NH_3 complexes (AH = proton donor) which involves an intermolecular C–H···N hydrogen bond at the B3LYP/6-31+G* level. The AH molecules examined include CH_4, CH_3Me, CH_2Me_2, $CHMe_3$, CH_3F, CH_2F_2, CHF_3, CH_3SO_2H, $CH_2(SO_2H)_2$, CH_3CN, $CH_2(CN)_2$ and $CH(CN)_3$. This list represents a wide range of proton donating ability. We have examined the interaction energies, geometrical parameters, vibrational frequencies as well as the topological properties which characterize the intermolecular C–H···N hydrogen bond.

As expected, an electron withdrawing substituent (F, CN or SO_2H) increases the proton donating ability, which leads to a stronger C–H···N intermolecular complex. As a consequence, the calculated interaction energies of the NH_3 complexes range from very weak (< 1 kJ mol^{-1}) to medium (~10 kJ mol^{-1}) to very strong (> 20 kJ mol^{-1}). Successive substitution of a substituent group leads to a rather uniform increment of interaction energy (Table 7.3). For the cyano series, a fairly large increment of ~12 kJ mol^{-1} for each CN group substitution is observed. The $HC(CN)_3$···NH_3 complex has the largest interaction energy of –37.9 kJ mol^{-1}, substantially larger than those with a typical conventional hydrogen bond. For comparison, the computed interaction energy of water dimer is –22.2 kJ mol^{-1} at the same level of theory. It is important to note that the B3LYP/6-31+G* level, include BSSE correction, employed here yield reliable estimates of the C–H···N interaction energies. This is supported by benchmark calculations on the CH_3F···NH_3 system. As evidenced in Table 7.4, various levels of correlation treatment and different basis sets yield similar results. In accordance with the interaction energy, the intermolecular C–H···N distance spans a wide range from 1.96 to 2.82 Å. A shorter C–H···N distance is associated with the stronger complex. The C–H···N angle is close to linearity in all cases (Table 7.3).

The stronger C–H···N complexes exhibit the characteristic of a normal hydrogen bond in which the C–H bond is lengthened upon complex formation. As a consequence, a red shift is observed for the C–H stretching frequency for these complexes (Table 7.3). On the other hand, the C–H bond is shortened upon hydrogen bond formation for the weaker complexes (< –10 kJ mol^{-1}). In these systems, the bond shortening is accompanied by an

increase in the C–H stretching frequency (i.e. a blue shift). For instance, the C–H bond length in $CHMe_3$ is shortened by 0.0022 Å upon formation of a hydrogen-bonded complex with ammonia. Accordingly, the C–H frequency undergoes a blue shift of 33 cm^{-1} in the complex. Hobza and co-worker called this type of interaction which shows a blue shift and bond contraction an ″anti″ hydrogen bond.[30] They concluded that dispersion forces play a major role in this form of interaction.

The C–H···N interaction in these complexes is characterized by a bond path and its associated bond critical point (bcp). The calculated values of electron density (ρ) and Laplacian of charge density ($\nabla_2\rho$) at the bcp are given in Table 3. The ranges of ρ (0.002 – 0.034 au) and $\nabla_2\rho$ (0.024 – 0.139 au) values lie in the ranges of the typical hydrogen-bonded systems.[29] This result confirms the hydrogen-bond nature of the C–H···N interaction in these intermolecular complexes. Previous studies have shown that the electron density (ρ) value at the bond critical point may be used to quantify the strength of bonding interaction involved.[31,32] As can be seen in Table 3, the electron density (ρ) correlates very well with the interaction energy (E_{int}) for the various intermolecular $AH\cdots NH_3$ complexes investigated here. This linear relationship is demonstrated in the correlation plot shown in Figure 3. Hence, the almost perfect linear fit (R^2 = –0.999) provides a simple equation to estimate C–H···N hydrogen bond strength based on calculated ρ value.

$$E_{int} = -1418.33\ \rho + 9.0199$$

Using above equation, we can estimate the strength of intramolecular C–H···N interaction in BPSDMBA**.** The calculated ρ values of the C–H···N hydrogen bond for BPSDMBA conformer **a** in the gas phase and in solution are 0.0159 and 0.0171 au, respectively, at the B3LYP/6-31+G* level. These ρ values yield interaction energies of 13.5 and 15.2 kJ mol^{-1} in the gas phase and in solution, respectively, for the intramolecular C–H···N hydrogen bond in BPSDMBA. Thus, the strength of the intramolecular C–H···N hydrogen bond in BPSDMBA is slightly increased in a dielectric solvent medium. Our calculated result is consistent with the experimental observation that the C–H···N hydrogen bond in BPSDMBA is prevailed in solution.[13]

7.3.5 C–H···O=S hydrogen bonds in BPSDMBA

As mentioned in Section 7.3.1, multiple intramolecular C–H···O contacts occur in most BPSDMBA conformers. Hydrogen bond involves sulfonyl oxygen has been reported previously.[33,34] To gauge the influence of this type of C–H···O=S hydrogen bond in BPSDMBA, we have adopted an approach similar to that of the C–H···N interaction to determine the bond strength of the C–H···O=S interaction. To this end, we have studied the correlation between interaction energy (E_{int}) and electron density (ρ) for a series of intermolecular C–H···O complexes, namely AH···OH_2 (AH = CH_4, CH_3F, CH_2F_2, CHF_3, CH_3CN, CH_2CN_2 and CH_3CN) and CH_4···HSO_2Ph complexes, at the B3LYP/6-31+G* level (Table 7.5) Not surprisingly, E_{int} correlates well with ρ (R^2 = –0.990) in Figure 7.4. The derived equation from the linear fit is E_{int} = –1438.89 ρ + 8.8289. The range of calculated ρ values for the various BPSDMBA conformers is 0.0063 – 0.0142. This leads

to an estimate of 0.3 – 11.5 kJ mol^{-1} for the C–H···O=S hydrogen bond in BPSDMBA. Although the magnitude of the interaction energy is significantly smaller than that calculated for the intramolecular C–H···N hydrogen bond, this stabilization effect is not negligible as there are multiple C–H···O=S contacts in each conformer. One would envisage that the C–H···O=S hydrogen bond is important for understanding conformational properties of compounds containing a sulfonyl functional group.

7.4 Conclusions

On the basis of ab initio MO calculations, 17 unique conformers of BPSDMBA have been identified. The intramolecular C–H···N and C–H···O hydrogen bonds and π-stacking interaction are important factors in governing the conformational preference of this molecule. The presence of the intramolecular hydrogen bonds was readily confirmed by the AIM theory of charge density analysis. For the intramolecular C–H···N hydrogen bond in BPSTMBA, the calculated structural parameters and ^1H NMR chemical shifts are in excellent accord with experimental results. A linear correlation was found between the interaction energy and electron density at the bond critical point for a series of intermolecular NH_3 complexes involving C–H···N hydrogen bond. Based on the linear fit, the interaction energy of the intramolecular C–H···N hydrogen bond in BPSDMBA is estimated to be 14 kJ mol^{-1}. Multiple C–H···O=S interactions are found in most conformers of BPSDMBA. Solvent effect calculations reveal that these weak intramolecular forces prevail in an aprotic dielectric medium.

7.5 References

1 Cappelli. A.; Giorgi, G.; Anzini, M.; Vomero, S.; Ristori, S.; Rossi, C.; Donati, A. *Chem. Eur. J.* **2004**. *10*. 3177.

2 Geffrey, G. A. *An Introduction to Hydrogen Bonding*, Oxford University Press, Oxford, **1997**.

3 Nishio, M.; Hirota, M.; Umezawa, Y. *CH/π Interaction: Evidence, Nature, and Consequence,* Wiley, New York, **1998**.

4 Desiraju, G. R.; Steiner, T. *The Weak Hydrogen Bond in Structural Chemistry and Biology*, Oxford University Press, Oxford, **1999**.

5 Desiraju, G. R. *Acc. Chem. Res*. **2002**, *35*, 565, and references therein.

6 Wetmore, S. D.; Schofield, R.; Smith, D. M.; Radom, L. *J. Phys. Chem. A* **2001**, *105*, 8718, and references therein.

7 Desiraju, G. R. *Chem. Commun*. **2005**, 2995, and references therein.

8 Nishio, M. *Cryst. Eng. Commun*. **2004**, *6*, 130, and references therein.

9 Donati, A.; Ristori, S.; Bonechi, C.; Panza, L.; Martini, G.; Rossi, C. *J. Am. Chem. Soc*. **2002**, *124*, 8778 .

10 Mizuno, K.; Ochi, T.; Shindo, Y. *J. Chem. Phys*. **1998**, *109*, 9502.

11 Jiang, L.; Lai, L. *J. Bio. Chem*. **2002**, *277*, 37732.

12 Alekseyeva, E. S.; Batsanov, A. S.; Boyd, L. A.; Fox, M. A.; Hibbert, T. G.; Howard, J. A. K.; MacBride, J. A. H.; Mackinnon, A.; Wade, K. *J. Chem. Soc. Dalton Trans*. **2003**, 475.

13 Arunima, N.; Kurur, D. *Chem. Phys. Lett*. **2005**, *401*, 470.

14 Harlow, R. L.; Li, C.; Sammes, M. P. *J. Chem. Soc., Chem. Commun*. **1984**, 818.

15 Li, C.; Sammes, M. P. *J. Chem. Soc, Perkin Trans. I* **1983**, 2193.

16 SPARTAN 5, Wavefunction Inc., Irvine, CA , **1997**.

17 Lee, C.; Yang, W.; Parr, R. G. *Phys. Rev. B* **1988**, *37*, 785.

18 Becke, A. D. *J. Chem. Phys*. **1993**, *98*, 5648.

19 Tarakeshwar, P.; Choi, H. S.; Kim, K. S. *Chem. Rev*. **2000**, *100*, 4245.

20 Wong, M. W.; Wiberg, K. B.; Frisch, M. J. *J. Am. Chem. Soc*. **1992**, *114*, 1645.

21 Boys, S. F.; Bernardi, F. *Mol. Phys*. **1970**, *19*, 553.

22 Bader, R. F. W. *Atoms in Molecules—A Quantum Theory*, Oxford Science Publications, Oxford, **1990**.

23 Popelier, P. L. A.; Bone, R. G. A. *MORPHY98,* UMIST, Manchester, **1998**.

24 Cheeseman, J. R.; Trucks, G. W.; Keith, J. K.; Frisch, M. J. *J. Chem. Phys*. **1996**,*104*, 5497.

25 Frisch, M. J. et al GAUSSIAN 03, Gaussian Inc., Wallingford, CT, **2004**.

26 Steiner, T.; Saenger, W. *J. Am. Chem. Soc*. **1992**, *114*, 10146.

27 Bondi, A. *J. Phys. Chem.* **1964**, *68*, 441.

28 Dahl, T. *Acta Chem. Scand*. **1994**, *48*, 95.

29 Kock, U.; Popelier, P. L. A. *J. Phys. Chem*. **1995**, *99*, 9747.

30 Hobza, P.; Havlas, Z. *Chem. Rev*. **2000**, *100*, 4253.

31 Knop, O.; Boyd, R. J.; Choi, S. *J. Am. Chem. Soc*. **1988**, *110*, 7299.

32 Bader, R. F. W.; Tang, T.-H.; Tal, Y.; Biegler-Konig, F. W. *J. Am. Chem. Soc*. **1982**, *104* 946.

33 Wong. M. W. *J. Org. Chem*. **2005**, *70*, 5487.

34 Salvatella, L.; Ruiz-Lo´pez, M. F. *J. Am. Chem. Soc*. **1999**, *121*, 10772.

7.6 Appendix

Table 7.1

Calculated relative energies[a] (ΔE, kJ mol^{-1}), solvation energies[b,c] ($\delta\Delta E$, kJ mol^{-1}), C–H···X interaction distances[d] (d, Å) and dipole moments[d] (μ, D) of various conformers of BPSDMBA

conformer	ΔE ($\varepsilon = 1$)	$\delta\Delta E$ ($\varepsilon = 40$)	d(C–H···N)[e]	d(C–H···O)[e]	μ
a	0.0	0.0	2.356 (2.319) 3.200 (3.167) π···π	2.478 (2.610) 2.858 (2.918)	7.01
b	0.7	9.5	2.251 (2.247)	2.431 (2.413) 2.494 (2.502) 2.727 (2.698)	1.44
c	6.8	–3.4	2.372 (2.352)	2.391 (2.414) 2.680 (2.901)	7.97
d	11.5	–4.7	2.384 (2.356) 2.905 (2.893) C-H···π		8.13
e	15.2	9.8		2.474 (2.467) 2.575 (2.577) 2.668 (2.652)	1.16
f	16.1	–2.4	2.975 (2.945) π···π	2.430 (2.395) 2.721 (2.881)	7.56
g	16.3	8.9		2.464 (2.472) 2.469 (2.458) 2.640 (2.609)	1.19
h	17.9	–4.6	2.893 (2.863) C-H···π	2.357 (2.342) 2.588 (2.647)	8.43
i	23.6	9.6		2.396 (2.404) 2.597 (2.619) 2.651 (2.647)	1.15
j	25.1	9.7		2.447 (2.445)	0.90

				2.434 (2.441) 2.667 (2.663)	
k	25.8	–3.1		2.402 (2.449) 2.775 (2.568)	7.81
l	27.6	–0.1		2.350 (2.314) 2.634 (2.542) 2.773 (2.814)	7.03
m	30.6	–4.0		2.481 (2.484) 2.678 (2.593)	8.02
n	32.8	–2.9		2.392 (2.413)	8.10
o	33.3	–1.2		2.445 (2.480) 2.748 (2.610)	7.29
p	33.4	–4.5		2.472 (2.409) 2.870 (2.654)	7.69
q	42.9	–2.7		2.719 (2.625)	7.32

[a] MP2/6-311+G**//B3LYP/6-31+G* level.

[b] B3LYP/6-311+G**//B3LYP/6-31+G* level.

[c] $\delta\Delta E = \Delta E\ (\varepsilon = 40) - \Delta E\ (\varepsilon = 1)$.

[d] Based on B3LYP/6-31+G* level.

[e] SCRF ($\varepsilon = 40$) value in parenthesis.

Table 7.2

Calculated structural parameters and ^{1}H NMR chemical shifts of BPSTMBA and BPSDMBA[a,b]

	d(H···N) [Å]		α(C–H···N) [°]		δH[c] [ppm]	
gas phase	2.287	(2.356)	135.6	(134.1)	6.60	(5.40)
solution (ε = 40)[d]	2.288	(2.319)	135.6	(135.5)	6.68	(5.87)
experiment	2.343[e]		138.2[e]		6.22[f]	(5.20)[e]

[a] B3LYP/6-31+G* level.

[b] BPSDMBA values are given in parentheses.

[c] ^{1}H chemical shift of the methane hydrogen (GIAO calculation).

[c] Based on SCRF solvation method.

[e] From Ref. [14].

[f] From Ref. [15].

Table 7.3

Binding properties of intermolecular $AH^{\cdots}NH_3$ complexes.[a]

AH molecule	E_{int}[b]	$d(H^{\cdots}N)$	$\alpha(CH^{\cdots}N)$	$\Delta d(C–H)$[c]	$\Delta\upsilon$[d]	ρ	$\nabla_2\rho$
	kJ mol^{-1}	Å	◦	Å	cm^{-1}	au	au
CH_4	–1.2	2.737	180.0	0.0006	–7.7	0.0074	0.0231
CH_3Me	–0.8	2.796	174.2	–0.0007	2.6	0.0067	0.0210
CH_2Me_2	–0.8	2.792	177.2	–0.0014	11.4	0.0069	0.0210
$CHMe_3$	–1.0	2.820	179.9	–0.0022	32.7	0.0067	0.0200
CH_3F	–6.8	2.488	178.5	–0.0004	7.1	0.0117	0.0345
CH_2F_2	–12.4	2.334	170.7	0.0002	–0.2	0.0158	0.0450
CHF_3	–18.4	2.226	180.0	0.0030	–42.8	0.0193	0.0540
CH_3SO_2H	–14.4	2.340	176.5	0.0049	–40.5	0.0154	0.0438
$CH_2(SO_2H)_2$	–25.1	2.115	179.5	0.0135	–256.6	0.0239	0.0640
CH_3CN	–12.3	2.345	177.5	0.0044	–40.8	0.0153	0.0436
$CH_2(CN)_2$	–24.5	2.136	173.0	0.0123	–207.1	0.0232	0.0615
$CH(CN)_3$	–37.9	1.959	179.2	0.0270	–399.2	0.0333	0.0828

[a] B3LYP/6-31+G* level.

[b] Interaction energy include BSSE correction.

[c] Bond lengthening on going from the AH monomer to the $AH^{\cdots}NH_3$ complex.

[d] C–H stretching frequency change on going from the AH monomer to the $AH^{\cdots}NH_3$ complex.

Table 7.4

Calculated interaction energies (E_{int}, kJ mol^{-1}) and intermolecular distance ($d(H^{\cdots}N)$, Å) of the $CH_3F^{\cdots}NH_3$ complex at various levels of theory[a]

Basis set	B3LYP		MP2		QCISD		CCSD(T)[b]
	E_{int}	$d(H^{\cdots}N)$	E_{int}	$d(H^{\cdots}N)$	E_{int}	$d(H^{\cdots}N)$	E_{int}
6-31G*	–7.1	2.519	–7.1	2.538	–6.8	2.561	–7.1
6-31+G*	–6.8	2.488	–7.0	2.474	–6.8	2.499	–7.5
6-311+G**	–6.7	2.529	–6.5	2.545	–6.3	2.572	–6.9
6-311++G**	–7.5	2.530	–6.6	2.541	–6.4	2.572	–6.9
cc-pVTZ	–5.8	2.557	–6.7	2.530	–6.4	2.569	–7.0
aug-cc-pVTZ	–5.6	2.654	–7.3	2.570	–7.1	2.603	–7.7

[a] Fully optimized at the level of theory specified unless otherwise noted.

[b] Based on QCISD/aug-cc-pVTZ optimized geometry.

Table 7.5

Binding properties of intermolecular $AH^{\cdots}H_2O$ and CH_4- SO_2H_2 and SO_2HPh complexes.[a]

AH molecule	E_{int}[b]	$d(H^{\cdots}N)$	$\alpha(CH^{\cdots}N)$	$\Delta d(C–H)$[c]	$\Delta\upsilon$[d]	ρ	$\nabla_2\rho$
	kJ mol^{-1}	Å	◦	Å	cm^{-1}	au	au
CH_4	-1.0	2.606	179.7	-0.0005	5.2	0.0067	0.0257
CH_3F	-5.7	2.408	169.2	-0.0015	21.5	0.0108	0.0368
CH_2F_2	-10.5	2.353	167.6	-0.0019	23.5	0.0147	0.0483
CHF_3	-14.9	2.157	175.7	-0.0010	23.6	0.0169	0.0571
$CH_3(CN)$	-10.1	2.366	173.4	-0.0024	26.5	0.0131	0.0434
$CH_2(CN)_2$	-20.0	2.100	172.1	-0.0038	37.8	0.0195	0.0628
$CH(CN)_3$	-28.2	1.974	173.8	-0.0074	99.3	0.0248	0.0810
$CH_4…SO_2H_2$	-0.4	2.786	177.0	-0.0006	6.3	0.0038	0.0156
$CH_4…SO_2HPh$	-0.7	2.747	175.2	-0.0007	7.4	0.0042	0.0172

[a] B3LYP/6-31+G* level.

[b] Interaction energy include BSSE correction.

[c] Bond lengthening on going from the AH monomer to the $AH^{\cdots}NH_3$ complex.

[d] C–H stretching frequency change on going from the AH monomer to the $AH^{\cdots}NH_3$ complex.

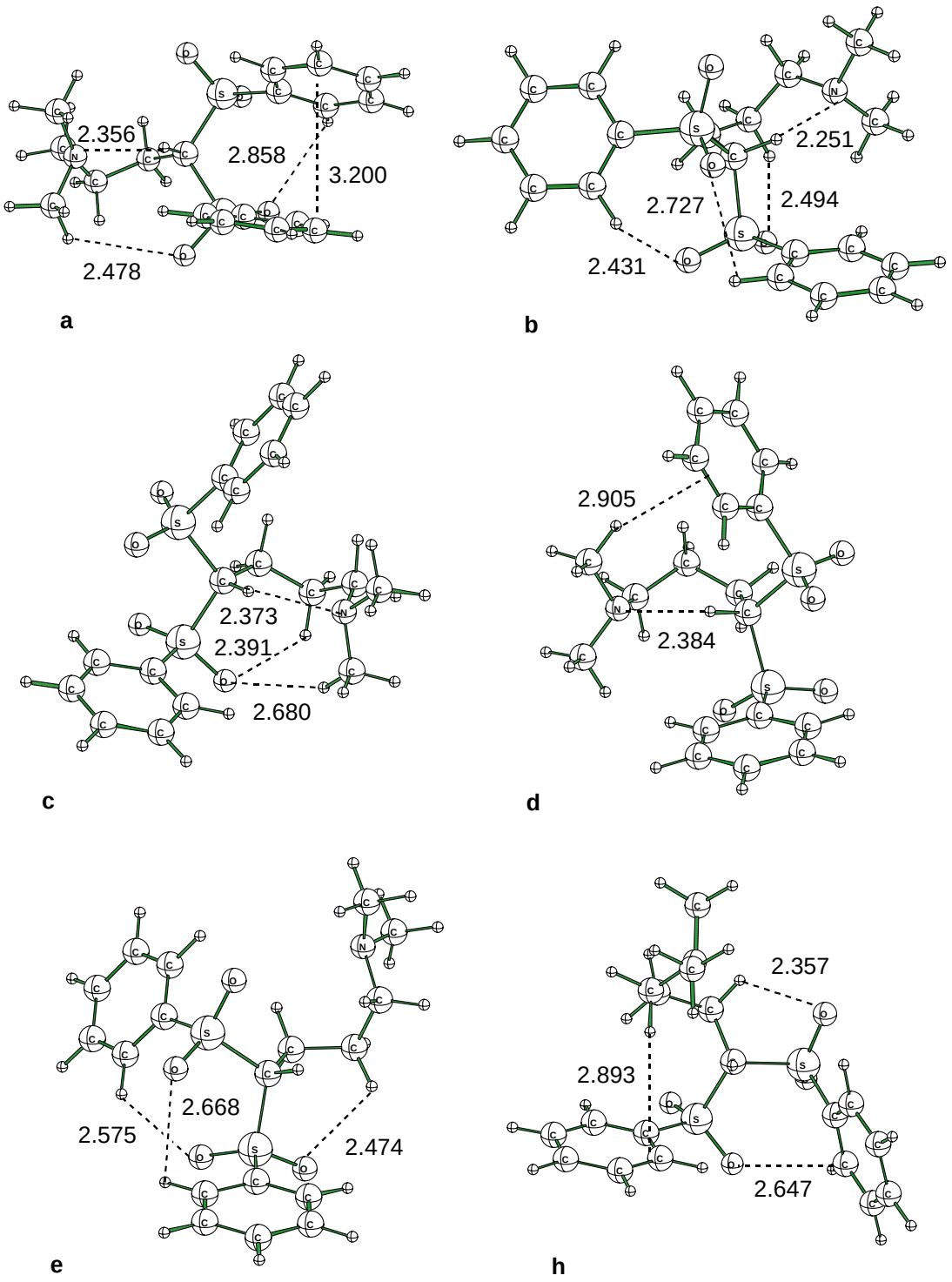

Figure 7.1 Optimized geometries [B3LYP/6-31+G*] of selected conformers of BPSDMBA (interaction distance in Å)

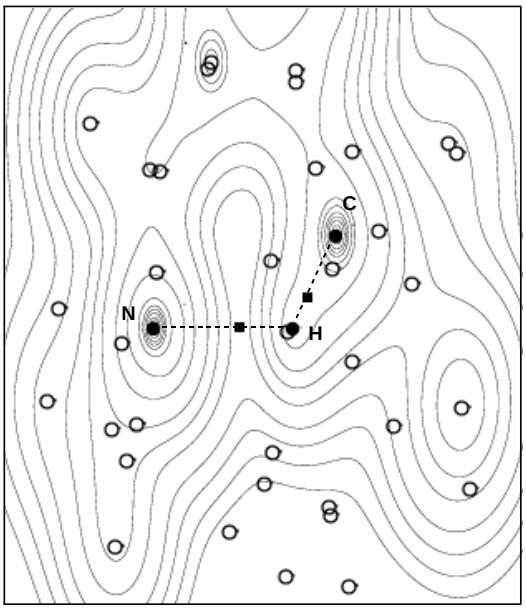

Figure 7.2 Contour line of charge density (ρ) with a relevant part of the molecular graph (C–H···N) of BPSDMA. The outline labels refer to atoms which are not lying in the plotting plane. The bond critical points are labeled as ″■″.

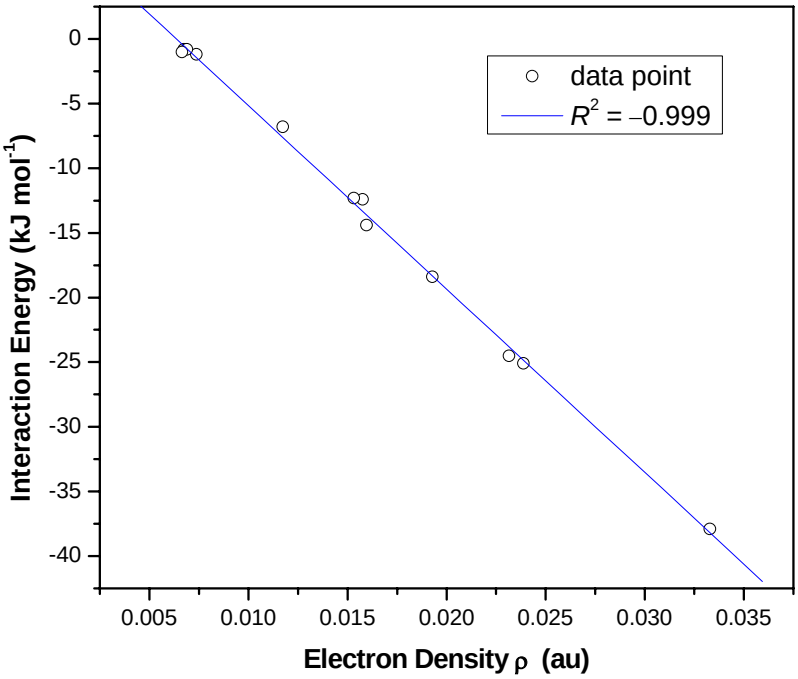

Figure 7.3 Plot of interaction energy against electron density (ρ) at bond critical point for the intermolecular AH···NH_3 complexes (AH = proton donor).

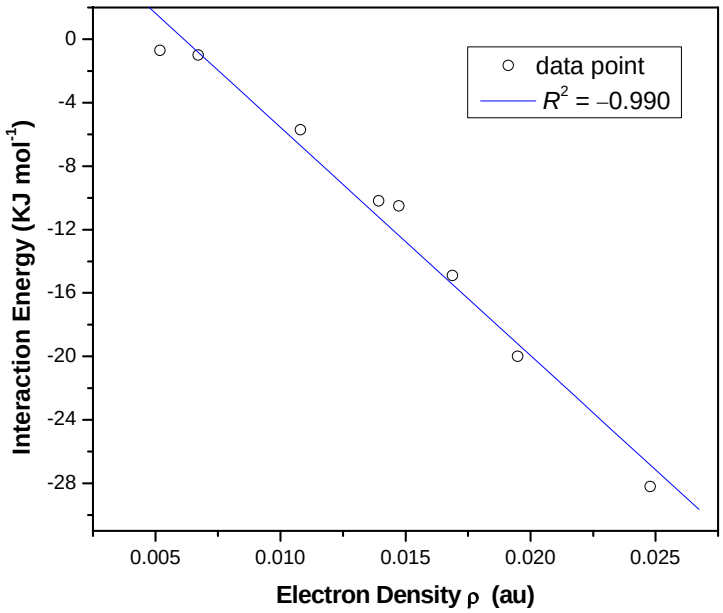

Correlation Plot for Intermolecular CH···O Complexes

Figure 7.4 Plot of interaction energy against electron density (ρ) at bond critical point for the intermolecular AH···H_2O complexes (AH = proton donor).